ACTIVITY OF ETHANOL EXTRACT OF *Pleurotus ostreatus* AGAINST MERCURIC CHLORIDE-INDUCED CEREBELLAR TOXICITY IN WISTAR RATS.

BY

AIG-UNUIGBE, JOHNFAVOUR EHIJIAGBON

PG/BMS1507490

DEPARTMENT OF ANATOMY

SCHOOL OF BASIC MEDICAL SCIENCES

COLLEGE OF MEDICAL SCIENCES

UNIVERSITY OF BENIN

JUNE, 2025.

ACTIVITY OF ETHANOL EXTRACT OF *Pleurotus ostreatus* AGAINST MERCURIC CHLORIDE-INDUCED CEREBELLAR TOXICITY IN WISTAR RATS.

BY

AIG-UNUIGBE, JOHNFAVOUR EHIJIAGBON
PG/BMS1507490
B.Sc. (UNIBEN, 2019)

A THESIS WRITTEN IN THE DEPARTMENT OF ANATOMY, SCHOOL OF BASIC MEDICAL SCIENCES AND SUBMITTED TO THE COLLEGE OF POSTGRADUATE STUDIES, IN PARTIAL FULFILMENT OF THE REQUIREMENTS FOR THE AWARD OF MASTER'S DEGREE (M.Sc.) IN ANATOMY OF THE UNIVERSITY OF BENIN, BENIN CITY.

JUNE, 2025.

AUTHOR'S STATEMENT

I hereby grant the University of Benin, through the University of Benin Library, a non-exclusive, worldwide right to reproduce and distribute my thesis and abstract (hereinafter "the Work"), in whole or in part, through any media, in its present form or any translated version for preservation and accessibility, provided such translation does not alter its content. This grant is royalty-free, and I retain the right to publish the Work in its current or future versions elsewhere.

Warranties

I further affirm that:

1. I am the sole author of the Work and grant the University of Benin the right to make it available four (4) years after the award of my doctorate degree, in compliance with the University of Benin Senate regulations.
2. The Work does not contain confidential information requiring third-party consent for disclosure.
3. I have exercised due diligence to ensure that the Work is original and does not breach any Nigerian law or infringe upon any third party's copyright or other Intellectual Property Rights, to the best of my knowledge.
4. Where the Work includes copyrighted material not owned by me, I have obtained unrestricted permission from the copyright holder to grant this license to the University of Benin Library. Such third-party materials are clearly identified and acknowledged within the Work.
5. In the event of any copyright dispute concerning the Work, I agree to indemnify and hold harmless the University of Benin, its officers, employees, and agents from any liability arising from the material authorized under this agreement.
6. The University of Benin is under no obligation whatsoever to take legal action on my behalf as the Depositor in the event of an intellectual property rights infringement or any other related dispute in the material deposited.

Author`s Name	Signature/Date	Email
Supervisor's Name	Signature/Date	Email

CERTIFICATION

This is to certify that this M.Sc. thesis was written by Aig-Unuigbe, JohnFavour Ehijiagbon in the Department of Anatomy, School of Basic Medical Sciences, University of Benin, Benin City, Nigeria.

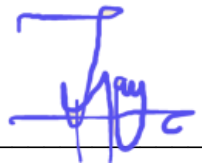

_____ _____

GERALD I. EZE (FWACP, PhD) **DATE**

Professor

Supervisor

_____ _____

ADAZE B. ENOGIERU (PhD) **DATE**

Associate Professor

Head of Department

_____ _____

EXTERNAL EXAMINER **DATE**

DEDICATION

To God, who grants wisdom to those who ask—

This is Yours before it is mine.

And to all who dare to chase knowledge, No matter the odds.

“For the Lord gives wisdom; from His mouth come knowledge and understanding.”
— Proverbs 2:6

ACKNOWLEDGEMENTS

This journey has been far more than a scholarly pursuit; it has been a pilgrimage of the mind and spirit, marked by grace, perseverance, and the quiet strength of those who believed in me. I owe heartfelt gratitude to Prof. Gerald Ikechi Eze, my supervisor, for his unwavering support, wise counsel, and mentorship that shaped both this work and my academic growth; and to Dr. Silvanus Olu Innih, whose timely guidance and steady presence provided clarity in moments of uncertainty.

To Dr. Adaze Bijou Enogieru, Head of Department, I am deeply grateful for your intellectual contributions, mentorship both within and beyond the classroom, and your sincere encouragement that never went unnoticed. I also remain indebted to the entire academic and non-academic staff of the Department of Anatomy, whose dedication and support fostered a truly enabling environment for this journey. I acknowledge with sincere gratitude the ANA-MED research team, whose collaboration, camaraderie, and meaningful contributions were instrumental to the success of this work. To my colleagues, thank you for your companionship and the shared pursuit of excellence that enriched this path. In particular, I am grateful to Miss Chioma and Mr. Raymond, whose presence, gentle encouragement, and steadfast support brought warmth and inspiration to this journey. Not also forgetting, Mr. Brownson, and Miss Adaeze, for their encouragement and support.

To my beloved parents, Rev. Dr. and Pastor (Mrs.) J. S. Aig-Unuigbe, your unwavering love, prayers, and wisdom have been the silent foundation beneath every page of this thesis. To my siblings, Jesuseme, Peace, and Evangeline, your light, laughter, and belief steadied me more than words can ever express. Finally, and most importantly, to God Almighty—the eternal light in my darkness, the still voice in my chaos, the hand that held mine through every silent struggle. This work is not mine alone—it is the quiet sum of many voices, the imprint of every hand that steadied mine, and the silent strength of hearts that walked beside me.

TABLE OF CONTENTS

ABBREVIATIONS

AICA	Anterior Inferior Cerebellar Artery
BBB	Blood-Brain Barrier
BDNF	Brain-Derived Neurotrophic Factor
CAT	Catalase
CNS	Central Nervous System
CuCT	Cuneocerebellar Tract
CVAAS	Cold Vapor Atomic Absorption Spectrometry
DNA	Deoxyribonucleic Acid
DPPH	2,2-diphenyl-1-picrylhydrazyl
DSCT	Dorsal Spinocerebellar Tract
GABA	Gamma-Aminobutyric Acid
GMA	Global Mercury Assessment
GPx	Glutathione Peroxidase
GR	Glutathione Reductase
GSH	Glutathione
Hg	Mercury
$HgCl_2$	Mercuric Chloride
IL-1β	Interleukin-1 beta
IL-6	Interleukin-6
MDA	Malondialdehyde
MeHg	Methylmercury
MIT	Movement Initiation Test
NK	Natural Killer Cells
NMDA	N-Methyl-D-Aspartate

OFT	Open Field Test
PBS	Phosphate Buffered Saline
PICA	Posterior Inferior Cerebellar Artery
RNA	Ribonucleic Acid
ROS	Reactive Oxygen Species
RSCT	Rostral Spinocerebellar Tract
SCA	Superior Cerebellar Artery
-SH	Thiol Groups
SOD	Superoxide Dismutase
TBARS	Thiobarbituric Acid Reactive Substances
TLRs	Toll-like receptors
TNF-α	Tumor Necrosis Factor-Alpha
UNEP	United Nations Environment Programme
VSCT	Ventral Spinocerebellar Tract
WHO	World Health Organisation

LIST OF FIGURES

LIST OF PLATES

LIST OF TABLES

ABSTRACT

Cerebellar disorders are a class of neurological impairments characterized by unsteady gait and uncoordinated movements, typically resulting from lesions or pathologies affecting the cerebellum. These disorders may arise from congenital anomalies, hereditary ataxias, or exposure to environmental neurotoxicants such as heavy metals. Mercury, a highly toxic heavy metal, is known to exert deleterious effects on the central nervous system. Its lipophilic nature enables it to cross the blood-brain barrier, where it accumulates and induces oxidative stress, leading to neuroinflammation, neuronal damage, and impaired motor coordination. Dietary antioxidants have shown promise in combating mercury-induced neurotoxicity. Accordingly, this study investigated the activity of ethanol extract of *Pleurotus ostreatus* (*P. ostreatus*) against mercuric chloride ($HgCl_2$) induced cerebellar toxicity in Wistar rats. In this study, forty-two (42) Wistar rats were randomly assigned into six groups (A-F). Group A rats served as control; Group B received 4 mg/kg body weight [bw] of $HgCl_2$ only; Group C received 4 mg/kg bw of $HgCl_2$+ 250 mg/kg of *P. ostreatus*; Group D received 4 mg/kg bw of $HgCl_2$ + 500 mg/kg of *P. ostreatus*; Group E received 250 mg/kg bw of *P. ostreatus* only and Group F received 500mg/kg bw of *P. ostreatus* only. All administrations were done orally for twenty-eight (28) days. Neurobehavioural activity was subsequently evaluated using the Open Field, String, Movement Initiation and Step Tests. Following the assessments, the experimental rats were sacrificed via cervical dislocation and the cerebellum harvested for antioxidant enzymes activity, lipid peroxidation, mercury concentration and histological assessments. The findings revealed that rats exposed to $HgCl_2$ exhibited significant ($p < 0.05$) weight loss, motor deficit, impaired antioxidant defense, elevated lipid peroxidation, elevated mercury levels and degeneration of Purkinje cells and molecular layer neurons. However, co-administration with *P. ostreatus* significantly ($p < 0.05$) mitigated these mercury-induced cerebellar alterations in Wistar rats. Overall, the findings from this study indicate that *P. Ostreatus* mitigates mercuric chloride-induced cerebellar toxicity, primarily through its antioxidant, neuroprotective, and metal-chelating properties, thus making it a promising agent for the development of novel therapeutic strategies aimed at managing mercury neurotoxicity and its associated motor impairments.

CHAPTER ONE

INTRODUCTION

1.1 BACKGROUND OF THE STUDY

The cerebellum, situated dorsally to the brainstem, constitutes a structurally and functionally specialized region of the vertebrate hindbrain (Khamas *et al*., 2024; Sagar *et al*., 2025). As a pivotal neural integrator, the cerebellum orchestrates a wide spectrum of sensorimotor activities, including the regulation of posture, balance, voluntary movement, and fine motor coordination (Marchand *et al*., 2025; Florio, 2025). Although it does not directly initiate motor output, the cerebellum plays a central role in refining and calibrating movement by processing afferent input from the spinal cord, vestibular nuclei, and various cortical and subcortical regions (Prati *et al*., 2024; Marchand *et al*., 2025). Through this integrative function, it ensures the precision, timing, and fluidity necessary for smooth motor execution. The cerebellum, traditionally linked to motor control, is now recognized for its role in cognitive and emotional functions, including attention, language, and memory (Habas, 2021; Grimaldi, 2021). By integrating input from proprioceptive and vestibular systems, it refines motor responses and adapts to environmental changes. Damage to the cerebellum can result in ataxia, dysmetria, dysarthria, and postural instability—key signs of cerebellar dysfunction (Grimaldi, 2021; Joshua *et al*., 2022).

Cerebellar motor disorders are a diverse group of neurological conditions marked by impaired motor coordination due to damage or dysfunction within the cerebellum (Grimaldi, 2021; Xia *et al*., 2023). Symptoms often include gait abnormalities, tremors, and postural instability, severely affecting mobility and quality of life. These disorders are more common than previously thought, with a global prevalence exceeding 20% (Xia *et al*., 2023). Their causes are varied, ranging from congenital malformations and hereditary ataxias to acquired insults such as infections, trauma, and neurotoxicity (Grimaldi, 2021). The cerebellum’s high

metabolic activity and limited repair capacity make it particularly susceptible to toxic damage, especially from heavy metals like mercury, which disrupts cerebellar function through oxidative stress, mitochondrial damage, and excitotoxicity (Althobaiti, 2024; Dubey *et al*., 2025).

Mercury is a globally widespread and highly toxic heavy metal existing in elemental, inorganic, and organic forms, each with distinct exposure routes and toxicological effects. Occupational exposure, especially in mining and industrial settings, primarily involves inhalation of elemental mercury vapours, while the general population is more frequently exposed to organic forms—particularly methylmercury—through consumption of contaminated seafood (Zafar *et al*., 2024; Charkiewicz *et al*., 2025). The cerebellum is one of the primary targets of mercury toxicity, due to its high lipid content, metabolic activity, and the sensitivity of Purkinje neurons (Novo *et al*., 2021). Mercury disrupts neural homeostasis by generating reactive oxygen species (ROS), impairing mitochondrial function, depleting antioxidants, and triggering neuroinflammation (Kaur *et al*., 2021; Novo *et al*., 2021). These mechanisms result in structural degeneration and motor deficits, including impaired coordination and balance. Mercury crosses the blood–brain barrier and accumulates in neural tissue, causing persistent motor impairments, especially during neurodevelopmental windows (Zafar *et al*., 2024).

Antioxidants are essential bioactive compounds that neutralize ROS and reduce oxidative stress, a key contributor to various degenerative diseases, including neurotoxicity (Olufunmilayo *et al*., 2023). Although synthetic antioxidants are used clinically, natural alternatives—particularly those from plants and fungi—are increasingly favoured due to their effectiveness, safety, and low toxicity (Maraveas *et al*., 2021; Stoia and Oancea, 2022). One such candidate is *Pleurotus ostreatus* (oyster mushroom), a functional food and medicinal fungus rich in antioxidant compounds such as flavonoids, phenolic acids, ergothioneine,

polysaccharides, selenium, and zinc (Mishra *et al*., 2022; Effiong *et al*., 2024). These components work synergistically to scavenge free radicals and modulate oxidative stress, thereby protecting cells from damage. The antioxidant and metal-chelating effects of *Pleurotus ostreatus* have been demonstrated in several *in vitro* and *in vivo* models, showing its ability to reduce heavy metal induced oxidative damage (Ćilerdžić *et al*., 2019; Fadugba *et al*., 2024). This is particularly relevant in mercury-induced neurotoxicity, which involves excessive ROS production, lipid peroxidation, and mitochondrial disruption—processes *Pleurotus ostreatus* can potentially counteract through both enzymatic and non-enzymatic mechanisms. In addition, its nutritional profile—comprising quality proteins, fibre, and essential vitamins—enhances its value as a therapeutic agent. Its anti-inflammatory and immune-modulating properties further support its potential role in protecting against cerebellar damage linked to oxidative stress. Consequently, the rich pharmacological properties of *Pleurotus ostreatus* highlights its promising use in therapeutic applications, thus, aligning with the wider trend towards leveraging the medicinal properties of natural antioxidants for comprehensive and sustainable healthcare solutions.

1.2 STATEMENT OF THE RESEARCH PROBLEM

Mercury contamination represents a persistent and under-addressed environmental and public health crisis, especially in regions with inadequate environmental controls and industrial regulation (Huo and Zhou, 2025; Fuller *et al*., 2025). Inorganic mercury compounds, particularly mercuric chloride ($HgCl_2$), are known for their high toxicity and neurodegenerative potential (Basu, 2023; Nawabjan *et al*., 2025). Globally, mercury exposure contributes to an increasing burden of disease, with the World Health Organization listing mercury among the top ten chemicals of major public health concern due to its irreversible effects on human health, particularly the nervous system (World Health Organisation, 2019).

In Nigeria, mercury exposure has become increasingly concerning, not just because of industrial and artisanal mining activities, but also due to its tendency to accumulate in the environment and the lack of effective regulatory enforcement (Awogbami *et al*., 2024; Anene *et al*., 2024). Reports from the Federal Ministry of Environment and independent monitoring agencies indicate increasing mercury levels in water bodies, soil, and food chains in mining-intensive regions such as Zamfara, Kebbi, and Osun states (Nigeria Health Online, 2019; WHO, 2019; Akinsooto *et al*., 2024). While widespread surveillance data remains limited, recent findings estimate that thousands of individuals in affected areas may be at risk of chronic mercury toxicity, including vulnerable populations such as pregnant women and children (Nigeria Health Online, 2019; Akinsooto *et al*., 2024). Yet, public awareness and intervention strategies remain grossly inadequate.

A major concern lies in the effect of mercury on the brain—particularly the cerebellum, a region critical for coordinating voluntary movement, maintaining balance and posture, and regulating fine motor control (Ganguly *et al*., 2022; Kumari *et al*., 2023). The cerebellum's highly oxidative environment, abundant mitochondria, and dense neuronal circuitry make it a prime target for mercury-induced neurotoxicity (Kang *et al*., 2024). Previous studies have demonstrated that even low-level exposure to inorganic mercury can result in significant cerebellar alterations, including Purkinje cell loss, glial activation, neuroinflammation, and impaired synaptic integrity (Chamoli and Karn, 2024; Kang *et al*., 2024; Zahed *et al*., 2024; Salavoura, 2025). These pathological changes often manifest clinically as motor deficits, such as truncal ataxia, tremor, impaired coordination, and dysmetria—all features of cerebellar motor disorders (Kumari and Chand, 2023; Chamoli and Karn, 2024).

In experimental models, exposure to $HgCl_2$ has been associated with elevated oxidative stress markers, mitochondrial dysfunction, and histopathological damage in the cerebellum (Douae *et al*., 2025; Nawabjan *et al*., 2025). Mercury's affinity for sulfhydryl groups on proteins leads

to glutathione depletion and disruption of antioxidant defenses, ultimately triggering neuronal apoptosis (Kang *et al*., 2024; Zahed *et al*., 2024). The chronic retention of mercury in nervous tissue further exacerbates its long-term impact, with a biological half-life ranging from several weeks in soft tissues to years in the brain and bones (Zafar *et al*., 2024)

Despite the seriousness of cerebellar motor disorders linked to heavy metal toxicity, existing treatment strategies remain limited (Rehman *et al.,* 2021). Most therapeutic approaches are symptomatic, focusing on relieving motor impairments rather than reversing the underlying pathology (Billeri and Naro, 2021). Pharmacological interventions, such as dopamine agonists, GABA modulators, or deep brain stimulation, have been employed to manage ataxia, tremor, or dystonia (Ranjan *et al.,* 2024). However, these interventions are not curative, often carry significant costs, and may not be accessible in low-resource settings like Nigeria. Furthermore, their efficacy is inconsistent and rarely targets the oxidative or inflammatory mechanisms central to heavy metal-induced cerebellar damage (Rehman *et al*., 2021; Althobaiti, 2024). The persistent burden of mercury exposure in Nigeria, combined with the vulnerability of the cerebellum to oxidative damage and the limitations of existing therapies, underscores the urgent need for novel, affordable, and mechanism-targeted interventions.

1.3 AIM OF THE STUDY

The aim of the study was to investigate the activity of ethanol extract of *Pleurotus ostreatus* against mercuric chloride-induced cerebellar toxicity in Wistar rats.

1.4 SPECIFIC OBJECTIVES

The specific objectives of the study were to:

i. Compare the brain and body weight changes in rats across the experimental groups

ii. Determine the neurobehavioral activities (Open field, Movement initiation, String and Step tests) in rats across the experimental groups.

iii. Evaluate the antioxidant enzymes (Catalase, Superoxide dismutase and Glutathione peroxidase) activity and lipid peroxidation (Malondialdehyde concentration) activity in the cerebellum of rats across the experimental groups.

iv. Quantify mercury concentration in the cerebellum of rats across the experimental groups

v. Examine the histology of the cerebellum of rats across the experimental groups

While also determining:

vi. the mycochemical constituents (qualitative and quantitative) and proximate analysis of ethanol extract of *Pleurotus ostreatus*

vii. the free radical scavenging activity of ethanol extract of *Pleurotus ostreatus* in comparison to a standard antioxidant (Ascorbic acid).

1.5 JUSTIFICATION OF THE STUDY

The increasing incidence of mercury-induced neurotoxicity, particularly in low-resource settings, underscores the urgent need for accessible and effective therapeutic interventions (Chamoli *et al*., 2024). Current treatment options are limited in scope, primarily addressing symptoms rather than targeting the underlying pathophysiological mechanisms. Specifically, they often fail to address the oxidative stress and inflammatory responses that drive cerebellar damage—a region especially vulnerable due to its high metabolic activity and intricate neuronal circuitry (Ganguly *et al*., 2022; Chamoli *et al*., 2024; Zahed *et al*., 2024).

In light of these therapeutic limitations, scientific attention has increasingly shifted toward the exploration of bioactive natural products with multitargeted pharmacological potential. Among these, edible and medicinal mushrooms—particularly *Pleurotus ostreatus* (commonly known

as the oyster mushroom)—have emerged as promising candidates. This fungus is rich in health-promoting compounds such as flavonoids, phenolic acids, terpenoids, polysaccharides, and essential trace elements like selenium (Mishra *et al*., 2022; Effiong *et al*., 2024; Fadugba *et al*., 2024). These constituents are well-known for their antioxidant, anti-inflammatory, and metal-chelating properties, all of which are mechanistically relevant in countering mercury-induced oxidative damage and neuroinflammation (Effiong *et al*., 2024; Fadugba *et al*., 2024). Although preliminary studies have demonstrated the neuroprotective potential of *Pleurotus ostreatus* in various models of oxidative stress (Ćilerdžić *et al*., 2019; Famii and Favour, 2019), there remains a critical gap in our understanding of its specific efficacy against mercury-induced cerebellar toxicity. This gap is particularly concerning given the cerebellum's essential role in motor coordination and its heightened susceptibility to heavy metal insults, such as those posed by mercury exposure.

Conventional therapeutic options remain largely inaccessible in many affected regions due to high costs, limited availability, and their primarily symptomatic nature. This reality highlights the pressing need for alternative, safer, and more affordable neuroprotective strategies. *Pleurotus ostreatus*, with its nutritionally rich profile and wide array of bioactive components, presents a viable and potentially transformative option in this regard. Evaluating the mushroom's capacity to mitigate mercury-induced cerebellar alterations could offer vital insights into the development of integrative and evidence-based interventions for heavy metal neurotoxicity. Ultimately, findings from this study may lay a strong foundation for future translational research and encourage the incorporation of natural product-based strategies in the management of mercury-related neurological disorders, particularly in resource-constrained regions.

CHAPTER TWO

LITERATURE REVIEW

2.1 THE BRAIN

The brain, protected within the bony neurocranium, is the central organ of the central nervous system, working in close coordination with the spinal cord (Junior *et al*., 2021; Palejwala *et al*., 2021). It governs a wide range of functions, from essential life-sustaining processes to complex cognitive activities. Structurally, the brain is organized into distinct regions, each exhibiting specialized functions and reflecting evolutionary development (Bhushan *et al*., 2022). Based on both anatomical structure and functional roles, the brain is commonly subdivided into the following key parts:

- **Telencephalon** – Representing the most evolutionarily advanced region of the brain, the telencephalon encompasses the cerebral hemispheres and cerebral cortex. It is responsible for higher-order functions, including reasoning, perception, voluntary movement, and memory (Palejwala *et al*., 2021).
- **Diencephalon** – Situated deep within the brain, the diencephalon comprises structures including the thalamus, hypothalamus, and metathalamus. It is crucial for relaying sensory information, controlling autonomic functions, and regulating endocrine activity. Along with the telencephalon, it constitutes the forebrain, also known as the prosencephalon (Bhushan *et al*., 2022).
- **Mesencephalon (Midbrain)** – A relatively small region, the midbrain comprises the tectum, tegmentum, and cerebral peduncles. Serving as a critical conduit for ascending and descending nerve tracts, it plays a key role in auditory and visual processing, and motor control (Bhushan *et al*., 2022).
- **Rhombencephalon (Hindbrain)** – This posterior section of the brain includes:

- ✓ The **metencephalon**, comprising the pons and the cerebellum, which coordinate movement and balance.
- ✓ The **myelencephalon**, which forms the medulla oblongata and manages vital autonomic functions such as heart rate and respiration (Junior *et al*., 2021; Bhushan *et al*., 2022).

Embedded within these regions lies the ventricular system, an interconnected network of cavities filled with cerebrospinal fluid that cushions the brain and meticulously regulates its chemical environment (Nazareth *et al*., 2021). Beyond its structural complexity, the brain's function is supported by glial cells such as astrocytes, oligodendrocytes, and microglia, which maintain homeostasis, support neurons, and defend against pathogens (Borst *et al*., 2021; Nazareth *et al*., 2021). Additionally, the blood-brain barrier ensures a tightly regulated environment by controlling substance exchange between the brain and bloodstream (Sultana *et al*., 2024).

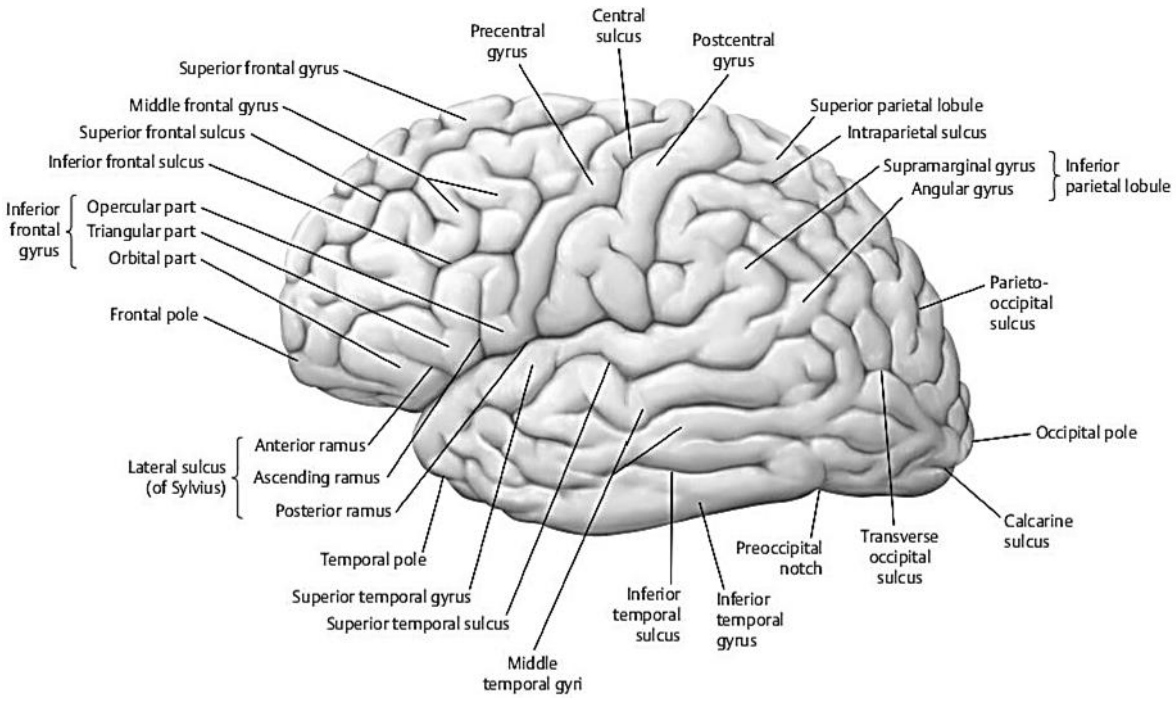

Figure 2.1: Gross Anatomy of the Brain (Bhushan *et al*., 2022)

2.2 THE CEREBELLUM

The cerebellum is the principal coordinator of muscle activity and plays a critical role in the acquisition and refinement of motor tasks (Miall *et al*., 2022). It synchronizes muscle contractions both within and across muscle groups, smoothing movements by finely regulating and modulating muscle tension (Lara-Aparicio *et al*., 2022). Consequently, the cerebellum is essential for maintaining equilibrium and muscle tone. Anatomically, it is situated in the posterior cranial fossa, beneath the tentorium cerebelli and posterior to the pons and medulla oblongata (Lara-Aparicio *et al*., 2022; Miall *et al*., 2022). The cerebellum processes sensory input related to ongoing motor activity entirely at an unconscious level. It does not contribute to conscious perception or higher cognitive functions such as intelligence.

Sensory input to the cerebellum originates from the vestibular system, stretch receptors (including neuromuscular spindles and Golgi tendon organs), and various somatosensory sources throughout the head and body (Miall *et al*., 2022; Kebschull *et al*., 2024). Additionally, auditory and visual systems project fibres to the cerebellum. These diverse inputs are functionally integrated into motor pathways, primarily through outputs to upper motor neurons and cerebellar feedback circuits that interconnect with the cerebral cortex, vestibular apparatus, and reticular formation of the brainstem (Kebschull *et al*., 2024).

2.2.1 Gross Anatomy of The Cerebellum

The cerebellum is located directly beneath the posterior aspects of the temporal and occipital lobes, within the posterior cranial fossa. It is structurally separated from the overlying cerebral cortex by the tentorium cerebelli, a dural reflection that forms a protective roof over its superior surface (Tanabe *et al*., 2018; Singh, 2020; Kebschull *et al*., 2024). Anteriorly, the cerebellum attaches to the brainstem at the level of the pons via three major fibre bundles known as the cerebellar peduncles. These include: the inferior cerebellar peduncle (restiform body), which carries both afferent and efferent fibres; the middle cerebellar peduncle (brachium pontis),

consisting entirely of afferent fibres from the contralateral pontine nuclei; and the superior cerebellar peduncle (brachium conjunctivum), which primarily conveys efferent fibres to the midbrain and thalamus (ten Donkelaar *et al*., 2020; Schmahmann, 2023).

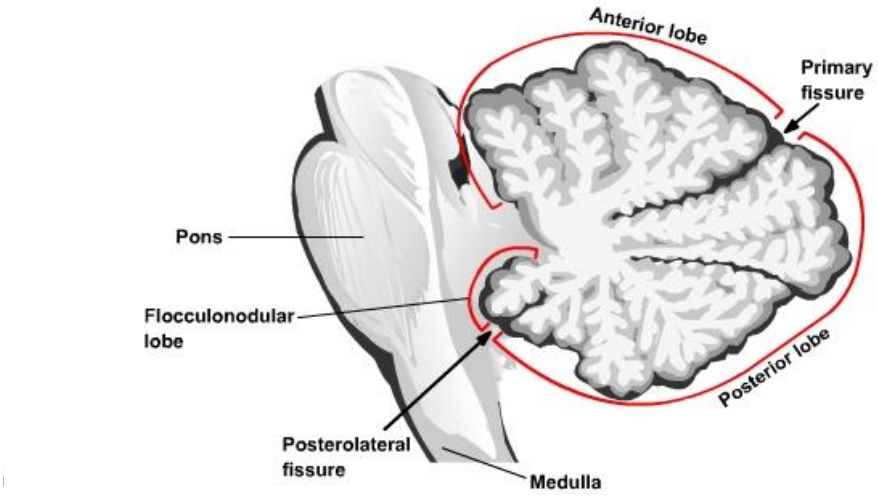

Figure 2.2: Structure of the Cerebellum (ten Donkelaar *et al*., 2020)

In situ, the most visually prominent features of the cerebellum are its two large hemispheres, characterized by transverse fissures and narrow, leaf-like ridges called folia (Kebschull *et al*., 2024). These surface features define the cerebellar hemispheres, which flank a centrally positioned, longitudinal structure know. Although the vermis is not readily visible externally, it runs along the midline from anterior to posterior and plays a central role in coordinating axial body movements (ten Donkelaar *et al*., 2020; Lara-Aparicio *et al*., 2022).

Approximately one-third of the distance from the brainstem along the dorsal surface lies the primary fissure, a prominent landmark that separates the cerebellum into two major lobes: the anterior lobe (rostral to the fissure) and the posterior lobe (caudal to it) (Schmahmann, 2023; Tanabe *et al*., 2018). Similar to the cerebral cortex, the cerebellum has undergone significant phylogenetic expansion, particularly in the posterior lobes of the hemispheres. This is reflected in the predominance of afferent projections to the posterior lobe from the cerebral cortex, highlighting its role in higher-order motor coordination (Lara-Aparicio *et al*., 2022; Miall,

2022). On the ventral surface, near the junction of the cerebellum and brainstem, are two small lateral protrusions known as the flocculi. Bridging these structures is the nodulus, typically concealed from view (Tanabe *et al*., 2018; Miall, 2022; Schmahmann, 2023). Collectively, the flocculi and nodulus form the flocculonodular lobe, which is the phylogenetically oldest part of the cerebellum and is primarily involved in vestibular function and balance (Miall, 2022; Schmahmann, 2023).

Another structural classification system divides the cerebellum into lobules, demarcated by other prominent surface fissures that span both the vermis and hemispheres. These lobules are identified by both descriptive names and Roman numerals: Lobules I–V constitute the anterior lobe, VI–IX the posterior lobe, and Lobule X corresponds to the flocculonodular lobe. (Kebschull *et al*., 2024). While these anatomical subdivisions are useful for descriptive and developmental purposes, functional divisions are more commonly employed in clinical contexts. These include the vestibulocerebellum, spinocerebellum, and cerebrocerebellum (also referred to as the pontocerebellum), each associated with distinct inputs, outputs, and physiological roles. These functional divisions will be discussed in greater detail in subsequent sections (ten Donkelaar *et al*., 2020; Sultana *et al*., 2024).

2.2.2 Connections of The Cerebellum

All afferent and efferent communication with the cerebellum occurs exclusively via the three cerebellar peduncles. The overall organizational scheme is relatively straightforward: with one notable exception for each, most afferent fibres enter the cerebellum through the inferior and middle cerebellar peduncles, while all efferent output exits through the superior cerebellar peduncle (Hatten *et al*., 2020; Carey, 2024). The cerebellum receives input from three principal sources: the spinal cord, brainstem nuclei, and the cerebral cortex. In general—and again, with a single major exception—afferent fibres originating from the spinal cord and brainstem nuclei

project to the cerebellum via the inferior cerebellar peduncle, whereas input from the cerebral cortex, transmitted through corticopontine pathways, reaches the cerebellum via the middle cerebellar peduncle (Hatten, 2020; Carey, 2024).

2.2.2.1 Inferior Cerebellar Peduncles

The inferior cerebellar peduncle (restiform body) serves as a major conduit for afferent input into the cerebellum, particularly from the spinal cord, medulla, and brainstem. Among the primary afferent pathways entering via this peduncle are the dorsal spinocerebellar tract (DSCT), which originates in the dorsal nucleus of Clarke, and the cuneocerebellar tract (CuCT), which arises from the lateral cuneate nucleus of the medulla. These tracts transmit non-conscious proprioceptive and kinesthetic information from muscle spindles and tendons—DSCT from the lower extremities and CuCT from the upper extremities (Fastenrath *et al*., 2022; Carey, 2024). The rostral spinocerebellar tract (RSCT), although less well defined, also enters through the inferior cerebellar peduncle and likely serves a role analogous to that of the ventral spinocerebellar tract (VSCT) for the upper limbs. Both RSCT and VSCT are thought to convey non-conscious somatosensory feedback, such as pressure, touch, and nociceptive inputs, as well as proprioceptive signals. Additionally, they may relay information related to spinal reflexes and intrinsic spinal cord activity via interneuronal circuits, influenced by descending corticospinal and bulbospinal inputs (Jossinger *et al*., 2020; Hatten, 2020; Lim *et al*., 2025).

The VSCT is unique among the spinocerebellar tracts in that it decussates within the spinal cord and then re-crosses within the brainstem, ultimately delivering predominantly ipsilateral input via the superior cerebellar peduncle (Lim *et al*., 2025). The trigeminocerebellar tract, originating in the principal sensory and spinal nuclei of cranial nerve V, also enters through the inferior peduncle. This pathway transmits proprioceptive and tactile information from the face and head and remains entirely ipsilateral (Sathyanesan *et al*., 2019; Hatten, 2020; Carey, 2024).

Additional significant afferent inputs via the inferior cerebellar peduncle arise from the vestibular nuclei, inferior and accessory olivary nuclei, and reticular nuclei. Vestibulocerebellar fibres are noteworthy in that, unlike most other inputs which project to both anterior and posterior lobes, they target primarily the flocculonodular lobe. These fibres travel through the juxtarestiform body, a medial subdivision of the inferior peduncle (Jang and Do Lee, 2020; Lim *et al*., 2025).

An important exception to the general rule that the inferior cerebellar peduncle carries only afferent fibres is that the juxtarestiform body also contains efferent projections. These arise from the flocculonodular lobe and associated fastigial nuclei and return to the vestibular and reticular nuclei, thus completing feedback loops vital for equilibrium and posture (Jossinger *et al*., 2020). The vestibular system, influenced by these cerebellar circuits, is essential for maintaining balance and coordinating eye movements. Its descending pathways, such as the vestibulospinal tract, exert excitatory effects on extensor motor neurons and inhibitory effects on flexor motor neurons, thereby supporting antigravity posture (Jossinger *et al*., 2020; Jang *et al*., 2020; Baran *et al*., 2022). Afferents from the inferior olivary complex are especially distinct. These fibres are entirely contralateral and project broadly across the cerebellar cortex. Unlike other cerebellar inputs, which take the form of mossy fibres synapsing on granule cells, the olivocerebellar fibres are climbing fibres that form powerful, exclusive synapses on Purkinje cells. These synapses are crucial for motor learning and cerebellar modulation of movement precision (Brownwonwi *et al*., 2019; Jang and Do Lee, 2020).

2.2.2.2 Middle Cerebellar Peduncles

The middle cerebellar peduncle, or brachium pontis, is by far the largest of the three cerebellar peduncles and serves as the principal route through which the cerebral cortex exerts its influence on the cerebellum. The majority of corticofugal fibres descending through the cerebral peduncles of the midbrain ultimately project to the cerebellum. These fibres terminate

ipsilaterally in the pontine nuclei, located in the anterior (basilar) portion of the pons (Çavdar *et al*., 2018; Stephen et aal., 2024). Neurons in the pontine nuclei then give rise to a massive band of transverse fibres that decussate across the midline and enter the cerebellum via the middle cerebellar peduncle, although a small proportion may remain uncrossed. This prominent fibre system contributes significantly to the characteristic transverse striation of the pons (Hamdy *et al*., 2022; Stephen *et al*., 2024).

The middle cerebellar peduncle conveys projections to all cerebellar regions except the flocculonodular lobe. Alongside climbing fibres from the inferior olivary nucleus, it constitutes a major source of input to the cerebellar hemispheres. The corticopontocerebellar pathway arises predominantly from the sensorimotor cortices surrounding the central sulcus. However, in humans, the prefrontal cortex, cortical association areas, and limbic cortices also contribute substantially to this pathway (Baran *et al*., 2022; Handy *et al*., 2022; Stephen *et al*., 2024). These extensive inputs suggest that the cerebellum not only receives information regarding ongoing motor activity and somatosensory feedback but also anticipates planned or intended movements. Moreover, it processes higher-order information, including visual, auditory, and affective signals, thereby supporting its emerging role in cognition and emotion in addition to motor coordination (Baran *et al*., 2022; Baran *et al*., 2022; Lim *et al*., 2025).

2.2.2.3 Superior Cerebellar Peduncles

The superior cerebellar peduncle, or *brachium conjunctivum*, serves as the principal efferent pathway from the cerebellum. A notable exception is the output from the flocculonodular lobe and the fastigial nuclei, which project to the vestibular and reticular nuclei via the inferior cerebellar peduncle (Lim *et al*., 2025). Although primarily an output structure, the superior cerebellar peduncle also conveys one major afferent pathway—the anterior (or ventral) spinocerebellar tract (VSCT). This tract transmits both peripheral and spinal cord information from the lower extremities and is unique in that it decussates twice, ultimately resulting in an

ipsilateral projection (Bruckert *et al*., 2019; Metwally *et al*., 2021). Some evidence also suggests that proprioceptive information from the muscles of mastication, transmitted via the mesencephalic nucleus of the trigeminal nerve, may enter the cerebellum through this peduncle (Bruckert *et al*., 2019; Stephen *et al*., 2024). With the exception of some direct projections from the flocculonodular lobe to the vestibular nuclei, virtually all cerebellar efferents originate from the deep cerebellar nuclei: the fastigial, globose, emboliform, and dentate nuclei. The fastigial nucleus projects fibres through both the inferior and superior cerebellar peduncles, primarily targeting the vestibular and lateral reticular nuclei. In contrast, efferents from the globose, emboliform, and dentate nuclei exit exclusively via the superior cerebellar peduncle (Çavdar *et al*., 2018; Hamdy *et al*., 2022; Stephen *et al*., 2024).

The major targets of these efferents include the contralateral inferior olivary nucleus, red nucleus, and ventrolateral nucleus of the thalamus. The latter projects to the primary motor and premotor cortices, thereby linking cerebellar output to motor planning and execution (Handy *et al*., 2022). Although these cerebellar pathways decussate, they influence motor systems—such as the corticospinal tract—that themselves cross the midline. Consequently, the cerebellum exerts an overall ipsilateral influence on motor control (Metwally *et al*., 2021; Handy *et al*., 2022). This complex arrangement allows the cerebellum to modulate motor activity at multiple hierarchical levels, ensuring coordination, timing, and precision of voluntary movement (Handy *et al*., 2022).

2.2.3 Cerebellar Cortex

Like the cerebrum, the cerebellum possesses a cortex, underlying white matter composed of afferent and efferent axonal fibres, and deep cerebellar nuclei (Van Essen *et al*., 2018; Hull and Regehr, 2022). However, the cerebellar cortex differs fundamentally from its cerebral counterpart in both structure and function. Unlike the multilayered cerebral cortex, the

cerebellar cortex consists of only three distinct layers (Sereno *et al*., 2020). This three-layered architecture is remarkably uniform throughout the cerebellum and features a highly organized, relatively straightforward neuronal arrangement. The three layers of the cerebellar cortex are: The molecular layer (outermost), the Purkinje cell layer (middle), and the granular layer (innermost) (Sereno *et al*., 2020; Guell and Schmahmann, 2020; Metwally *et al*., 2021).

2.2.3.1 Molecular Layer

The molecular layer is the most superficial and has the lowest neuronal density of the three layers. It contains two main types of inhibitory interneurons: stellate cells and basket cells. Despite its relative paucity of cell bodies, the molecular layer is densely packed with neuronal processes. Most prominent among these are the expansive dendritic arbors of the Purkinje cells and the parallel fibres originating from granule cells in the granular layer (Metwally *et al*., 2021).

The dendritic trees of Purkinje cells are highly branched yet constrained to a single sagittal plane, perpendicular to the longitudinal axis of the cerebellar folia. In contrast, the parallel fibres run transversely across the molecular layer, intersecting the dendritic planes of Purkinje cells at right angles. This orthogonal arrangement allows each parallel fibre to synapse with potentially thousands of Purkinje cell dendrites, providing a broad excitatory input (Van Essen *et al*., 2018; Sereno *et al*., 2020).

Stellate cells, with their relatively short dendrites, form inhibitory synapses with the dendrites of a limited number of nearby Purkinje cells. Basket cells, which have more extensive dendritic arbors, exert their inhibitory influence directly on the Purkinje cell soma and proximal dendrites. Both cell types receive excitatory input from the parallel fibres and act as modulatory interneurons by dampening Purkinje cell activity through GABAergic synapses (Guell and Schmahmann *et al*., 2020; Sereno *et al*., 2020).

2.2.3.2 Purkinje Layer

The Purkinje layer forms the narrow middle tier of the cerebellar cortex and is composed exclusively of the large, flask-shaped Purkinje cell bodies, which are among the most prominent and morphologically distinctive neurons in the central nervous system. These cells serve as the sole output neurons of the cerebellar cortex (Van Essen *et al*., 2018; Sereno *et al*., 2020). The extensive dendritic arbors of Purkinje cells ascend into the overlying molecular layer, where they form a dense, planar network that receives synaptic input primarily from parallel fibres and climbing fibres. In contrast, the axons of Purkinje cells project downward through the granular layer to synapse on neurons in the deep cerebellar nuclei, exerting GABAergic inhibitory control. These inhibitory projections form the primary efferent pathway from the cerebellar cortex to the cerebellar output centers (Bruckert *et al*., 2019; Hull and Regehr, 2022; Metwally *et al*., 2021).

Notably, a subset of Purkinje cells, particularly those located in the vermal region and flocculonodular lobe, send their axons directly to the vestibular nuclei in the brainstem, bypassing the deep cerebellar nuclei. These projections also convey inhibitory output and are essential for vestibular regulation and balance (Hamdy *et al*., 2022; Stephen *et al*., 2024). Additionally, the Purkinje layer contains fibres in transit between other cortical layers. These include climbing fibres (originating from the inferior olive), aminergic fibres (modulatory inputs), and processes of granule cells, Golgi cells, and basket cells, many of which terminate on or near the Purkinje cell soma (Guell and Schmahmann, 2020; Hull and Reghe, 2022).

2.2.3.3 Granular Layer

The innermost layer of the cerebellar cortex, the granular layer, is characterized by an exceptionally high density of small neurons, primarily granule cells, along with Golgi type II cells. Despite their diminutive size, granule cells are the most numerous neurons in the human brain (Consalez *et al*., 2021; D'Angelo, 2021). Granule cells serve as the excitatory

interneurons of the cerebellar cortex. Their axons ascend into the molecular layer, where they bifurcate into parallel fibres that course transversely and form excitatory synapses with the dendrites of Purkinje cells, as well as with basket and stellate cells. This parallel fibre system is central to the integration and distribution of afferent input within the cerebellum (D'Angelo, 2021; Florimbi *et al*., 2021).

The second principal cell type in this layer, the Golgi cells, function as inhibitory interneurons. While some of their dendritic processes extend into the molecular layer to interact with parallel fibres, their axons form inhibitory synapses with granule cell dendrites within specialized structures called glomeruli. Through these inhibitory synapses, Golgi cells modulate granule cell activity, forming a key component of the cerebellar cortical feedback circuit (Lackey *et al*., 2018; D'Angelo, 2021; Poudel *et al*., 2023). Together, the granule and Golgi cells establish a tightly regulated balance of excitation and inhibition within the cerebellar cortex, critical for the timing and precision of cerebellar processing (Poudel *et al*., 2023).

2.2.4 Cerebellar Nuclei

Embedded within the white matter at the anterior aspect of the cerebellum are several pairs of deep nuclei that serve as the primary output centers of the cerebellar circuitry. In humans, these are, from medial to lateral: the fastigial, globose, emboliform, and dentate nuclei (Boyken *et al*., 2018; Urrutia Desmaison *et al*., 2023). The globose and emboliform nuclei are often collectively referred to as the interposed nuclei due to their intermediate anatomical position between the fastigial and dentate nuclei, and their shared functional characteristics. These nuclei receive converging inputs from two principal sources:

- collateral branches of afferent fibres entering the cerebellum, and
- inhibitory efferents from Purkinje cells in the overlying cerebellar cortex (Urrutia Desmaison *et al*., 2023).

With the exception of a subset of Purkinje axons from the flocculonodular lobe that terminate directly in the vestibular nuclei, virtually all cerebellar output is mediated through these deep cerebellar nuclei (Bostan and Strick, 2018; Urrutia Desmaison *et al*., 2023). The fastigial nucleus, the most medially located, lies adjacent to the roof of the fourth ventricle and primarily receives inputs from the vermal and flocculonodular cortical regions, particularly those involved in balance and postural control. Its projections are directed to the vestibular nuclei and reticular formation, thus participating in the regulation of axial musculature and vestibulospinal reflexes (Willet *et al*., 2019; Urrutia Desmaison *et al*., 2023).

The interposed nuclei—comprising the globose and emboliform—are more prominent in higher primates, including humans. These nuclei receive afferent input mainly from the paravermal regions of the cerebellar cortex, which process spinal proprioceptive signals, especially from the limbs (Bostan and Srick, 2018; Willet *et al*., 2019). In addition to cortical input, they receive direct collaterals from ascending spinal afferents and other subcortical sources, including the reticular formation, inferior olivary complex, and potentially the red nucleus (Sarnaik ad Raman, 2018; Boyken *et al*., 2018). The dentate nucleus, the most laterally situated and phylogenetically the newest of the cerebellar nuclei, is the largest and most structurally complex. It receives dominant input from the lateral cerebellar hemispheres, particularly from regions implicated in planning and coordination of voluntary movement. It also receives some input from the anterior lobe (Boyken *et al*., 2018). Like the interposed nuclei, the dentate also receives collateral afferents from extracerebellar sources, although the precise afferent contribution patterns are still under active investigation (Bostan and Striick, 2018; Boyken *et al*., 2018).

Output from the dentate and interposed nuclei is relayed primarily via the superior cerebellar peduncle, targeting the contralateral red nucleus and the ventrolateral thalamic nuclei, the latter of which project to motor and premotor cortical areas (Wllet *et al*., 2019). The dentate nucleus

preferentially projects to the thalamus, whereas the interposed nuclei maintain stronger connections with the red nucleus. Both nuclei also send fibres to other brainstem targets, including the inferior olive, reticular formation, and superior colliculus, thus participating in multiple feedback and modulatory circuits (Wllet *et al*., 2019; Poudel *et al*., 2023). Several fundamental organizational principles of cerebellar output are evident. Firstly, the cerebellum exerts an ipsilateral influence on movement. This results from the double-crossing of its major output pathways (e.g., cerebellar projections to contralateral motor centers that themselves project to the contralateral body), meaning that lesions in a given cerebellar hemisphere affect movement on the same side of the body (Sarnaik and Raman, 2018; Florimbi *et al*., 2021; Urrutia Desmaison *et al*., 2023).

Secondly, the cerebellum engages in indirect modulation of spinal motor circuits through its projections to supraspinal centers such as the thalamus, red nucleus, vestibular nuclei, and reticular formation, which in turn influence the corticospinal, rubrospinal, vestibulospinal, and reticulospinal tracts (Florimbi *et al*., 2021; Urrutia Desmaison *et al*., 2023). Furthermore, the cerebellum is integrated into reentrant feedback loops that refine motor planning and execution. A key example includes the circuit: *dentate nucleus → thalamus → cerebral cortex → corticopontine fibres → pontocerebellar pathway*, thereby allowing the cerebellum to monitor and fine-tune cortical motor output (Sarnaik and Raman, 2018). Additional loops include reciprocal interactions between the vestibular nuclei and the flocculonodular lobe, essential for balance, equilibrium, and coordination of eye movements (Florimbi *et al*., 2021).

2.2.5 Functional Sub-Divisions of The Cerebellum

The cerebellum is functionally organized into three major divisions: the vestibulocerebellum, spinocerebellum, and cerebrocerebellum (also referred to as the pontocerebellum). These subdivisions are delineated not only by their primary sources of afferent input but also by their

distinct roles in motor coordination, postural control, and, more recently, higher-order cognitive and affective processes (Diedrichsen *et al*., 2019; Miall, 2022; Donnelly, 2023). An appreciation of this functional compartmentalization benefits from a brief anatomical orientation. Running along the midline of the cerebellum is the vermis, named for its worm-like appearance, which extends in the anterior-posterior direction (Diedrichsen *et al*., 2019). Flanking the vermis are the cerebellar hemispheres, which represent the most lateral regions of the cerebellum. The intermediate region between these two, lacking clearly defined anatomical borders, is known as the paravermal zone (Guell *et al*., 2018; Diedrichsen *et al*., 2019; Miall, 2022).

The vermal zone is primarily associated with control of axial musculature, including the muscles of the head, neck, and trunk. It plays a crucial role in balance, postural equilibrium, and associated reflexive motor responses. In addition to its established somatic functions, there is emerging evidence suggesting that anterior portions of the vermis may participate in modulating affective behaviours (Diedrichsen *et al*., 2019; Donnelly, 2023). The paravermal zone is more closely linked with regulation of appendicular movements, particularly those of the arms and legs. It is functionally involved in the coordination and correction of limb movements, relying heavily on proprioceptive feedback (Guell *et al*., 2018; Bostan and Strick, 2018). The lateral cerebellar hemispheres, particularly within the posterior lobes, are implicated in the modulation of executive motor functions such as motor planning, motor learning, and the formation of habitual responses. Increasingly, this region is also being recognized for its contributions to non-motor processes, including aspects of cognition, language, and emotional regulation (King *et al*., 2019; ten Donkelaar *et al*., 2020).

Each of these zones has relatively specific connections to the deep cerebellar nuclei, which serve as their principal output structures (Donnelly, 2023). These functional and anatomical relationships support the following tripartite division of cerebellar function:

2.2.5.1 Vestibulocerebellum

Comprising primarily the flocculonodular lobe and closely associated with the fastigial nucleus, this division receives input from the vestibular system and is essential for balance, gaze stabilization, and vestibulo-ocular reflexes (Guell *et al*., 2018; Bostan *et al*., 2018; King *et al*., 2019). The vestibulocerebellum is the phylogenetically oldest part of the cerebellum, often referred to as the archicerebellum. It comprises the flocculonodular lobe, including the nodulus (part of the anterior vermis) and the flocculus. This region receives its primary input from the vestibular nuclei, although like all cerebellar divisions, it also receives substantial afferent input from the inferior olivary nucleus (Guell *et al*., 2018; Donnelly, 2019).

Anatomically, the vestibulocerebellum partially overlaps with the anterior regions of the vermal zone. The Purkinje cells within this region project mainly to the fastigial nuclei, though some fibres project directly back to the vestibular nuclei, bypassing the deep cerebellar nuclei entirely (Guell *et al*., 2018; Bostan *et al*., 2018). Functionally, the vestibulocerebellum is essential for the modulation of postural tone and equilibrium in response to vestibular inputs. It plays a central role in the control of gait, balance, and reflexive eye movements. Lesions in this region are often associated with truncal ataxia, gait instability, and disturbances in the vestibulo-ocular reflex (Sarnail and Raman, 2018; King *et al*., 2019).

2.2.5.2 Spinocerebellum

The spinocerebellum comprises portions of both the vermal and paravermal zones, and receives significant afferent input from the spinal cord. These spinal afferents include proprioceptive signals, cutaneous sensory input, and analogous sensory information from the trigeminal nuclei. The vermis also receives secondary vestibular input, further integrating balance-related information (King *et al*., 2019; Diedrichsen *et al*., 2019). This division is also referred to as the paleocerebellum, reflecting its evolutionary development. Functionally, the vermal region of the spinocerebellum is primarily concerned with the regulation of muscle tone, synergistic

muscle coordination, and the postural adjustments required during ongoing, semi-automatic motor activities such as walking or running (Guell *et al*., 2018). Although such actions are consciously initiated, the cerebellum ensures their fluid and adaptive execution (Mariën and Borgatti, 2018; Guell *et al*., 2018; Donnelly, 2023). The paravermal zones are more involved in limb movement control, particularly in relation to fine-tuning of speed, force, direction, and the temporal sequencing of voluntary motor actions (Mariën and Borgatti, 2018). These areas likely operate in conjunction with the lateral hemispheres to support skilled motor performance, especially when dynamic or variable adjustments are needed (Mariën and Borgatti, 2018; King *et al*., 2019; Diedrichsen *et al*., 2019).

2.2.5.3 Pontocerebellum (Cerebrocerebellum)

The cerebrocerebellum, also known as the pontocerebellum or neocerebellum, corresponds to the lateral hemispheric zones of the cerebellum. It receives its predominant input from the cerebral cortex, especially from the prefrontal, frontal, and parietal lobes, via the corticopontine tract. These cortical fibres synapse in the pontine nuclei, from which secondary fibres project to the cerebellum through the middle cerebellar peduncle (Mariën and Borgatti, 2018; King *et al*., 2019). This division is the most evolutionarily recent and has undergone considerable expansion in concert with the growth of the cerebral hemispheres.

Functionally, the cerebrocerebellum is implicated in the planning, timing, and learning of complex motor activities, including visually guided movements, tool use, and other forms of motor memory (Bostan and Strick, 2018; Willett *et al*., 2019; Urrutia Desmaison *et al*., 2023). Recent evidence further suggests that the pontocerebellum contributes to non-motor functions, such as working memory, attention, language processing, and executive function (Rousseau *et al*., 2022). These cognitive roles are believed to emerge through cerebellar connections with prefrontal cortical areas via the dentate nucleus and thalamic relays (Rousseau *et al*., 2022; Donnelly, 2023).

Table 2.1: Functional Division of the Cerebellum

Division	Primary Function(s)	Primary Input(s)	Associated Nuclei
Vestibulocerebellum (flocculonodular lobe and adjacent portions of vermis)	Balance, equilibrium, gait, reflex eye movements	Vestibular, inf. olivary	Fastigial
Spinocerebellum (paravermal and vermal regions)	Muscle tone, control of axial (vermis), and limb (paravermal region) movements	Spinal cord, inf. olivary, vestibular, reticular	Emboliform, globose, and fastigial (with vermis)
Cerebrocerebellum or pontocerebellum (cerebellar hemispheres)	Modulation, memory of skilled motor, and voluntary eye movements	Cerebral cortex (via pontine n.), inf. Olivary	Dentate

2.2.5 Development of The Cerebellum

The hindbrain, or rhombencephalon, represents the most caudal segment of the embryonic brain and gives rise to several key structures, including the cerebellum (Badura *et al*., 2018). During early development, the hindbrain undergoes segmentation into a series of transient, bilaterally symmetrical bulges known as rhombomeres. These eight rhombomeres (Rh1–Rh8) serve as fundamental patterning units that guide the spatial and functional organization of neural structures (Rahimi-Balaei *et al*., 2018; Badura *et al*., 2018). The cerebellum specifically originates from the dorsal aspect (alar plate) of the neural tube and emerges from two key regions: rhombomere 1 (Rh1) caudally and the isthmic organizer rostrally, at the midbrain–hindbrain boundary (Badura *et al*., 2018; Van Essen *et al*., 2018). These domains coordinate

developmental signaling that delineates cerebellar identity within the broader architecture of the neural tube (Van Essen *et al*., 2018)

Two distinct neurogenic zones give rise to the major neuronal populations of the cerebellum:

- **The Ventricular Zone:**

  Located in the roof of the fourth ventricle, this zone originates from the neuroepithelium of the alar plate and generates GABAergic inhibitory neurons, including Purkinje cells and neurons of the deep cerebellar nuclei—the principal output elements of the cerebellar cortex and the cerebellum as a whole (Van Essen *et al*., 2018; Rahimi-Balaei *et al*., 2018). These cells form the backbone of cerebellar circuitry responsible for integrating and modulating motor commands (Rahimi-Balaei *et al*., 2018).

- **The Rhombic Lip:**

  Situated at the dorsolateral margin of the fourth ventricle, the rhombic lip is a secondary germinal zone that gives rise to glutamatergic excitatory neurons, including granule cells, unipolar brush cells, and large projection neurons of the cerebellar nuclei (Rahimi-Balaei *et al*., 2018; Badura *et al*., 2018). These cells migrate extensively during development and play essential roles in forming the layered cerebellar cortex and establishing long-range cerebellar connections (Badura *et al*., 2018).

The distinction between these two germinal sources is not only anatomical but also neurochemical: neurons derived from the ventricular zone are predominantly GABAergic, whereas those from the rhombic lip are mainly glutamatergic. This dichotomy underpins the functional diversity of cerebellar microcircuits and reflects the evolutionary specialization of cerebellar processing (Badura *et al*., 2018).

2.2.6 Arterial Supply and Venous Drainage of the Cerebellum

The cerebellum receives its vascular supply from three principal arteries, which originate from the vertebrobasilar system. These arteries ensure perfusion to distinct cerebellar territories and also contribute to the blood supply of associated brainstem and ventricular structures (Błaszczyk *et al*., 2024).

- ***Superior Cerebellar Artery (SCA):***

  The SCA arises bilaterally from the distal portion of the basilar artery, immediately inferior to the origin of cranial nerve III (oculomotor nerve). It courses dorsally around the midbrain and supplies the superior aspect of the cerebellar hemispheres, superior vermis, superior medullary velum, portions of the pons, and occasionally the pineal gland (Martirosyan *et al*., 2011). Its precise perfusion territory makes it vital for maintaining the functional integrity of the cerebellar cortex and brainstem interface (Miao *et al*., 2020; Arslan *et al*., 2018).

- ***Anterior Inferior Cerebellar Artery (AICA):***

  The AICA arises from the basilar artery at the pontomedullary junction, typically just inferior to cranial nerve VI (abducens nerve). It courses laterally and posteriorly to supply the anterior inferior portion of the cerebellum, particularly the flocculus, middle cerebellar peduncle, and adjacent portions of the pons (Scremin, 2015). Due to its proximity to cranial nerve VII (facial nerve), vascular compromise in this region is often associated with neurovascular syndromes involving cranial nerves (Tripathi and Sieber, 2019; Miao *et al*., 2020).

- ***Posterior Inferior Cerebellar Artery (PICA):***

  The PICA typically arises from the vertebral artery proximal to its junction with the basilar artery, usually just superior to the rootlets of cranial nerve XI (accessory nerve). It is the largest and most variable of the cerebellar arteries and supplies the posterior

inferior surface of the cerebellum, including the inferior vermis and deep cerebellar nuclei (Tatu *et al*., 2012). It also perfuses the dorsolateral medulla, thus its involvement is commonly associated with Wallenberg syndrome (Arslan *et al*., 2018; Tripathi *et al*., 2019).

Venous outflow from the cerebellum is coordinated by an intricate network of superficial and deep cerebellar veins that collectively form the cerebellar venous system (Blaszczyk *et al.*, 2024). This system plays a critical role in maintaining intracranial venous homeostasis by channeling blood efficiently into the major dural venous sinuses (Arslan *et al*., 2018; Miao *et al.*, 2020). The superficial venous system includes the superior cerebellar veins, which drain the dorsal cerebellar surface and empty predominantly into the straight sinus and superior petrosal sinus (Miao *et al.*, 2020). The posterior inferior cerebellar veins drain the inferior aspects of the cerebellum, directing blood toward the transverse and occipital sinuses (Miao *et al.*, 2020).

In addition to these superficial pathways, deep cerebellar structures also contribute venous return through connections with the great cerebral vein (vein of Galen), thereby linking infratentorial drainage with supratentorial venous circuits (Miao *et al.*, 2020; Blaszczyk *et al.*, 2024). This hierarchical venous architecture not only ensures efficient removal of metabolic byproducts but also provides functional redundancy, allowing bidirectional communication between different venous territories (Arslan *et al*., 2018). Disturbances in this system—such as venous sinus thrombosis or compression—can compromise drainage, leading to cerebellar congestion, edema, and in severe cases, venous infarction, all of which significantly impair cerebellar function (Blaszczyk *et al.*, 2024).

2.3 CEREBELLAR DISORDERS

Cerebellar disorders constitute a diverse spectrum of neurological conditions resulting from dysfunction or structural damage to the cerebellum—a region of the brain fundamentally involved in the coordination, precision, and temporal regulation of movement (Grimaldi, 2021; Joshua *et al*., 2022). Given its central role in integrating sensory input with motor commands, the cerebellum is essential for both gross motor functions such as gait and balance, and fine motor skills, including tasks like handwriting or speech articulation (Sathyanesan *et al*., 2019).

Damage to the cerebellum disrupts the cerebellar circuits that underlie sensorimotor integration and feedforward control, resulting in deficits in movement accuracy, timing, and adaptability (Grimaldi, 2021). Furthermore, growing evidence has expanded our understanding of the cerebellum's role beyond motor control, implicating it in a range of cognitive and affective processes. Consequently, cerebellar pathology can lead to both motor and non-motor dysfunctions, often with a profound impact on an individual's daily functioning and overall quality of life (Sathyanesan *et al*., 2019; Grimaldi, 2021).

2.3.1 Ataxia and Associated Cerebellar Motor Disorders

Ataxia is the hallmark motor manifestation of cerebellar dysfunction and broadly refers to impairments in the coordination and execution of voluntary movements. It reflects deficits in the timing, force, amplitude, and direction of movement, resulting in poor balance, instability, and imprecise motor control (Sathyanesan *et al*., 2019; D'Arrigo *et al*., 2021). Several distinct motor abnormalities commonly co-occur under the umbrella of cerebellar ataxia, each revealing different aspects of disrupted cerebellar processing (Joshua *et al*., 2022).

One key feature is dysmetria, characterized by the inability to properly scale movement amplitude. This may manifest as either overshooting (hypermetria) or undershooting (hypometria) a target. Dysmetria is particularly evident during rapid, goal-directed, or multi-

joint movements and is thought to result from impaired temporal coordination between agonist and antagonist muscle groups, as well as altered contraction timing (Joshua *et al*., 2022; Iskusnykh *et al*., 2024). Patients often display abnormal muscle co-contraction and delayed movement initiation, pointing to dysfunction in motor planning circuits involving the dentate nucleus and motor cortex (Iskusnykh *et al*., 2024). Dysmetria may also stem from difficulties in sensory prediction and movement outcome estimation.

The rebound phenomenon, or lack of check, reflects difficulty in terminating a movement after resistance is removed. It is typically demonstrated during resisted elbow flexion, where sudden release of the resistance causes an exaggerated rebound motion due to delayed antagonist muscle response (Sathyamesam *et al*., 2019; Grimaldi, 2021; Iskusnykh *et al*., 2024). Similarly, dysdiadochokinesia, the inability to perform rapid alternating movements, leads to irregular, clumsy actions, especially during repetitive tasks like tapping or forearm pronation-supination. These signs indicate a failure of the cerebellum to switch smoothly between opposing muscle groups (Grimaldi, 2021).

Intention tremor, a hallmark of cerebellar dysfunction, appears during voluntary movements and intensifies near the endpoint. Unlike the resting tremors seen in basal ganglia disorders, cerebellar tremors stem from poor timing and control during deceleration, often worsening with visual input. Some patients also exhibit postural or truncal tremor (titubation) when attempting to stay still (McCreary *et al*., 2018; Paredes-Acuna *et al*., 2024).

Dyssynergia, the disruption of multi-joint coordination, results in fragmented, stepwise movements instead of smooth, integrated actions, as seen in the heel-to-shin test. This reflects a failure to properly activate and stabilize synergistic muscle groups (Stoffel, 2016). Hypotonia, or reduced resistance to passive movement, often co-occurs and may present with pendular reflexes. While its cause is unclear, it may involve altered spinal reflexes or decreased muscle spindle sensitivity (Stephen *et al*., 2019; Joshua *et al*., 2022).

Dysarthria, another common symptom, affects the motor execution of speech. Though phoneme articulation remains intact, speech becomes slow, slurred, and scanning due to poor coordination of the oral and respiratory muscles (Tanaka *et al*., 2015; Duffy *et al*., 2018). Nystagmus, an involuntary oscillation of the eyes, reflects cerebellar-vestibular dysfunction and, in unilateral lesions, may cause the eyes to drift toward the lesion, impairing gaze stability (MacLean *et al*., 2018; Stephen *et al*., 2019).

2.3.2 Motor Performance Deficits

A hallmark of cerebellar dysfunction is ataxic gait, marked by a wide stance, irregular foot placement, reduced stride length, and instability (Pillay *et al*., 2019). These abnormalities are amplified during tandem walking, which often reveals dysmetria, mistimed steps, and variability in trajectory (Martini and Broglio, 2018; Neely *et al*., 2019; Pillay *et al*., 2019). Tandem walking is useful for both diagnosis and tracking progress in rehabilitation. Postural adjustments that normally stabilize the body during voluntary movement are often impaired in cerebellar disorders (Arumugam and Parasher, 2019). Patients struggle to maintain balance, particularly during quiet standing or when reacting to shifts in body mass. This instability arises from poor temporal coordination of muscle activity and may be worsened by vestibular or visual processing deficits (Martini and Broglio, 2018).

Tasks like rising on tiptoes highlight deficits in timing and muscle coordination. Patients often display delayed or poorly sequenced activation of key muscles such as the tibialis anterior and quadriceps, resulting in failure to complete the movement or a return to heel contact (Martini and Broglio, 2018). These patterns reflect dyssynergia—disruption of smooth muscle integration (Arumugam and Parasher, 2019). Postural sway during standing is often increased in cerebellar patients, though in some cases, such as vermal lesions, reduced sway has been observed. This suggests that lesion location affects balance strategies, though the clinical

relevance of sway remains debated due to natural variability among healthy individuals (Martini and Broglio, 2018). Upper limb movements such as reaching or tracking reveal dysmetria and poor coordination, especially during rapid actions. Patients show excessive muscle co-contraction, prolonged agonist activity, and delayed antagonist response, all contributing to instability (O'Leary *et al*., 2018; Pillary *et al*., 2019; Neely *et al*., 2019). Even during slower movements, deficits persist. In tasks like repetitive throwing, cerebellar patients struggle to maintain consistent hand trajectories and fail to adjust for joint interaction torques, indicating impaired internal models for motor prediction and control (Neely *et al*., 2019; Arumugan *et al*., 2019).

2.3.3 Aetiology of Cerebellar Disorders

Cerebellar disorders arise from a diverse array of causes and may occur as isolated conditions or as part of broader neurological or systemic diseases. These disorders can stem from structural, genetic, autoimmune, infectious, vascular, toxic, metabolic, or idiopathic origins, and may also be associated with malignancies through paraneoplastic mechanisms (Zwergal *et al*., 2020; Reumers *et al*., 2025).

- ***Structural Abnormalities:***

  One of the primary aetiologies is structural damage to the cerebellum. Such lesions may result from developmental anomalies (e.g., Arnold–Chiari malformation, Dandy–Walker syndrome), birth-related complications (e.g., hypoxia), traumatic brain injury, neoplasms, strokes, or infections such as encephalitis (Geng *et al*., 2020). Additionally, structural cerebellar involvement may occur in demyelinating conditions like multiple sclerosis, hereditary diseases such as Friedreich's ataxia, and in various degenerative, metabolic (e.g., Wilson's disease, myxoedema), vascular (e.g., vertebrobasilar

insufficiency), and toxic contexts, including drug or alcohol intoxication (Geng *et al*., 2020; Sahoo *et al*., 2022; Reumers *et al*., 2025).

- ***Genetic Factors:***

  Genetic contributions are significant in cerebellar pathology. A range of hereditary syndromes are implicated, including spinocerebellar ataxias—progressive neurodegenerative disorders marked by cerebellar degeneration. Other genetically linked conditions such as Friedreich's ataxia also leads to cerebellar dysfunction, typically following autosomal recessive or dominant inheritance patterns (Geng *et al*., 2020; Sahoo *et al*., 2022).

- ***Autoimmune Disorders:***

  Autoimmune mechanisms can similarly underlie cerebellar disorders. In these cases, aberrant immune responses target cerebellar tissue, as observed in gluten ataxia—a condition associated with celiac disease where antibodies cross-react with cerebellar antigens. This results in coordination deficits and progressive ataxia (Reumers *et al*., 2025).

- ***Infections:***

  Certain infections also have a direct cerebellar impact. Viral agents like varicella-zoster virus and Epstein–Barr virus can cause cerebellitis, an acute inflammatory condition affecting the cerebellum. Such infections often result in transient or sometimes permanent cerebellar dysfunction (Geng *et al*., 2020; Reumers *et al*., 2025).

- ***Vascular Lesions:***

  Vascular causes, including cerebellar infarctions, haemorrhages, or ischemic strokes, can compromise the cerebellum by disrupting its blood supply. Insufficient perfusion leads to neuronal injury, with both acute and chronic implications for cerebellar function (Zwergal *et al*., 2020; Sahoo *et al*., 2022).

- ***Idiopathic Causes:***

  In some cases, the underlying cause remains unknown, leading to a diagnosis of idiopathic cerebellar disorder. These instances are particularly challenging in clinical practice due to the absence of identifiable pathology and are likely influenced by multifactorial interactions that remain poorly understood (Pontillo *et al*., 2020).

- ***Paraneoplastic Syndromes:***

  Paraneoplastic cerebellar degeneration represents a rare but important aetiology, typically occurring in the context of malignancy. In these syndromes, the immune response to neoplastic antigens cross-reacts with cerebellar tissue, resulting in progressive cerebellar symptoms. Treating the underlying cancer may lead to symptom stabilization or partial recovery (Yshii *et al*., 2020; Loehrer *et al*., 2021).

- ***Toxic and Metabolic Factors:***

  Toxic and metabolic factors are well-established contributors to cerebellar damage (Penticoff and Fortin, 2023). Chronic alcohol use is notably associated with cerebellar degeneration, particularly targeting the anterior superior vermis (Hammoud and Jimenez-Shahed, 2019).

  Metabolic conditions such as Wilson's disease also affect the cerebellum through abnormal copper accumulation (Lorincz, 2018). Heavy metals, like Mercury (Hg), represent potent neurotoxins with established cerebellar effects, including ataxia and tremor (Cariccio *et al*., 2019; Ganguly *et al*., 2022).

2.4 MERCURY

Mercury (Hg) is a naturally occurring heavy metal ubiquitously distributed across the environment, posing a substantial global public health concern (Basu, 2023). Its widespread presence means that all human beings are routinely exposed to certain quantities of mercury, ranging from low background levels to higher concentrations in specific contexts (Wu *et al*., 2024). This pervasive exposure, even at low levels, can induce molecular, cellular, developmental, and behavioural alterations in various organisms, including humans (Basu, 2023; Wu *et al*., 2024). The World Health Organization (WHO) recognizes mercury as one of the top ten chemicals of major public health concern, and chronic mercury poisoning holds the distinction of being one of the oldest occupational diseases (WHO, 2024). The constant, low-level background exposure for the general population implies that the cumulative effect over a lifetime or during critical developmental windows could have widespread, subtle, and potentially under-recognized neurotoxic consequences across populations, extending beyond acute poisoning incidents (Basu, 2023; WHO, 2024; Wu *et al*., 2024). Mercury exists in several distinct chemical forms: elemental (metallic) mercury (Hg), inorganic mercury compounds (e.g., mercuric chloride, $HgCl_2$, or Hg^{2+}), and organic mercury compounds (e.g., methylmercury, MeHg) (Kalisińska *et al*., 2019; Wu *et al*., 2024).

2.4.1 Human Exposure to Mercury

Mercury (Hg) remains a significant public health concern due to its widespread environmental presence and persistence. Human exposure occurs primarily through anthropogenic activities that release mercury into the atmosphere and aquatic systems (Calao-Ramos *et al*., 2021). According to the Global Mercury Assessment (GMA) 2018 conducted by the United Nations Environment Programme (UNEP), the major sources of global mercury emissions include artisanal and small-scale gold mining (ASGM), accounting for 37.7% of total emissions;

stationary combustion of fossil fuels and biomass (21%); non-ferrous metal production (15%); and cement production (11%) (UNEP, 2019).

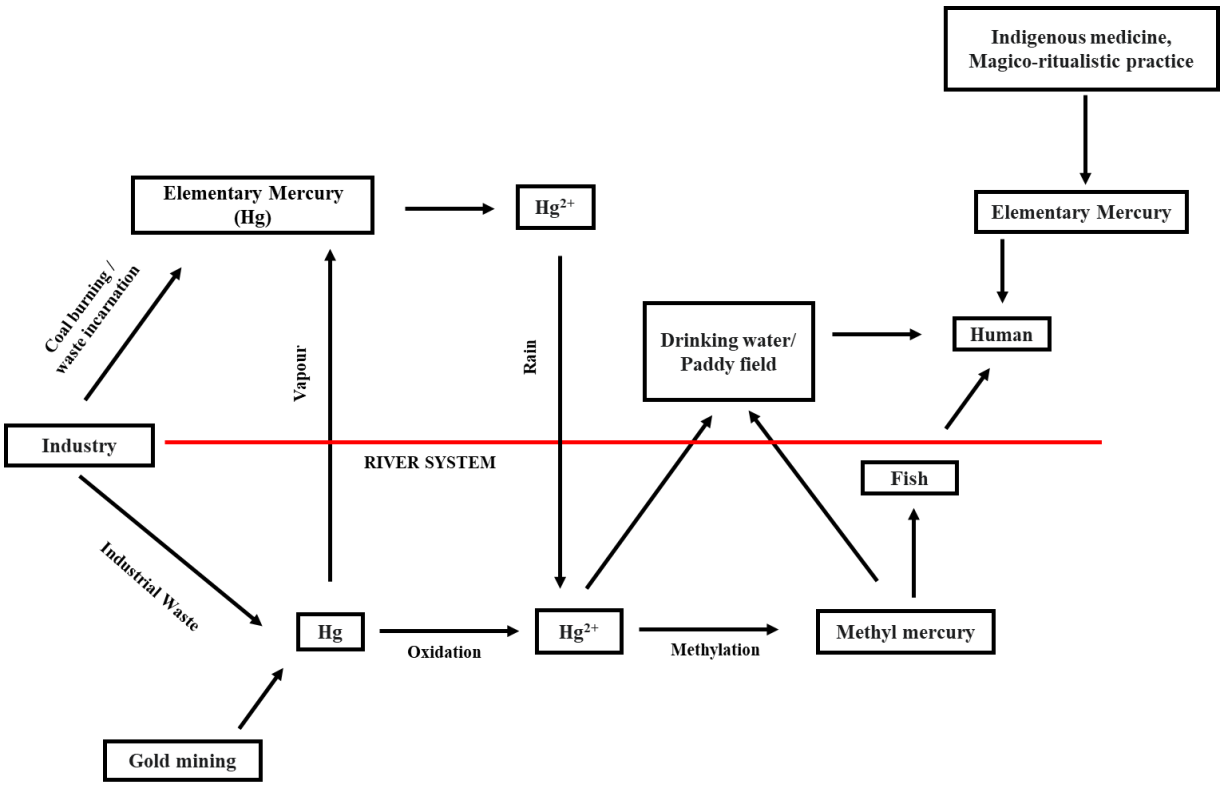

Figure 2.3: Human exposure to elemental and Organic Mercury

ASGM is particularly hazardous, as it employs mercury to form amalgams with gold. This process releases mercury vapors when the amalgam is heated, resulting in significant inhalational exposure among workers and surrounding communities (Henriques *et al.*, 2019). Additionally, elemental mercury released into water bodies undergoes microbial methylation, forming methylmercury, a highly bioavailable and toxic organic form (Zulaikhah *et al.*, 2020; Calao-Ramos *et al.*, 2021). Methylmercury accumulates in aquatic organisms and magnifies through the food chain, making dietary intake—especially through fish and seafood—a primary route of exposure for the general population (Calao-Ramos *et al.*, 2021).

Occupational exposure remains a concern not only in mining but also in sectors such as chlor-alkali production, dentistry, and manufacturing involving electrical components and

fluorescent lighting. In many developing regions, inadequate regulation and safety practices further exacerbate mercury exposure risks in these environments (Vianna *et al*., 2019; Calao-Ramos *et al*., 2021). Environmental contamination from mercury also contributes to indirect exposure via soil, air, and water. Communities living near industrial sites or mercury-contaminated ecosystems are particularly vulnerable. Inhalation of mercury vapor, ingestion of contaminated food or water, and dermal contact represent key pathways through which mercury enters the human body (Henriques *et al*., 2019; Zulaikhah *et al*., 2020; Calao-Ramos *et al*., 2021).

2.4.2 Toxicokinetics and Exposure Pathways of Mercuric Chloride

The toxicokinetics of mercuric chloride ($HgCl_2$), an inorganic mercury compound, dictate its absorption, distribution, metabolism, and excretion within the body, profoundly influencing its neurotoxic potential. The predominant route of human exposure for $HgCl_2$ is ingestion (Cappelletti *et al*., 2019; Zulaikhah *et al*., 2020). Upon oral intake, approximately 7% to 15% of the ingested dose is absorbed through the gastrointestinal tract (Cappelletti *et al*., 2019). While less common, dermal absorption is also a documented pathway, particularly from historical or illicit topical applications of ointments containing inorganic mercury salts (Zhao *et al*., 2022; Zhao *et al*., 2025). Inhalation of inorganic mercury salts is rare, as these compounds are typically non-volatile solids at ambient temperatures (Cappelletti *et al*., 2019; Zhao *et al*., 2022).

Once absorbed, inorganic mercury is distributed systemically to all tissues. However, it preferentially accumulates in the kidneys, which are recognized as a major target organ for inorganic mercury toxicity (Zulaikhah *et al*., 2020; Zhao *et al*., 2025). Within the kidney, the proximal tubule is the primary site of mercuric ion uptake and accumulation (Zhao *et al*., 2025). Intracellularly, Hg^{2+} exhibits a strong and detrimental affinity for endogenous biomolecules

containing thiol (-SH) groups. This includes essential proteins, small molecular weight peptides such as glutathione, and amino acids like cysteine (Zulaikhah *et al*., 2020). This binding disrupts critical metabolic processes, inhibits enzymatic activities, and interferes with normal cellular functions and detoxification pathways (Cappelletti *et al*., 2019; Zhao *et al*., 2022; Zhao *et al*., 2025).

$HgCl_2$ has a poor lipid solubility, hence, only a small fraction of inorganic mercury readily crosses the blood-brain barrier (BBB) and the placental barrier (Gu *et al*., 2023; Auza *et al*., 2024). Despite this limited permeability, multiple studies have unequivocally demonstrated that inorganic mercury (Hg^{2+}) can reach the brain and accumulate there, leading to neurotoxic effects (Auza *et al*., 2024; Zhao *et al*., 2025). This observation highlights a critical aspect: while the initial rate and quantity of $HgCl_2$ crossing the BBB may be lower compared to highly lipid-soluble forms, the cumulative accumulation over time, even of small amounts, is sufficient to induce significant neurotoxicity. This is particularly critical for the immature brain, which exhibits heightened susceptibility (Gu *et al*., 2023). The poor lipid solubility might indicate that alternative, perhaps slower, transport mechanisms (e.g., specific ion channels, transporters, or even subtle disruptions of BBB integrity under chronic exposure) facilitate its brain uptake, allowing for persistent accumulation. This implies that even chronic, low-level exposure to inorganic mercury, despite its perceived limited BBB permeability, can still pose a substantial neurological risk, especially for vulnerable populations, necessitating careful long-term monitoring (Cappelletti *et al*., 2019; Auza *et al*., 2024).

Excretion of $HgCl_2$ predominantly occurs through urine and faeces (Parida and Patel, 2023; Uddin *et al*., 2023). The excretion rate is typically biphasic, characterized by an initial rapid phase followed by a slower, more prolonged elimination. The biological half-life of inorganic mercury is estimated to be approximately 60 days (Uddin *et al*., 2023). Urinary mercury is considered an ideal biomarker for assessing long-term exposure to inorganic mercury and

serves as a reliable indicator of the overall body burden (Parida and Patel, 2023). Given the kidney's prominent role as a major target organ and primary excretion route for inorganic mercury, monitoring renal health and urinary mercury levels is not solely for assessing kidney damage but also functions as a crucial indirect biomarker for the overall systemic inorganic mercury burden. This systemic burden, even if only a small fraction ultimately reaches the brain, is indicative of potential neurological risk, particularly when considering the immature brain's heightened susceptibility (Parida and Patel, 2023; Uddin *et al*., 2023; Auza *et al*., 2024).

2.4.3 Mechanisms of Neurotoxicity

The neurotoxic effects of $HgCl_2$ are mediated by a complex interplay of cellular and molecular mechanisms, primarily centred around oxidative stress, disruption of protein function, and damage to critical organelles.

2.4.3.1 Oxidative Stress

Oxidative stress is widely recognized as a predominant mechanistic pathway in mercury neurotoxicity (Antunes dos Santos *et al*., 2018; Farina and Aschner, 2019; Novo *et al*., 2021). $HgCl_2$ exposure in animal models, such as rats, consistently leads to a significant increase in lipid peroxidation, as evidenced by elevated levels of thiobarbituric acid reactive substances (TBARS) and malondialdehyde (MDA) (Jalili *et al*., 2021; Naraki *et al*., 2025). This indicates extensive damage to cellular membranes. Concurrently, $HgCl_2$ treatment results in a significant decrease in the levels of reduced glutathione (GSH), a crucial endogenous antioxidant that plays a vital role in cellular defense against oxidative damage (Raeeszadeh *et al*., 2021; Naraki *et al*., 2025).

Furthermore, $HgCl_2$ profoundly alters the activity of key antioxidant enzymes. Studies show a significant decrease in the enzymatic activity of superoxide dismutase (SOD), catalase (CAT), and glutathione peroxidase (GPx) (Aysin *et al*., 2020; Raeeszadeh *et al*., 2021). Conversely,

there is a significant increase in glutathione reductase (GR) levels (Raeeszadeh *et al*., 2021; Naraki *et al*., 2025). This imbalance in the antioxidant defense system leads to an exacerbated production of reactive oxygen species (ROS) (Naraki *et al*., 2025). Brain tissues are particularly vulnerable to oxidative damage due to their high metabolic rate, elevated oxygen consumption, and relatively lower antioxidant capacity compared to other organs (Aysin *et al*., 2020; Jalili *et al*., 2021; Naraki *et al*., 2025). The reaction of mercury with glutathione peroxidase, specifically via thiol and/or selenol groups, further impairs this critical enzyme (Jalili *et al*., 2021; Naraki *et al*., 2025).

2.4.3.2 Protein and Enzyme Disruption

A fundamental aspect of $HgCl_2$ toxicity stems from its strong affinity for endogenous biomolecules containing thiol (-SH) groups (Perrone *et al*., 2023). This includes a wide array of essential proteins, small molecular weight peptides like glutathione, and amino acids such as cysteine (Piscopo *et al*., 2020; Perrone *et al*., 2023). This robust binding disrupts critical metabolic processes and can profoundly alter the structure and function of numerous proteins (Jha *et al*., 2019; Piscopo *et al*., 2020). Beyond thiol interactions, mercury also causes irreversible inhibition of selenoenzymes, such as thioredoxin reductase, which are vital for regenerating reduced forms of vitamins C and E and other important antioxidant molecules (Piscopo *et al*., 2020). The depletion of cellular selenium and selenoproteins further compromises the body's intrinsic antioxidant defenses against mercury-induced damage (Aysin *et al*., 2020; Perrone *et al*., 2023). The binding to thiol groups appears to be a foundational event that triggers a cascade of downstream cellular damage, including oxidative stress, mitochondrial dysfunction, and changes in antioxidant enzyme activities.

2.4.3.3 Mitochondrial Dysfunction, Apoptosis, and Endoplasmic Reticulum Stress

Heavy metals, including mercury, induce cytotoxicity through a complex and interconnected network of molecular mechanisms, prominently featuring oxidative stress, mitochondrial

dysfunction, apoptosis (programmed cell death), and endoplasmic reticulum (ER) stress (Rojas-Franco *et al*., 2019; Gao *et al*., 2023). Mercury exposure leads to a deterioration of mitochondrial quality and function, thereby impairing cellular energy production (Rojas-Franco *et al*., 2019; Gao *et al*., 2023). The disruption of intracellular calcium homeostasis, often intricately linked to mitochondrial dysfunction, can trigger apoptosis in cells, ultimately leading to neurodegenerative damage (Rojas-Franco *et al*., 2019). Histological observations in animal models reveal that $HgCl_2$ can induce fragmentation of the rough endoplasmic reticulum and ballooning of the Golgi apparatus, clear indicators of significant cellular stress (Van Noorden *et al*., 2005; Rojas-Franco *et al*., 2019; Gao *et al*., 2023). This implies a cascading effect where initial damage in one pathway (e.g., excessive ROS production) rapidly propagates and exacerbates dysfunction in others (e.g., mitochondrial impairment), thereby amplifying cellular injury.

2.4.3.4 Impact on Neurotrophic Factors and Neuroinflammation

Brain-Derived Neurotrophic Factor (BDNF) plays a crucial role in neuronal survival, growth, neurotransmitter modulation, and neuronal plasticity—all essential for learning and memory (Said *et al*., 2021). Mercury-induced BDNF expression in astrocytes has been observed to protect neurons against metal toxicity (Corrêa *et al*., 2020; Said *et al*., 2021). Mercury-induced inhibition of neurodifferentiation and neurogenesis is mechanistically associated with epigenetic alterations in critical genes, including BDNF (Kang *et al*., 2024). While astrocytes may upregulate BDNF as an acute or compensatory protective response at certain exposure levels, chronic or specific mercury exposures can lead to epigenetic alterations in BDNF genes, potentially impairing the long-term function or expression of BDNF, which is crucial for ongoing neurodevelopment and neurogenesis. Beyond direct cellular damage, previous studies report the modulation of the neuroimmune system, including the selective release of

inflammatory mediators in the CNS, as a significant mechanism of mercury neurotoxicity (Corrêa *et al*., 2020; Said *et al*., 2021; Kang *et al*., 2024).

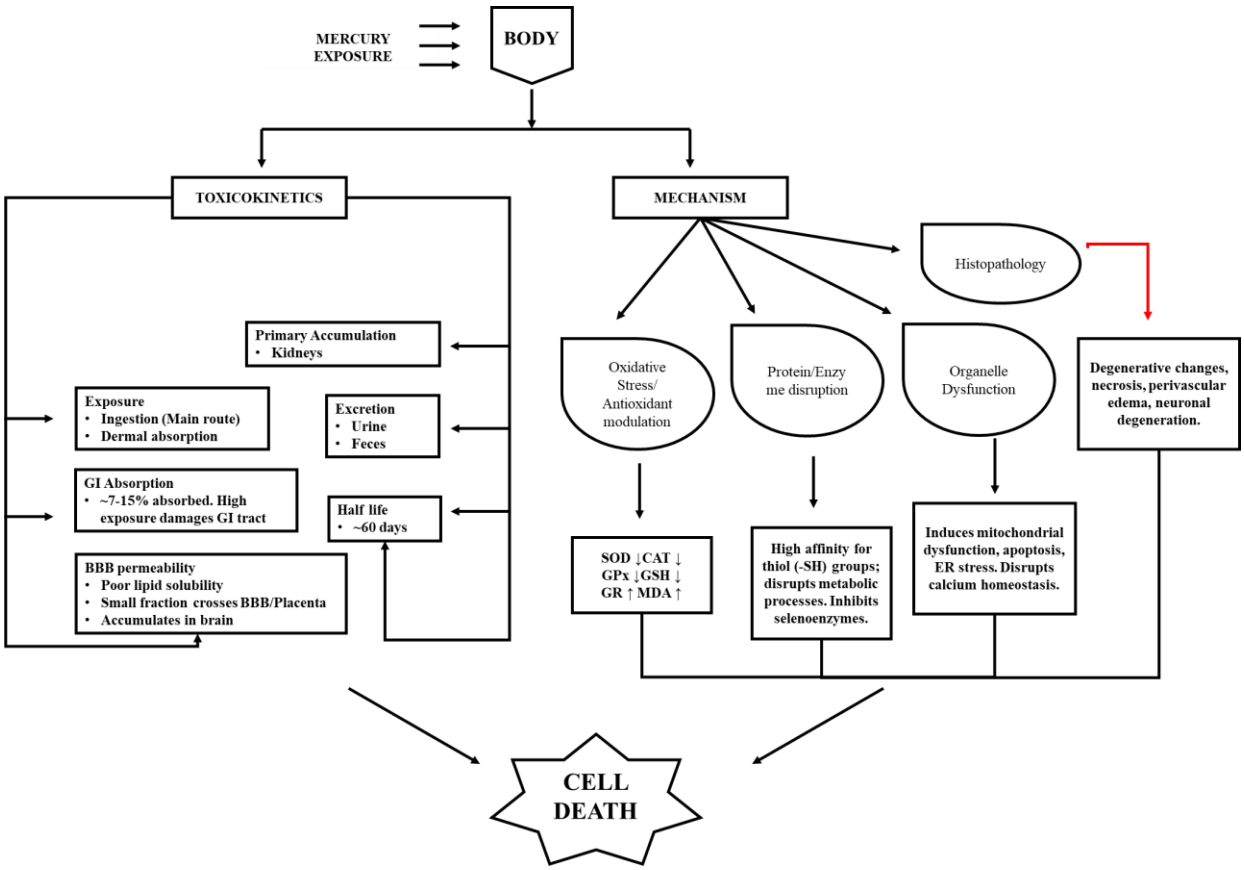

Figure 2.4: Toxicokinetics and Cellular Mechanisms of Mercury neurotoxicity

2.4.4 Effect of Hg on the Cerebellum

The cerebellum exhibits a pronounced vulnerability to mercury toxicity, a susceptibility primarily attributed to its elevated metabolic rate and inherent sensitivity to oxidative stress. Mercury, in its various forms including methylmercury (MeHg) and inorganic mercury, readily traverses the blood-brain barrier, thereby exerting deleterious effects on both cerebellar structure and function.

Developmental exposure to mercury is particularly insidious, as evidenced by studies demonstrating irreversible cognitive and motor deficits. Farina *et al*. (2012) reported that maternal consumption of contaminated fish, leading to developmental Hg exposure, precisely

targets the cerebellum. Their research elucidated oxidative stress as a primary mechanism of damage, characterized by reduced glutathione levels and inhibition of crucial antioxidant enzymes such as glutathione peroxidase (GPx) and glutathione reductase (GR). Further substantiating this, Ceccatelli *et al*. (2010) demonstrated that Hg exposure induces apoptosis in developing cerebellar neurons, particularly granule cells. These apoptotic events were intimately linked to caspase activation and profound mitochondrial dysfunction. The enduring impact of in utero mercury exposure on cerebellar development was further underscored by Hematian (2013), who observed a dose-dependent reduction in the thickness of cerebellar grey and white matter, along with a decrease in cellular density within these layers in the offspring of pregnant rats exposed to mercuric oxide.

In the adult brain, inorganic mercury, commonly encountered as mercury vapor, also exerts significant neurotoxicity. Altunkaynak *et al*. (2019) reported a significant reduction in cerebellar volume and Purkinje cell numbers following mercury vapor exposure. Histological analyses revealed severe cellular damage, including the presence of pyknotic nuclei and vacuolization. These findings were corroborated by Sørensen *et al*. (2000), who observed a 12.7% loss of Purkinje cells and a 15.6% loss of granule cells in rats exposed to mercury vapor. Importantly, their comparative analysis indicated distinct toxicity profiles between mercury vapor and MeHg, with inorganic mercury demonstrating a more pronounced central nervous system (CNS) focus.

Bittencourt *et al*. (2021) utilized proteomic analysis to investigate long-term inorganic mercury exposure, revealing increased cerebellar mercury levels, oxidative stress, and mitochondrial dysfunction. Altered expression of proteins critical for synaptic transmission and energy metabolism suggested a progression towards neurodegeneration. Warfvinge (2000) provided crucial insights into mercury accumulation patterns, identifying its presence in Purkinje cells, Bergmann glia, Golgi cells, and granule cells in both neonatal and adult monkey brains, with

the cerebellar nuclei exhibiting the highest concentrations. This consistent accumulation pattern across developmental stages points to similar uptake mechanisms despite varying age-related vulnerabilities.

The predominant mechanisms underlying mercury-induced cerebellar damage appear to be oxidative stress and apoptosis. Early evidence by Chang and Hartmann (1972) demonstrated that mercury impairs RNA and protein synthesis in neurons, with cerebellar granule cells exhibiting particular sensitivity. Farina *et al*. (2012) highlighted the disruption of redox homeostasis via MeHg's interaction with sulfhydryl groups on glutathione, culminating in excessive reactive oxygen species (ROS) accumulation. Sumathi *et al*. (2012) further confirmed that MeHg exposure inhibits key antioxidant enzymes such as superoxide dismutase (SOD), catalase (CAT), and GPx. Bittencourt *et al*. (2021) reinforced these mechanistic findings with proteomic data, unequivocally demonstrating that oxidative stress, mitochondrial dysfunction, and apoptosis collectively contribute to cerebellar degeneration.

The histological and molecular damage observed in the cerebellum has direct functional consequences, notably impairing motor functions. Enogieru and Inneh (2022) reported significant motor deficits in mercury-exposed rats, including impaired locomotion and reduced exploratory behavior, which correlated with the degeneration of Purkinje cells. Animoku *et al*. (2019) similarly observed necrosis, vacuolation, and disorientation of Purkinje cells in the cerebellum of mercury-exposed rats, changes that were directly linked to deficits in motor performance.

Table 2.2: Effect of Mercury on the cerebellum

Mercury Type & Dosage	Duration	Model of Study	Histopathological Findings	Mechanism of Action	Reference
Methylmercury (low dose, maternal fish consumption)	Gestational	Humans (epidemiological)	Cognitive/motor deficits, cerebellum as primary target	Oxidative stress, reduced glutathione, GPx, GR	Farina *et al.* (2012)
Methylmercury	Acute (*in vitro*)	Cerebellar cell culture	Apoptosis of granule neurons	Caspase activation, mitochondrial dysfunction	Ceccatelli *et al*. (2010)
Mercuric oxide (unspecified)	Gestation	Pregnant rats	Reduced thickness of cerebellar layers, decreased cell numbers	Oxidative stress	Hematian *et al*. (2013)
Mercury vapor	Sub-chronic	Adult rats	Reduced cerebellar volume, pyknotic Purkinje cells, vacuolization	Oxidative stress, neurodegeneration	Altunkaynak *et al*. (2018)
Mercury vapor	11 weeks	Adult rats	12.7% Purkinje cell loss, 15.6% granule cell loss	Neuronal toxicity	Sørensen *et al*. (2000)
Inorganic mercury	Chronic	Adult rats	Increased Hg in cerebellum, altered protein expression, mitochondrial dysfunction	Oxidative stress, apoptosis, synaptic disruption	Bittencourt *et al*. (2021)
Methylmercury (unspecified)	Prenatal	Pregnant monkeys	Accumulation in Purkinje cells, Golgi cells, granule cells	Transplacental uptake, cellular toxicity	Warfvinge (2000)
Mercury chloride (unspecified)	Acute	Animal (unspecified)	RNA/protein synthesis inhibition, granule cell loss	Oxidative damage, transcription inhibition	Chang and Hartmann (1972)
Methylmercury + antioxidant	4 weeks	Adult rats	Reduced SOD, CAT, GPx; improvement with *Bacopa monniera*	Antioxidant depletion, ROS accumulation	Sumathi *et al*. (2012)
Methylmercury (unspecified)	30 days	Adult rats	Degeneration of Purkinje cells, motor coordination deficit	Neurotoxicity linked to structural cerebellar damage	Enogieru and Inneh (2022)
Mercury (unspecified)	28 days	Adult rats	Necrosis, vacuolation, Purkinje cell disorientation; improvement with ascorbic acid	Oxidative stress, antioxidant protection	Sule *et al*. (2021)

2.4.5 Current Treatment Options for Cerebellar Disorders and Hg Toxicity

Effective treatment for cerebellar disorders involves an integrated strategy. Pharmacological interventions primarily modulate neurotransmitter systems: dopaminergic agents (e.g., levodopa) restore dopamine balance, while GABA-enhancing drugs (e.g., benzodiazepines, baclofen) alleviate symptoms like spasticity (Nimgampalle *et al*., 2023). Additional drugs include anticholinergics (e.g., trihexyphenidyl) for tremor and rigidity (LeWitt *et al*., 2024), beta-blockers (e.g., propranolol) for intention tremors (Frei and Truong, 2022), and anticonvulsants (e.g., phenytoin) for seizures. NMDA receptor modulators (e.g., memantine) offer neuroprotection (LeWitt *et al*., 2024), and immunosuppressants (e.g., corticosteroids) may be used for autoimmune causes (Frei and Truong, 2022).

For heavy metal neurotoxicity, especially mercury (Hg), treatment focuses on reducing the body's metal burden. Chelation therapy, using agents like DMSA, facilitates metal excretion. However, caution is needed due to potential side effects (Kim *et al*., 2019). Nutritional interventions are also crucial: calcium supplementation inhibits Hg absorption (Kim *et al*., 2019), and a diet rich in iron, zinc, and vitamin C aids detoxification (Flora *et al*., 2022).

Antioxidants are vital in counteracting oxidative stress from heavy metals. Hg elevate ROS, causing neuronal damage (Cariccio *et al*., 2019). Vitamins C and E neutralize ROS, protecting neural tissue (Cariccio *et al*., 2019). Heavy metals disrupt mitochondrial function, leading to cell death (Sun *et al*., 2022). Antioxidants help restore mitochondrial function and cellular balance. Notably, alpha-lipoic acid has both antioxidative and mild chelating properties, enhancing its neuroprotective effects (Sun *et al*., 2022). Naturally-derived antioxidants are also gaining recognition for their role in mitigating metal toxicity.

2.5 *Pleurotus ostreatus*

Pleurotus ostreatus, commonly known as the oyster mushroom, is among the most widely cultivated edible fungi globally. It ranks as the second most commercially produced mushroom worldwide (Effiong *et al*., 2024).

Figure 2.5: Image showing *Pleurotus ostreatus* [Oyster mushroom] (Majesty *et al*., 2019)

2.5.1 Botanical and Organoleptic Characteristics

The basidiocarp of *Pleurotus ostreatus* typically presents with a broad, reniform to infundibuliform pileus, ranging in diameter from 2 to 30 cm. Natural specimens exhibit a chromatic spectrum from albescent to argenteous or fulvous to fuscous. The pileus margin is characteristically involute in juvenile stages, subsequently becoming smooth and frequently undulate or lobed (Majesty *et al*., 2019; Effiong *et al*., 2024). The context (flesh) is pallid, firm, and exhibits variable thickness contingent upon the stipe's arrangement. The lamellae are adnate to decurrent, ranging in color from white to cream. In instances where a stipe is present, the lamellae descend along its length. The stipe, if manifest, is typically eccentric with a lateral attachment to the substratum (Vlasenko and Kuznetsova, 2020). The resultant sporaprint is albescent to lilac-grey, optimally observed against a dark background for enhanced contrast.

The stipe of *P. ostreatus* is frequently rudimentary or absent; when present, it is characterized by a short, robust morphology. A distinctive organoleptic attribute is the presence of a bittersweet aroma, attributable to benzaldehyde, a compound also characteristic of bitter almonds (Semenova *et al*., 2023; Effiong *et al*., 2024).

2.5.2 Nomenclature and Etymology

Both the binomial Latin and vernacular appellations for *P. ostreatus* directly reference the morphology of its fruiting body (Seethapathy *et al*., 2023). The genus epithet *Pleurotus*, derived from Greek, signifies "side-ear," alluding to the characteristic lateral growth of the stipe relative to the pileus (Seethapathy *et al*., 2023; Effiong *et al*., 2024). The specific epithet *ostreatus*, alongside the common English name "oyster mushroom," refers to the pileus's resemblance to the eponymous bivalve mollusc (Li *et al*., 2019). An alternative etymological hypothesis suggests the "oyster" descriptor may also originate from the mushroom's characteristic lubricous texture. The common name "grey oyster mushroom" is frequently employed to denote *P. ostreatus* (Majesty *et al*., 2019; Semenova *et al*., 2023; Seethapathy).

Table 2.3: Scientific Classification of *Pleurotus ostreatus*

Domain	Eukaryota
Kingdom:	Fungi
Division:	Basidiomycota
Class:	Agaricomycetes
Order:	Agaricales
Family:	Pleurotaceae
Genus:	*Pleurotus*
Species:	*Ostreatsus*
Scientific name:	*Pleurotus ostreatus*

2.5.3 Distribution, Habitat and Ecology

The oyster mushroom is widespread in many temperate and subtropical forests throughout the world, although it is absent from the Pacific Northwest of North America, being replaced by P. pulmonarius and P. populinus. It is a saprotroph that acts as a primary decomposer of wood, especially deciduous trees, and beech trees in particular. It is a white-rot wood-decay fungus (González *et al*., 2021). The standard oyster mushroom can grow in many places, but some other related species, such as the branched oyster mushroom, grow only on trees. While this mushroom is often seen growing on dying hardwood trees, it only appears to be acting saprophytically, rather than parasitically (Ackay *et al*., 2023). As the tree dies of other causes, *P. ostreatus* grows on the rapidly increasing mass of dead and dying wood. They actually benefit the forest by decomposing the dead wood, returning vital elements and minerals to the ecosystem in a form usable to other plants and organisms (Fufa *et al*., 2021; Muswati *et al*., 2021). Oyster mushrooms bioaccumulate lithium. Although predatory behavior on nematodes has evolved independently in all major fungal lineages, *P. ostreatus* is one of the few known carnivorous mushrooms. Its mycelia can kill and digest nematodes, which is believed to be a way in which the mushroom obtains nitrogen (Akcay *et al*., 2023; Effiong *et al*., 2024; Zhao *et al*., 2024).

2.5.4 Traditional Uses

In ethnomedicine, *Pleurotus ostreatus* is primarily valued as a nutritious edible mushroom, but it also holds medicinal significance in some cultures. Documented ethnographic surveys indicate that *P. ostreatus* are incorporated into traditional remedies by various West African communities. For example, in Nigeria among the Igala people, the “Pearl oyster” (*P. ostreatus*) is eaten as a healthful food and employed topically or orally as a folk medicine (Johnson Afolabi *et al*., 2024). Igala informants report using *P. ostreatus* to treat asthma and respiratory

complaints, heal skin wounds and burns, and to manage hypertension (Johnson Afolabi *et al*., 2024; Ojone and Ayodele, 2025).

Elsewhere in Africa, *Pleurotus* mushrooms (notably wild species like P. tuber-regium) are traditionally used to treat fevers, coughs, gastrointestinal disorders and pain, suggesting a shared cultural appreciation of oyster-type mushrooms in folk medicine (Fernandes *et al*., 2021; Adetunji *et al*., 2022; Johnson Afolabi *et al*., 2024). Although specific records of *P. ostreatus* per se are limited, its properties are consistent with these practices. Ethnomycological compilations note that *P. ostreatus* and related *Pleurotus* species are reputed to possess antimicrobial activity and to bolster general wellness (Adetunji *et al*., 2022; Ojone and Ayodele, 2025).

2.5.5 Pharmacological activities

While *Pleurotus ostreatus* is widely recognized for its culinary value, it has also been reported to possess notable pharmacological properties and potential health-promoting effects. These include the following:

2.5.5.1 Antibacterial and Antimicrobial Activities

Pleurotus ostreatus has been consistently recognized for its significant and broad-spectrum antibacterial properties, extending beyond simple inhibition to encompass complex immunomodulatory effects. A study by Elhusseiny *et al*. (2021) highlighted the isolation of a crucial β-D-glucan, known as pleuran, from the fruiting bodies of *P. ostreatus*. This specific polysaccharide demonstrated a remarkable ability to enhance survival rates in murine models subjected to bacterial challenges, suggesting its role in fortifying host defense mechanisms. The antibacterial effects of *P. ostreatus* are indeed multifactorial, stemming from a synergistic interplay of various bioactive compounds. β-glucans, such as pleuran, are potent biological response modifiers. Their mechanism of action primarily involves the activation of innate

immune cells, including macrophages, neutrophils, and natural killer (NK) cells, through specific pattern recognition receptors like Dectin-1 and Toll-like receptors (TLRs). This activation leads to a cascade of events, including enhanced phagocytosis, increased production of ROS, and the release of pro-inflammatory cytokines (e.g., TNF-α, IL-1β, IL-6), all of which contribute to an effective antimicrobial response (Mishra *et al*., 2022).

Beyond the immunomodulatory polysaccharides, *P. ostreatus* contains a rich array of secondary metabolites, notably phenolic compounds and tannins. These phytochemicals exert direct antimicrobial effects through distinct molecular mechanisms. Phenolic compounds, encompassing flavonoids, phenolic acids, and lignans, can disrupt microbial cell membrane integrity, leading to leakage of intracellular contents and eventual cell lysis. They are also known to inhibit vital microbial enzymes involved in cell wall synthesis, DNA replication, and protein synthesis. Furthermore, tannins can interfere with microbial adhesins and biofilm formation, thereby preventing bacterial colonization and subsequent infection (Cowan, 1999).

The comprehensive study by Khinsar *et al*. (2021) provided empirical evidence for this broad-spectrum efficacy, demonstrating potent inhibitory effects of petroleum ether and acetone extracts against both Gram-positive (e.g., *Staphylococcus aureus*) and Gram-negative bacteria (e.g., *Escherichia coli*, *Pseudomonas aeruginosa*). Interestingly, their findings also revealed solvent-dependent selectivity, with methanolic and chloroform extracts exhibiting a more pronounced activity against Gram-positive species, underscoring the importance of extraction methodologies in isolating specific bioactive components. This multifaceted antibacterial action, encompassing both immune enhancement and direct antimicrobial effects, positions *P. ostreatus* as a promising source for novel antibacterial agents, particularly in an era of increasing antibiotic resistance.

2.5.5.2 Antifungal and Antimicrobial Properties

Expanding upon its antibacterial capabilities, *P. ostreatus* also exhibits a significant antifungal and broader antimicrobial spectrum, which is critically influenced by the extraction solvent. Research by Gashaw *et al*. (2020) and Liu *et al*. (2020) collectively elucidated the comprehensive antimicrobial profile of methanolic extracts from *P. ostreatus*. These extracts demonstrated efficacy against a diverse panel of pathogenic microorganisms, including clinically significant bacteria such as *Escherichia coli*, *Staphylococcus aureus*, *Bacillus megaterium*, and *Klebsiella pneumoniae*. More importantly, these studies confirmed potent antifungal activity against a range of fungal pathogens, specifically targeting *Candida* species (e.g., *C. albicans*), *Trichophyton* species (a common dermatophyte responsible for ringworm), and *Epidermophyton* species (another group of dermatophytes). This broad activity against both bacterial and fungal pathogens highlight its potential as a dual-action antimicrobial agent.

The observed antimicrobial activity was notably solvent-dependent, a phenomenon crucial for the targeted isolation of specific bioactive compounds. For instance, ether extracts were found to be more effective against Gram-negative organisms, likely due to their ability to extract non-polar compounds that can readily permeate the outer membrane of Gram-negative bacteria Törős *et al*. (2023). Conversely, acetone extracts, while still active, showed different profiles. This differential efficacy based on solvent polarity suggests the presence of distinct antimicrobial compounds with varying chemical properties within *P. ostreatus*. The identification of such a broad antimicrobial spectrum, encompassing common bacterial and fungal strains relevant to human health, positions *P. ostreatus* as a valuable candidate for further pharmacological exploration, particularly in the development of natural antimicrobial remedies or as a source for lead compounds against multi-drug resistant pathogens.

2.5.5.3 Antiviral Potential

The antiviral properties of *P. ostreatus* represent a highly promising area of research, primarily associated with the presence of specific protein-based components such as laccases and ubiquitin-like factors. A study by Elhusseiny *et al*. (2021) provided compelling evidence for the anti-hepatitis C virus (HCV) activity of *P. ostreatus* laccase. Laccases are multi-copper oxidoreductases widely distributed in fungi, known for their ability to oxidize phenolic compounds. In this context, the *P. ostreatus* laccase demonstrated its capacity to inhibit HCV entry into HepG2 cells, a crucial step in the viral life cycle, and subsequently impede viral replication. This suggests that laccase might interfere with host-cell receptor interactions or directly target viral proteins involved in replication. The low cytotoxicity observed in these studies further enhances its therapeutic appeal, differentiating it from many conventional antiviral drugs that often come with significant side effects.

Furthermore, the isolation of a distinct ubiquitin-like protein from *P. ostreatus* by Pérez-Bassart *et al*. (2024) revealed its potential against human immunodeficiency virus type 1 (HIV-1). This protein was shown to impede HIV-1 reverse transcriptase activity, an enzyme critical for the conversion of viral RNA into DNA within the host cell. Inhibition of reverse transcriptase is a well-established therapeutic target for HIV-1, and the discovery of such a natural inhibitor with potentially novel binding sites could offer a new avenue for antiretroviral drug development. The low cytotoxicity and reduced propensity for viral resistance, as suggested by the preliminary findings, are critical advantages in the context of long-term antiviral therapy, where drug resistance remains a significant challenge. These findings collectively underscore *P. ostreatus* as a valuable bioresource for the discovery and development of novel antiviral compounds, potentially broadening the therapeutic arsenal against persistent viral infections (Seo and Choi, 2021).

2.5.5.4 Antidiabetic Effects

The growing body of scientific literature robustly supports the significant hypoglycemic and broader antidiabetic effects of *P. ostreatus*, particularly evidenced in various diabetic animal models. The work by Nweze *et al*. (2020) revealed intriguing synergistic glucose-lowering effects when *P. ostreatus* was co-administered with other botanicals in alloxan-induced diabetic rats. Alloxan selectively destroys pancreatic β-cells, inducing a type 1 diabetes-like state; therefore, the observed improvements suggest *P. ostreatus* may either protect residual β-cells, stimulate their regeneration, or enhance insulin sensitivity in peripheral tissues. Agunloye and Oboh (2022) provided further depth, demonstrating that high-dose *P. ostreatus* extract was remarkably effective in reducing not only hyperglycemia but also associated diabetic complications, including DNA damage, chromosomal aberrations, and even sperm abnormalities, surpassing the efficacy of the standard antidiabetic drug, amaryl (glimepiride). This suggests *P. ostreatus*'s action extends beyond glycemic control to mitigating oxidative stress and genotoxicity commonly linked to chronic hyperglycemia.

Further corroborating these findings, Nnemolisa *et al*. (2024) reported comprehensive improvements in diabetic mice treated with *P. ostreatus*, observing amelioration of hyperglycemia, hyperlipidemia (abnormal lipid levels), and renal dysfunction, all hallmarks of advanced diabetes. These systemic benefits point to a multifaceted mechanism of action. Proposed mechanisms include direct activation of glucokinase, a pivotal enzyme in glucose metabolism that phosphorylates glucose to glucose-6-phosphate, thereby increasing glucose utilization. Furthermore, *P. ostreatus* may stimulate insulin secretion from pancreatic β-cells, potentially through protection against oxidative damage or by enhancing their secretory capacity. Inhibition of glycogen synthase kinase is another postulated mechanism, which would promote glycogen synthesis and storage in the liver and muscles, thereby reducing circulating glucose levels. Importantly, human trials involving diabetic and hypertensive

patients have echoed these preclinical observations, showing statistically significant reductions in fasting glucose, glycated hemoglobin (HbA1c, a long-term glycemic control marker), and blood pressure, critically without adverse renal or hepatic effects. This clinical translation potential, coupled with its safety profile, positions *P. ostreatus* as a promising dietary intervention or complementary therapeutic agent for managing diabetes and its associated complications.

2.5.5.5 Antioxidant and Anti-Aging Properties

Pleurotus ostreatus is replete with compounds that confer robust antioxidant activity, making it a subject of significant interest for anti-aging and health promotion. Abdelkader *et al*. (2024) provided compelling evidence for its role in mitigating age-related oxidative stress by observing enhanced catalase expression and reduced protein oxidation in aged rats following *P. ostreatus* intake. Catalase is a crucial endogenous antioxidant enzyme that catalyzes the decomposition of hydrogen peroxide to water and oxygen, thereby neutralizing a potent reactive oxygen species. Reduced protein oxidation, a marker of oxidative damage to cellular components, further signifies the protective effect of *P. ostreatus* against cellular senescence.

According to Paterska *et al*. (2024) and Luo *et al*. (2024), beyond bolstering endogenous antioxidant defenses, various extracts of *P. ostreatus* demonstrate direct scavenging capabilities. Ethanol extracts, for example, have shown potent *in vitro* scavenging of superoxide radicals (O2·−), hydroxyl radicals (OH·), and ferrous ions (Fe2+), all of which are highly reactive species implicated in cellular damage and aging. Moreover, these extracts exhibited significant inhibition of lipid peroxidation, a process where free radicals attack lipids, leading to cellular membrane damage and dysfunction. Polysaccharide fractions, such as PSPO-1a, have also contributed substantially to this antioxidant profile, exhibiting strong DPPH (2,2-diphenyl-1-picrylhydrazyl) radical scavenging activity and effective nitric oxide (NO) inhibition. NO, while a vital signaling molecule, can form highly reactive peroxynitrite

in excess, contributing to oxidative stress. Collectively, these findings underscore the multifaceted antioxidant defense provided by *P. ostreatus*, acting both through direct radical neutralization and by enhancing the body's intrinsic antioxidant machinery. This comprehensive antioxidant capacity strongly supports its utility as a functional food additive or a nutraceutical to combat age-related oxidative stress and associated chronic diseases, potentially extending healthy lifespan (Rukhsar *et al*., 2025).

2.5.5.6 Antitumor and Anticancer Activity

The antitumor and anticancer potential of *P. ostreatus* is extensively documented, with research spanning several decades. Findings by Elhusseiny *et al*. (2021) were pivotal in identifying antitumor β-glucans within this mushroom, laying the groundwork for subsequent detailed investigations. These findings have been corroborated by numerous *in vitro* and *in vivo* studies, which have elucidated complex mechanisms of action (Khinsar *et al*., 2021; Mishra *et al*., 2022). For instance, hot-water extracts of *P. ostreatus* have demonstrated significant inhibitory effects against a panel of human cancer cell lines, including PC-3 (prostate adenocarcinoma), MCF-7 (breast carcinoma), HT-29, and HCT-116 (colon carcinoma) (Khinsar *et al*., 2021; Mishra *et al*., 2022). The observed cytotoxicity was attributed to the induction of apoptosis, a programmed cell death pathway, often mediated through both extrinsic (death receptor-dependent) and intrinsic (mitochondrial-dependent) pathways. Furthermore, these extracts induced cell-cycle arrest, specifically at the G0/G1 phase, thereby halting uncontrolled proliferation by preventing DNA replication and cell division. Modulation of key tumor suppressor pathways, such as p53/p21, was also noted, indicating that *P. ostreatus* components can reactivate critical cellular checkpoints that are often dysfunctional in cancer cells.

Beyond polysaccharides, protein extracts from *P. ostreatus* have also shown remarkable anticancer activity, notably by triggering reactive oxygen species (ROS)-mediated apoptosis in leukemic cells such as SW480 (colon cancer) and THP-1 (acute monocytic leukemia). While

ROS can be detrimental at high levels, their controlled increase within cancer cells can overwhelm antioxidant defenses, leading to mitochondrial dysfunction and apoptotic initiation. *In vivo* studies have further validated these antitumor effects. Mycelial proteoglycans, complex molecules combining proteins and polysaccharides, have been shown to significantly reduce the growth of sarcoma-180 tumors in animal models (Mishra *et al*., 2022). This effect was not solely direct but also highly immunomodulatory, involving the enhancement of natural killer (NK)-cell cytotoxicity and increased macrophage nitric oxide production. NK cells are crucial components of the innate immune system, capable of recognizing and destroying tumor cells without prior sensitization. Macrophage activation, leading to increased nitric oxide production, contributes to the antitumor microenvironment. These immunomodulatory effects are partially attributed to the binding of *P. ostreatus* compounds with glucose/mannose-specific lectins present on the surface of immune cells, facilitating their activation and downstream immune responses (Elhusseiny *et al*., 2021). The confluence of direct cytotoxic effects, cell cycle perturbation, and immune-mediated tumor regression highlights the profound potential of *P. ostreatus* as a source of anticancer biotherapeutics.

2.5.5.7 Immunomodulatory Effects

The immunomodulatory potential of *Pleurotus ostreatus* stems from its rich content of bioactive compounds—particularly polysaccharides, lectins, and protein-polysaccharide complexes. These molecules act as biological response modifiers by engaging pattern recognition receptors like Dectin-1 and CR3 on macrophages and neutrophils, triggering intracellular signaling that enhances phagocytosis and reactive oxygen species (ROS) production. They also promote cytokine secretion (e.g., TNF-α, IL-1β, IL-6) and chemokine-mediated immune cell recruitment (Wang *et al*., 2022; Du *et al*., 2024).

Both fruiting-body and mycelial extracts have been shown to increase neutrophil oxidative burst and stimulate proliferation of lymphocytes and splenocytes, enhancing overall immune

surveillance. These effects are largely mediated by the binding of mushroom-derived lectins to immune cell receptors, triggering signal transduction pathways that support immune cell activation, differentiation, and maturation. This capacity to modulate and strengthen immune responses highlights *P. ostreatus* as a promising adjunct in immunotherapy and infection control (Llauradó Maury *et al*., 2021).

2.5.5.8 Hypocholesterolemic and Hypolipidemic Effects

Pleurotus ostreatus has a well-established history and a growing body of contemporary research supporting its significant cholesterol-lowering (hypocholesterolemic) and lipid-lowering (hypolipidemic) properties. The key bioactive compounds responsible for these effects include specific dietary β-glucans and, notably, statin-like compounds, with lovastatin being a well-identified example. These compounds collectively exert their effects by favorably modulating the lipid profile, leading to significant reductions in low-density lipoprotein (LDL) cholesterol ("bad" cholesterol), very-low-density lipoprotein (VLDL) cholesterol, and triglycerides, while simultaneously promoting an increase in high-density lipoprotein (HDL) cholesterol ("good" cholesterol) (Iqbal *et al*., 2024).

The mechanisms underpinning these beneficial lipid alterations are multifaceted. One primary route involves the impaired intestinal absorption of dietary lipids and cholesterol. β-glucans, being viscous soluble fibres, form a gel-like matrix in the digestive tract, which can entrap bile acids and dietary cholesterol, thereby preventing their absorption and promoting their excretion. This forces the liver to synthesize more bile acids from endogenous cholesterol, further reducing circulating cholesterol levels. A more direct and potent mechanism involves the inhibition of hepatic HMG-CoA reductase, the rate-limiting enzyme in cholesterol biosynthesis. The presence of lovastatin-like compounds in *P. ostreatus* directly interferes with this enzyme, mimicking the action of prescription statin drugs and thereby reducing endogenous cholesterol production.

Empirical evidence from rodent models, encompassing normal, genetically hypercholesterolemic, and Triton WR-1339–induced hyperlipidemia, consistently demonstrates the efficacy of *P. ostreatus*. Administration of ethanol extracts or dietary inclusion of 5–10% *P. ostreatus* biomass consistently achieved substantial reductions (ranging from 20–65%) in total cholesterol and triglycerides. Human clinical trials have further validated these preclinical findings. Dyslipidemic and diabetic patients who incorporated *P. ostreatus* into their diet experienced similar lipid-lowering effects, indicating the translational potential of these findings (Abidin *et al*., 2017). Advanced gene expression analyses conducted in these studies have identified the modulation of key genes involved in lipid metabolism, such as *Dgat1* (diacylglycerol acyltransferase 1), an enzyme crucial for triglyceride synthesis, and various lipid transport genes. This molecular insight reinforces the comprehensive nature of *P. ostreatus*'s hypolipidemic action, suggesting its utility as a natural adjunct in the management of dyslipidemia and cardiovascular risk (Abidin *et al*., 2017; Sultan and Abed, 2023; Iqbal *et al*., 2024).

2.5.5.9 Hepatoprotective Effects

While perhaps less extensively investigated compared to its other renowned properties, the hepatoprotective activity of *Pleurotus ostreatus*, particularly its polysaccharide-rich extracts, is an emerging area of significant interest. Liver injury, often caused by xenobiotics, oxidative stress, or inflammation, leads to cellular damage and impaired hepatic function. Polysaccharide fractions from *P. ostreatus* have been shown to exert protective effects by enhancing the activity of critical hepatic antioxidant enzymes. These include catalase, superoxide dismutase (SOD), and potentially glutathione peroxidase. SOD converts superoxide radicals to hydrogen peroxide, which is then neutralized by catalase and glutathione peroxidase. By bolstering these endogenous antioxidant defenses, *P. ostreatus* extracts help to mitigate oxidative stress-

induced damage within hepatocytes, preserving cellular integrity and function (Famii and Ebuka, 2019; Osman and Toliba, 2019).

Furthermore, these extracts have been observed to significantly reduce the levels of necrotic markers in serum, specifically aminotransferases such as alanine aminotransferase (ALT) and aspartate aminotransferase (AST), and alkaline phosphatase (ALP). Elevated serum levels of these enzymes are classical indicators of hepatocellular injury, as they leak from damaged liver cells into the bloodstream. The reduction in these markers in various toxicological models (e.g., carbon tetrachloride-induced or paracetamol-induced liver injury) demonstrates the ability of *P. ostreatus* to prevent or attenuate liver cell necrosis. The proposed mechanisms likely involve not only direct antioxidant effects but also anti-inflammatory properties and stabilization of hepatocyte membranes. The findings by Duan *et al*. (2020) underscore the potential of *P. ostreatus* as a natural hepatoprotective agent, warranting further in-depth research to fully elucidate its mechanisms and therapeutic applications in liver diseases.

Table 2.4: Summary of The Pharmacological properties of *Pleurotus ostreatus*

Pharmacological Property	Key Bioactive Compounds	Study Methods & Models	Main Findings & Mechanistic Insights	References
Antibacterial / Antifungal	Methanol/chloroform extracts, panisaldehyde, AgNPs, tannins, phenolics	*In vitro* (agar diffusion, broth dilution)	Broad-spectrum activity; disrupts membrane, inhibits enzymes	Gashaw *et al*. (2020); Liu *et al*. (2020); Törős *et al*. (2023)
Antiviral	Laccase, ubiquitin, β-glucans	*In vitro* (HIV, HCV, HSV, Influenza A)	Inhibits HIV-1 RT, blocks HCV entry, HSV-1, West Nile virus	Elhusseiny *et al*. (2021); Seo and Choi (2021); Pérez-Bassart *et al*. (2024)
Antidiabetic / Antihyperglycemic	Polysaccharides, phenols, flavonoids, saponins, terpenoids	*In vitro* (enzyme assays); In vivo (alloxan, STZ models); Clinical (diabetics)	↓ Glucose, HbA1c, lipids; inhibits α-amylase, α-glucosidase; improves insulin secretion	Nweze *et al*. (2020); Agunloye and Oboh (2022); Nnemolisa *et al*. (2024)
Antioxidant / Anti-Aging	Phenolics (flavonoids, gallic acid, etc.), β-glucans, ergothioneine, vitamins C & E, carotenoids, saponins	*In vitro* (DPPH, β-carotene inhibition); *In vivo* (Wistar/hypercholesterolemic rats)	Scavenges ROS, inhibits lipid peroxidation, upregulates SOD & catalase, chelates metal ions	Abdelkader *et al*. (2024); Paterska *et al*. (2024); Luo *et al*. (2024); Rukhsar *et al*. (2025)
Antitumor / Anticancer	β-glucans, proteoglycans, POPS-1, Pleuran, POMP-2, methyl gallate, flavonoids	*In vitro* (MCF-7, HT-29, HepG2); In vivo (sarcoma-180, DMBA); Limited clinical use	Induces apoptosis, inhibits proliferation, arrests cell cycle, immune activation (NK, macrophages)	Elhusseiny *et al*. (2021); Khinsar *et al*. (2021); Mishra *et al*. (2022)
Immunomodulatory	Polysaccharide–protein complexes, β-glucans, lectins, PSP	*In vivo* (mice, children); Clinical (HIV+, GI cancer)	↑ IL-2, TNF-α, CD4+/CD8+ ratio, ROS burst; activates macrophages, neutrophils	Llauradó Maury *et al*. (2021); Wang *et al*. (2022); Du *et al*. (2022)
Hypocholesterolemic / Hypolipidemic	β-glucans, lovastatin analogs, chrysin, gallic acid	*In vivo* (hyperlipidemic rats); Clinical (HIV+ patients)	↓ LDL, VLDL, TG; ↑ HDL; improves lipid metabolism gene expression	Abidin *et al*. (2017); Sultan and Abed (2023); Iqbal *et al*. (2024)
Hepatoprotective	Polysaccharides, phenolics, antioxidants	*In vivo* (toxin-challenged or stressed rats)	↓ ALT, AST; protects from oxidative injury, improves hepatic enzymes	Famii and Ebuka (2019); Osman and Toliba (2019); Duan *et al*. (2020)

CHAPTER THREE

MATERIALS AND METHODS

3.1 ETHICAL APPROVAL

Ethical approval was obtained before the commencement of this study from the Research Ethics Committee (REC), College of Medical Sciences, University of Benin, Benin City, Nigeria with REC Approval Number: **CMS/REC/2024/792.**

3.2 REAGENTS AND CHEMICALS

Mercuric chloride (MOLYCHEM – P. Code: 15700 – MCR-27769: Badiapur District, India) was purchased and used for the study. A previously reported oral dose of 4 mg/Kg body weight was used to induce neurotoxicity (Owoeye *et al*., 2018; Ajibade *et al*., 2019).

3.3 COLLECTION AND EXTRACTION OF MYCO-MATERIAL

Fresh *Pleurotus ostreatus* was obtained from the African Centre for Mushroom Research and Technology Innovations (ACMRTI), University of Benin, Benin City, Nigeria. A total of 3000g of fresh fungi material was cleaned thoroughly, air-dried and blended into fine powder using a mechanical blender. For extraction, 1 L of Ethanol was added to 1000g of extract and then allowed to sit at room temperature for 72 hours with periodical stirring – after every 6 hours. The mixture was then filtered using Whatman No. 1 filter paper. The solvent was concentrated by evaporating the ethanol extract at 40^{o}C using a water bath. The resulting extract was stored at 4^{o}C until further use. The extract was reconstituted in distilled water to the desired working concentrations used in this study.

3.4 MYCOCHEMICAL SCREENING

Mycochemical screening is the systematic analysis of fungal extracts to detect and characterize the presence of bioactive compounds. This process includes both qualitative and quantitative assessments aimed at identifying key secondary metabolites which contribute to the medicinal and nutritional properties of the fungus.

3.4.1 Qualitative Mycochemical Screening

The mycochemical examinations was carried out by dissolving 1.0 g of the ethanol extract in 50 mL of 95% ethanol in a 100 mL beaker. The solution was transferred to a 100 mL standard flask. The beaker was rinsed three times with 10 mL portions of ethanol and added to the flask. The volume was made up to the mark with ethanol, corked, mixed thoroughly, and kept aside for mycochemical analysis. The final solution had a concentration of 10,000 µg/mL. The mycochemical examinations were carried out using standard methods as described by Tiwari *et al*. (2016).

3.4.1.1 Test for alkaloids (Mayer's reagent test)

This was done by evaporating 2.0 ml of the fungus extract to dryness. Then the resultant residues were dissolved in 5ml of HCl (2 mol/ dm^3) and filtered. The filtrate was divided into two test tubes. To the first test tube, a few drops of Mayer's reagent were added, and the formation of a yellow-coloured precipitate indicates the presence of alkaloids. The second test tube was treated with a few drops of Wagner's reagent, and the brownish-red precipitate formation indicates alkaloids (Tiwari *et al*. (2016).

3.4.1.2 Test for Glycoside

Ethanol extract (0.5 mg) was dissolved in 1 mL of ethanol. A few drops of aqueous sodium hydroxide (NaOH) solution were then added. The appearance of a yellow coloration was taken as a positive indication for the presence of glycosides (Tiwari *et al*., 2016).

3.4.1.3 Tests for Tannins

To 1.0 mL of the ethanol extract, 1.0 mL of 1% gelatin solution containing sodium chloride was added. The mixture was observed for the formation of a white precipitate, which indicates the presence of tannins (Tiwari *et al*., 2016).

3.4.1.4 Tests for Phenols

To 1.0 mL of the ethanol extract, 4 drops of ferric chloride ($FeCl_3$) solution were added. The appearance of a bluish-black coloration was taken as a positive indication for the presence of phenolic compounds (Tiwari *et al*., 2016).

3.4.1.5 Tests for Saponins

Saponin detection was carried out using both the foam test and froth test methods. In the foam test, 0.5 g of the ethanol extract was shaken vigorously with 2.0 mL of distilled water. The formation of a stable foam that persisted for at least 10 minutes was taken as a positive indication of saponins. In the froth test, 5.0 mL of the ethanol extract was diluted to 20.0 mL with distilled water in a 50 mL graduated cylinder, then shaken vigorously for 15 minutes. The development of a persistent foam layer approximately 1 cm in height indicated the presence of saponins (Tiwari *et al*., 2016).

3.4.1.6 Tests for Flavonoids

Flavonoid detection was carried out using the alkaline reagent test and the lead acetate test. In the alkaline reagent test, the ethanol extract was treated with a few drops of 2 mol/dm³ sodium hydroxide (NaOH) solution. The appearance of an intense yellow coloration that became colorless upon the addition of dilute hydrochloric acid (2 mol/dm³ HCl) indicated the presence of flavonoids. In the lead acetate test, the ethanol extract was treated with a few drops of lead acetate solution. The formation of a yellow precipitate was taken as a positive result for flavonoids (Tiwari *et al*., 2016).

3.4.1.7 Tests for Eugenols

Approximately 2.0 mL of the ethanol extract was mixed with 5.0 mL of 5% potassium hydroxide (KOH) solution. The resulting mixture was allowed to separate, and the aqueous layer was carefully filtered. A few drops of hydrochloric acid (HCl) were then added to the filtrate. The formation of a pale-yellow precipitate was considered a positive indication (Tiwari *et al*., 2016).

3.4.1.8 Tests for Steroids

Steroid detection was performed using the Salkowski test. To 0.5 g of the ethanol extract, 2.0 mL of acetic anhydride was added, followed by 2.0 mL of concentrated sulfuric acid (H_2SO_4). A color change from violet to blue or green was considered indicative of the presence of steroids (Tiwari *et al*., 2016).

3.4.1.9 Tests for Terpenoid

Terpenoid detection was carried out using the Salkowski test. Approximately 0.2 g of the ethanol extract was mixed with 2.0 mL of chloroform ($CHCl_3$), and 3.0 mL of concentrated sulfuric acid (H_2SO_4) was carefully added to form a separate layer. The appearance of a reddish-brown coloration at the interface was taken as a positive indication for the presence of terpenoids (Tiwari *et al*., 2016).

3.4.2 Quantitative Mycochemical Screening

Quantitative mycochemical analysis provides accurate estimations of the concentrations of key bioactive constituents within fungal extracts (Tiwari Pandey *et al*., 2021). In this study, the quantitative evaluation of *Pleurotus ostreatus* ethanol extract was conducted according to established methods. The analysis included the determination of total phenolic content, alkaloid, flavonoid, total saponin and tannin contents.

3.4.2.1 Total Phenolic Content Estimation

The total phenolic content of the *Pleurotus ostreatus* ethanol extract was determined using the Folin–Ciocalteu method as described by Ainsworth and Gillespie (2007). Tannic acid was used as the standard. Briefly, 1.0 mL of the extract solution (250 µg/mL) was transferred into a test tube, followed by the addition of 1.0 mL of Folin–Ciocalteu reagent. The mixture was vortexed and allowed to stand for 5 minutes at room temperature. Subsequently, 15.0 mL of 20% sodium carbonate (Na_2CO_3) solution was added, and the reaction mixture was incubated at room temperature for 2 hours. The absorbance was measured at 760 nm using a UV-Visible spectrophotometer (Jenway 6100, Dunmow, Essex, U.K.). The total phenolic content was calculated and expressed as micrograms of tannic acid equivalents (µg TAE), using a standard calibration curve generated from known concentrations of tannic acid.

3.4.2.2 Alkaloid Content Estimation

The total alkaloid content of *Pleurotus ostreatus* ethanol extract was determined using the method described by Sharma *et al*. (2021). Briefly, 5 g of the dried ethanol extract was placed in a 250 mL beaker, and 100 mL of 20% acetic acid in ethanol was added. The mixture was covered and allowed to stand at room temperature for 2 hours to ensure complete extraction. It was then filtered, and the filtrate was concentrated to one-quarter of its original volume using a water bath. Concentrated ammonium hydroxide was added dropwise to the concentrated extract until complete precipitation of alkaloids was achieved. The solution was allowed to settle, and the resulting precipitate was collected by filtration, washed with 1% ammonia solution, dried, and weighed. All samples were analyzed in triplicates, and the results were expressed as a percentage of the total extract weight.

$$\text{Alkaloid (\%)} = [\text{Weight of residue} / \text{Weight of sample}] \times 100$$

3.4.2.3 Flavonoid Content Estimation

The total flavonoid content of *Pleurotus ostreatus* ethanol extract was determined using the method described by Kamtekar *et al*. (2014). Quercetin was used as the reference standard, and the results were expressed as micrograms of quercetin equivalent per gram of extract (µg QE/g). Briefly, 30 µL of the ethanol extract was transferred into a test tube and diluted with 90 µL of methanol. To this, 6 µL of 10% aluminum chloride ($AlCl_3$) solution and 6 µL of 1 M sodium acetate (CH_3CO_2Na) were added. Finally, 170 µL of methanol was added to bring the total reaction volume to 302 µL. The mixture was incubated at room temperature for 30 minutes, and the absorbance was measured at 415 nm using a UV-Vis spectrophotometer. All samples were analyzed in triplicate, and flavonoid content was quantified based on a quercetin standard calibration curve.

3.4.2.4 Total Saponins Content Estimation

The total saponin content of *Pleurotus ostreatus* ethanol extract was estimated using the vanillin–sulfuric acid colorimetric method as described by Mir *et al*. (2016). Briefly, 50 µL of the ethanol extract was mixed with 250 µL of distilled water in a test tube. Then, 250 µL of vanillin reagent (prepared by dissolving 800 mg of vanillin in 10 mL of 99.5% ethanol) was added, followed by 2.5 mL of 72% sulfuric acid (H_2SO_4). The mixture was vortexed and incubated in a water bath at 60°C for 10 minutes. After incubation, the reaction mixture was immediately cooled in ice-cold water, and the absorbance was measured at 570 nm using a UV-Vis spectrophotometer. Standard saponin solutions (0–25 ppm) were prepared from a stock solution and treated in the same way as the test samples. Total saponin content was calculated from the standard calibration curve and expressed in parts per million (ppm).

3.4.2.5 Tannin Content Estimation

The total tannin content of *Pleurotus ostreatus* ethanol extract was determined using the Folin–Denis method. Precisely 0.20 mL of the ethanol extract was added to 20 mL of 50% methanol

in a test tube and incubated in a water bath at 77–80°C for 1 hour, with intermittent shaking. The resulting extract was quantitatively filtered through a double-layered Whatman No. 1 filter paper. To the filtrate, 20 mL of distilled water, 2.5 mL of Folin–Denis reagent, and 10 mL of 17% sodium carbonate (Na_2CO_3) solution were added and mixed thoroughly. The mixture was allowed to stand at room temperature for 20 minutes to allow for full color development. A series of standard tannic acid solutions were prepared in methanol and treated similarly. The absorbance of both standards and samples was measured at 760 nm using a UV-Visible spectrophotometer. Total tannin content was calculated from the tannic acid standard calibration curve and expressed as µg tannic acid equivalents (TAE) per gram of extract (Mir *et al.*, 2016).

3.5 PROXIMATE ANALYSIS

3.5.1 Ash Content

The ash content of *Pleurotus ostreatus* was determined using the dry ashing method. Two grams (2 g) of the dried sample was accurately weighed into a pre-weighed porcelain crucible. The crucible was then placed in a preheated muffle furnace set at 900°C and incinerated for 1 hour to ensure complete combustion of organic matter. After ashing, the crucible was carefully transferred to a desiccator and allowed to cool to room temperature. The final weight of the crucible and its inorganic residue (ash) was recorded. The percentage ash content was calculated using the formula:

$$\text{Ash} = 100\ W_{ash}\ (\%) / W_o$$

Where, W_{ash} = content weight after final drying.

W_o = the dried weight of the sample.

3.5.2 Moisture Content

The moisture content of *Pleurotus ostreatus* was determined using the oven-drying method (Agbagwa *et al*., 2020). Two grams (2 g) of the sample was accurately weighed and placed in

a clean, dry moisture dish. The sample was then dried in a hot air oven at a controlled temperature (typically 105°C). The sample was reweighed at 10-minute intervals until a constant weight was achieved, indicating that all moisture had been evaporated. The moisture content (%) was calculated using the following formula:

$$[(W_0 - W_{dry}) / W_0] \times 100$$

Where, W_0 = initial weight

W_{dry} = dry weight (final weight)

3.5.3 Crude Fibre Content

Crude fibre content was determined following the standard method described by Agbagwa *et al*. (2020). Exactly 4 g of moisture-free sample was weighed into a 250 mL beaker, followed by the addition of 50 mL of 4% sulfuric acid (H_2SO_4) and distilled water to a total volume of 200 mL. The mixture was brought to a boil and maintained at boiling for 30 minutes, with constant stirring using a rubber-tipped glass rod.

The volume was kept constant throughout by adding hot distilled water. After 30 minutes, the mixture was filtered through a Buchner funnel fitted with ashless Whatman No. 40 filter paper and connected to a vacuum pump. The beaker and residue were thoroughly rinsed with hot distilled water until the filtrate was acid-free, confirmed using litmus paper. The residue was then transferred back into the beaker, using 5% sodium hydroxide (NaOH) and hot distilled water to reach 200 mL.

The mixture was again boiled for 30 minutes, with continuous stirring and volume adjustment. It was then filtered and rinsed thoroughly with hot water until alkali-free, followed by two washes with 2 mL of 95% ethanol. The final residue, including the filter paper, was transferred into a pre-weighed porcelain crucible, dried in an oven at 110°C to constant weight, cooled in a desiccator, and weighed. The crucible was then ignited in a muffle furnace at 550°C for 8

hours, cooled, and reweighed. All analyses were carried out in triplicate. The percentage crude fibre content was calculated using the formula:

$$\text{Crude Fibre (\%)} = [100\ (y - a)] / x$$

Where, x = Weight of sample (g)

y = Weight of insoluble matter (g)

a = Weight of Ash (g)

3.5.4 Crude Fat Content

Crude fat content was determined using the Soxhlet extraction method as described by Irshad *et al*. (2023). This method is based on the principle that non-polar lipids are readily soluble in organic solvents such as petroleum ether. Exactly 3.0 g of oven-dried (moisture-free) sample was weighed into a fat-free thimble, which was then plugged with glass wool. The thimble was inserted into a Soxhlet extractor containing 160 mL of petroleum ether (boiling point 60–80°C). A clean, dry, and pre-weighed receiver flask was attached to the extractor.

The Soxhlet unit was assembled and extraction was performed for 8 hours, with continuous circulation of cold water through the condenser and the water bath maintained at 60°C. After extraction, the thimble was removed and dried in a hot air oven at 70°C for 3 hours to ensure complete removal of solvent. It was then cooled in a desiccator and weighed to a constant weight using an analytical balance. The crude fat content was calculated as:

$$\%\ \text{Fat} = [X - Y] / Z$$

Where, x = Weight sample and thimble and oil

Y = Weight of empty thimble

Z = Weight of sample

3.5.5 Crude Protein Content

Crude protein content of the defatted *Pleurotus ostreatus* samples was determined using a micro-Kjeldahl method as described by Chromý *et al*. (2015). Three grams (3g) each of the

defatted samples were separately weighed on pre-weighed into micro-Kjeldahl digestion flask together with few anti bumping granules. Two grams of catalyst mixture ($CuSO_4$: Na_2SO_4: SeO_2, 5:1:02 w/w) was added to each flask and then 10 mL nitrogen free concentrated H_2SO_4 also added to each flask. The flasks were placed in inclined position on a heating mantle in a fume cupboard. Digestion was started at temperature of 30°C until frothing ceased and then heating was increased to 50°C for another 30 min and finally at full heating (100°C) until a clear solution was obtained. Simmering was continued below boiling point for another 30 min to ensure complete digestion and conversion of nitrogen to ammonium sulphate. After digestion was completed, samples were allowed to cool and then transferred quantitatively to 100 mL volumetric flasks with washing and cooling to room temperature. Volumes were made up to mark with distilled water.

Afterwards, 5ml of the filtrate from the digest was transferred with the aid of a 10ml pipette into a 25ml standard flask. 2.5ml of the Alkaline Phenate was added and the solution shaken to mix properly. Then 1ml of Sodium Potassium Tartarate was added, shaken properly followed by the addition 2.5ml of sodium hypochlorite. There after the solution was made up to the 25ml mark with distilled water and the absorbance of the resultant solution measured with the aid of UV/visible spectrophotometer, at 630nm. The Nitrogen standards were treated the same way with the sample. The crude protein content was calculated using the formula:

%N = [Instrument. Reading x Slope Reciprocal x Color Vol. x Digest Vol.] / Weight of Sample x Aliquot Taken x 10000

% Crude Protein = % Nitrogen × 6.25

3.5.6 Estimation of total carbohydrate

The total carbohydrate content of the diet samples was obtained by subtracting the sum of the percentage crude protein, crude fat, Moisture, Fibre, and ash from 100.

Carbohydrate content = 100% - (moisture + crude protein + crude fat + ash + crude fiber)%

3.6 DPPH RADICAL SCAVENGING SCREENING ACTIVITY

From the stock extract solution which contains 10000µg/ml, five different concentrations (250, 200,150,100, and 50µg/ml) were prepared, using the dilution formula of $C_1V_1 = C_2V_2$**.** The free radical scavenging activities of each of the plant extracts were assayed using a stable DPPH standard method as described by Musa *et al*. (2016) and Siripongvutikorn *et al*. (2024). 2 ml of each diluted extract was placed in test tubes that had been washed, rinsed with distilled water, dried, and labelled accordingly. Also, 2 ml of methanol was added to another test tube labelled control. Thereafter 2ml of the prepared DPPH solution was added to each of the test tubes. The test tubes were agitated a little for proper mixing of the content and then incubated in the dark for 30 minutes. The absorbance of the reaction mixtures was measured using a UV/Visible Spectrophotometer at 518 nm wavelength, and the ability of the extracts to scavenge DPPH radical were calculated by following the equation:

$$Scavenging\ activity\ (\%) = \frac{(A_0 - A_1)}{A_0} \times 100$$

Where, A_0 = the absorbance of the control

A_1 = the absorbance of extract/standard taken as ascorbic acid.

3.7 PROCUREMENT AND CARE OF EXPERIMENTAL ANIMALS

A total of forty-two (42) adult Wistar rats, weighing between 170–190 g, were procured and acclimatised for 2 weeks in the Animal House of the Department of Anatomy, School of Basic Medical Sciences, College of Medical Sciences, University of Benin, Benin City, Nigeria. The animals were housed in clean polypropylene cages under standard laboratory conditions and maintained at ambient room temperature with 12-hour light/dark cycles. All rats had *ad libitum* access to water and were fed with Chikun Feed Grower Mash (Olam Agri Holdings Pte Ltd., Lagos State, Nigeria). Body weights were measured weekly, starting before the commencement of treatment and continuing throughout the duration of the experiment, using

a calibrated digital weighing scale (Mettler Toledo, LLC – Columbus, United States). Weight values were recorded to the nearest gram. All experimental procedures complied with the National Research Council's Guide for the Care and Use of Laboratory Animals (2011).

3.8 EXPERIMENTAL DESIGN

After the period of acclimatization (2 weeks), the animals were randomly assigned into six (6) groups (A, B, C, D, E, and F) of seven (7) rats each (n=7). Doses 250 mg/kg and 500 mg/kg body weight of *Pleurotus ostreatus* ethanol extract were adopted for this study as previously reported by Zitte and Bernard (2019) and Valappil *et al*. (2020).

Table 3.1: Summary of Experimental Design

GROUP	TREATMENT
Group A	Control
Group B	4 mg/Kg body weight of mercuric chloride only
Group C	4 mg/Kg body weight of mercuric chloride + 250 mg/kg body weight of *Pleurotus ostreatus*
Group D	4 mg/Kg body weight of mercuric chloride + 500 mg/kg body weight of *Pleurotus ostreatus*
Group E	250 mg/kg body weight of *Pleurotus ostreatus* only
Group F	500 mg/kg body weight of *Pleurotus ostreatus* only

Administration lasted for twenty-eight (28) days. All administrations were carried out via oral route using an orogastric tube.

3.9 NEUROBEHAVIOURAL ASSESSMENTS

On day 28, following the final administration of treatments, neurobehavioural evaluations were conducted to assess the functional integrity of the central nervous system. Neurobehavioural assessment involves the systematic observation of behavioural patterns to detect changes indicative of neurological dysfunction (Echefu *et al*., 2025). It is an essential investigative tool

for distinguishing between organically driven impairments and behaviours that are secondary or reactive to neurological injury (Cozza and Boccardi, 2023). To evaluate the effects of treatments on neurobehavioral activities, the tests that were carried out include; open field test (OFT), step test, string test, and movement initiation test (MIT).

3.9.1 Open Field Test

This test was performed according to the method of Olopade (2020). The open field test is widely used to evaluate exploratory and locomotory activities in rodents. The test assesses the rat's overall locomotor activity by measuring parameters such as distance traveled, velocity, and time spent moving as well as exploratory patterns, including entries into different zones within the open field. Briefly, each rat was placed in an open field, a 72 by 72 cm square box with lines on the floor dividing it into 18 by 18 cm square that allowed the definition of central and peripheral parts.

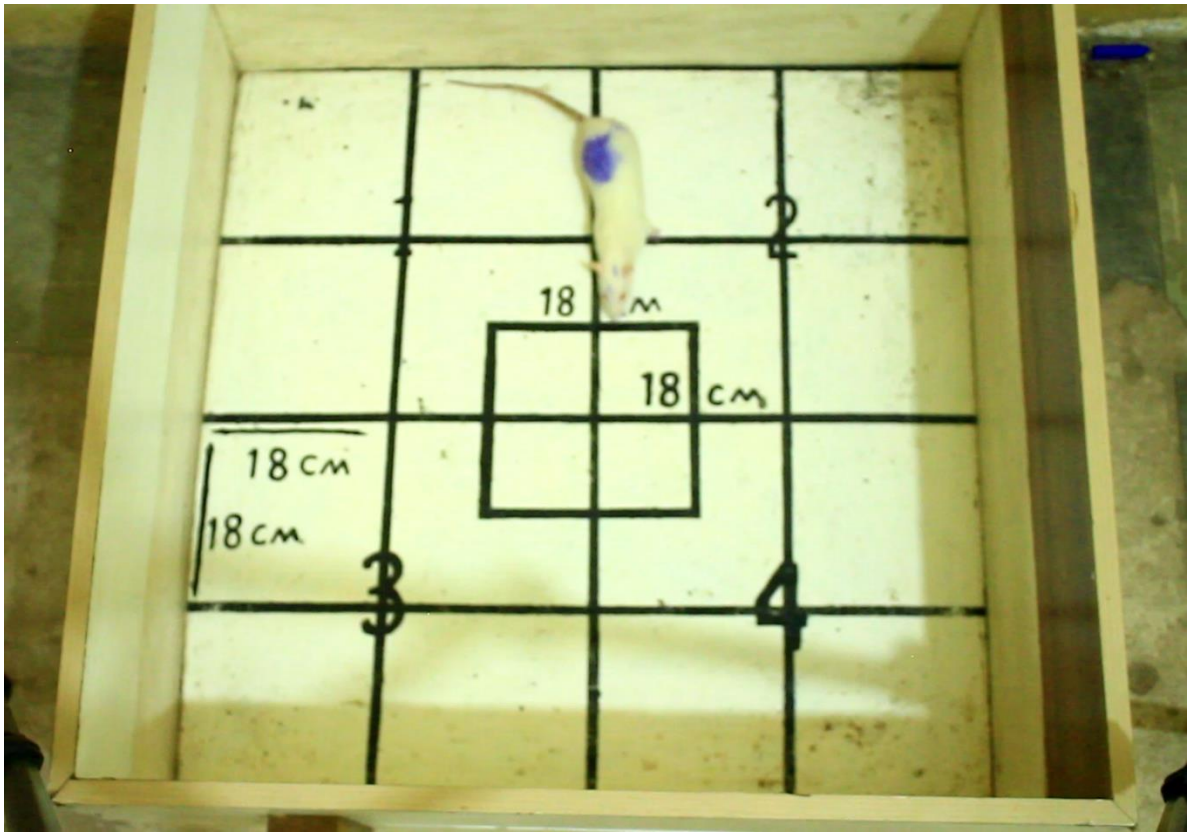

Figure 3.1: Open Field Test Apparatus

Each animal was then placed in the center of the field and the following parameters were measured:

- ✓ **Rearing:** frequency with which the animal stands on their hind limbs and raise their upper body vertically (erect postures).
- ✓ **Grooming:** Self-grooming behaviour is demonstrated by licking or scratching various regions of the body, including the face, head, fur, paws, and tail.
- ✓ **Ambulation:** total time of locomotor activity or movement within the open field arena.
- ✓ **Immobility:** absence or minimal movement of the rat within the open field arena.
- ✓ **Sniffing:** total time of sniffing behavior
- ✓ **Thigmotaxis:** the frequency with which the animal stays close to walls when exploring an open field box
- ✓ **Crossing:** total number of the square crossing during the test period
- ✓ **Central square entry:** total number of times the animal enters the central square with all four paws.

After each test, the open field box was cleaned with 70 % ethanol and allowed to dry before introducing another rat. This was done to eliminate olfactory bias.

3.9.2 String Test

The string test was used to assess grip strength and limb impairment. The steel wire is positioned at a height of 50 cm over a cushion support, and the rat is allowed to hold it with its forepaws (2 mm in diameter and 60 cm in length). The parameters measured include; latency to grip loss and limb impairment score. A cut-off time of 180 seconds was used to measure how long the rat was able to retain the wire before it broke. According to Ijomone *et al*. (2014), this latency to grip loss is regarded as a proximate indicator of grip strength. To assess limb impairment, rats were scored 3 for grasping the wire with both of their hind paws, 2 for using

one hind paw to grasp the wire and 1 for not using either hind paw to grasp the wire. The total score was used to represent the results (Ijomone *et al*., 2014).

Figure 3.2: String Test Apparatus

3.9.3 Movement Initiation Test

An isolated forelimb test was used in the MIT to evaluate the stepping movements made by each forelimb (Tillerson *et al*., 2002). To hold the weight of the animal's body with just one forelimb, the rat was hoisted above the surface of a table by its hind limbs and held by its torso. The time to initiate one step is recorded for each forelimb. To establish a score, the average of the initiation time of the two forelimbs was taken (Flemming *et al*., 2004).

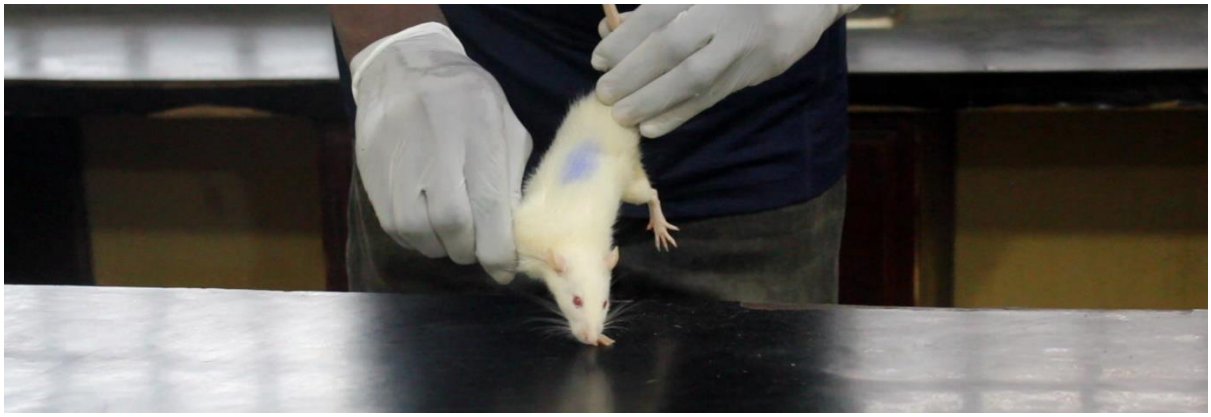

Figure 3.3: Movement Initiation Test Apparatus

3.9.4 Step Test

Postural stability is evaluated using the step test (Idemudia and Enogieru, 2025). Animals were supported throughout this test in the same way it was done during the movement initiation test, where one forelimb supports the animal's weight. The parameters measured include; right forelimb and left forelimb test. Over the course of 5 seconds, the animal is transported laterally across a tabletop at a distance of 90 cm. Each forelimb's adjustment steps are counted as the animal is moved over the table. Each forelimb's average step count over three trials is used for analysis (Ijomone *et al*., 2014).

Figure 3.4: Step Test Apparatus

3.10 EVALUATION OF BODY AND BRAIN WEIGHTS

Following completion of the neurobehavioural assessments, the rats were euthanized under low level anaesthesia, followed by cervical dislocation to ensure humane sacrifice. The brains were carefully excised, freed from adherent blood and connective tissue, and blotted dry with filter paper. Each brain was then immediately weighed using a precision electronic balance calibrated in milligrams, and the weights were recorded to the nearest two decimal places. The relative brain weights were calculated as follows:

Relative brain weight = [$absolute\ brain\ weight$ (g) / b$ody\ weight\ of\ rat$ (g)] x 100

Relative cerebellar weight = [$cerebellar\ weight\ (g)$ / f$inal\ body\ weight\ of\ rat$ (g)] x 100

Cerebellum/brain weight ratio = $cerebellar\ weight$ (g) / a$bsolute\ brain\ weight$

3.11 CEREBELLAR OXIDATIVE STRESS ASSESSMENTS

The cerebellum was removed from the brain after being harvested, blotted of blood, and weighed right away with an electronic balance calibrated in milligrams and recorded to the nearest two decimal places. The harvested and weighed hippocampi were washed twice in cold phosphate buffered saline (PBS), homogenized using acid-washed sand and PBS in porcelain mortar and pestle. The homogenate was centrifuged at 10,000 ×g for 15 minutes at 4°C. The supernatants were collected for the estimation of the various biochemical assays.

3.11.1 Estimation of Superoxide Dismutase (SOD) Activity

This was determined according to the method of Misra and Fridovich (1972)

Principle: Adrenaline undergoes autoxidation rapidly to adrenochrome whose concentration can be determined at 420 nm with the aid of a spectrophotometer. The auto-oxidation of adrenaline depends on the presence of superoxide anions. Superoxide dismutase inhibit auto-

oxidation of adrenaline by catalyzing the breakdown of superoxide anion. The degree of inhibition reflects the activity of SOD which is determined at 420 nm.

Preparation of reagents: Carbonate buffer (0.05 M) pH 10.2: this was prepared by dissolving 0.2014 g of Na_2CO_3, 0.2604 g of $NaHCO_3$ and 0.0372 g of EDTA in 100 ml of distilled water. Hydrochloric acid (0.005 M): this was prepared by adding 0.044 concentrated HCl to 99.96 ml of distilled water. Adrenaline solution (0.3 mM): this was prepared by dissolving 0.01098 g of Adrenaline in 100 ml of 0.005 M HCl solution.

Procedure: Supernatant volume of 0.2 ml was mixed with 2.5 ml of carbonate buffer and 0.3 ml of adrenaline solution; 0.2 ml of distilled water was mixed with 2.5 m of carbonate buffer and 0.3 ml adrenaline as reference sample. These were mixed and absorbance read at 420 nm.

$$\% \text{ inhibition} = [(\text{O. D test} - \text{O.D ref}) \times 100] / \text{O.D test}$$

Enzyme activity was thus calculated thus:

$$\text{SOD activity (Unit / mg protein)} = \% \text{ inhibition} / (50 \times Y)$$

Where Y = mg of protein in the volume of sample used.

3.11.2 Estimation of Catalase (CAT) Activity

This was determined by the method of Cohen *et al*. (1970).

Principle: Catalase is present in nearly all animal, plant, and bacteria cells. It acts to prevent the accumulation of noxious H_2O_2 which is converted to O_2 and H_2O.

Preparation of reagent: 0.01M KMnO4 was prepared by dissolving 0.158g of $KMnO_4$ in 100ml of distilled water; Phosphate buffer (pH 7.4); 0.426 of NaHPO4 NaH_2PO_4 was weighed and dissolved in 100ml of distilled water; 6M H_2SO_4: 32.3ml of conc. H_2SO_4 was added to 66.7 ml of distilled water 30Mm H_2O_2 solution was prepared by measuring 0.34ml of 30% of H_2O_2 in 1001ml of phosphate buffer.

Procedure: To a known volume of supernatant (0.5ml), 5.0ml of H_2O_2 was added. This was then mixed by inversion and allowed to stand for 30 minutes. The reaction was stopped by adding 6M H_2SO_2. The absorbance was taken at 480nm within 30-60 seconds against distilled water.

$$\text{Activity} = [\text{OD} \times \text{min} \times \text{Vt}] / [\text{M} \times \text{V} \times \text{L} \times \text{Y}]$$

Where, OD = absorbance

L = light path = 1cm

V1 = total volume of the reaction sample

M = molar extinction co-efficient of H_2O_2 (40/M/cm).

3.11.3 Estimation of Glutathione Peroxidase (GPx) Activity

This was determined by the method of Rotruck *et al*., (1973).

Principle: This is based on the oxidation of pyrogallol to purpurogallin by peroxidase activity, resulting to a deep brown colour disposition, read at 430 nm.

Preparation of reagent: Pyrogallol (20 mM): 0.2552g of pyrogallol was dissolved in 100 ml of distilled water.

Procedure: To an aliquot of supernatant (0.2 ml), 2.5 ml of phosphate buffer, 2.5ml of H2O2, 1.5ml of distilled water and 2.5 ml of pyrogallol was added. The reaction was allowed to stand for 30 minutes at room temperature. A deep brown color was formed which was read at 420nm.

$$\text{Activity} = [(\text{OD} / \text{Min}) \times (\text{Vt} \times \text{Df})] / [\text{E} \times \text{Vs} \times \text{Y}]$$

Where, OD = Absorbance of test

Vt = Total volume of reaction mixture

Df = Dilution factor = 1

E = Molar extinction coefficient (12/M/cm)

Vs = Volume of sample

Y = mg of protein used

3.11.4 Estimation of Malondialdehyde Concentration

Malondialdehyde was determined using the thiobarbituric acid assay (Buege and Aust, 1978).

Principle: Malondialdehyde which is a product of lipid peroxidation reacts with thiobarbituric acid to give a red species.

Preparation of reagent: Stock TCA-TBA-HCL was prepared by mixing 15 g of trichloroacetic acid, 0.375 g of thiobarbituric acid and 0.25 N hydrochloric acid. This solution was mildly heated to assist in the dissolution of the thiobarbituric acid.

Procedure: A volume of supernatant (1.0 ml) was added to 2.0 ml of TCA-TBA-HCL and mixed thoroughly. The solution was heated for 15 minutes in a boiling water bath. After cooling, the flocculent precipitate was removed by centrifuging at 1000 g for 10 minutes. The absorbance was determined at 535nm against a blank. The concentration of MDA was determined using the formula:

$$\text{MDA (unit/mg protein)} = (A \times Vt \times 1000) / (M \times V \times 1 \times Y)$$

Where, A = absorbance of sample test at 535nm

Vt = total volume of the reaction = 3ml

M = molar extinction co-efficient of product = 1.56 × 105m-1cm-1

l = light path = 1cm

V = volume of tissue extract used = 1ml

Y = mg of tissue in the volume of sample used

3.12 ESTIMATION OF MERCURY CONTENT

Mercury retention in brain tissue was determined using a mercury analyzer equipped for cold vapor atomic absorption spectrometry (CVAAS). At the end of the experimental period, brain tissues were excised, blotted dry, and accurately weighed. Samples were then digested with a

mixture of nitric acid and sulfuric acid under controlled temperature conditions until a clear solution was obtained. The digests were cooled, filtered, and analyzed for total mercury content using the mercury analyzer according to the manufacturer's protocol. The mercury concentrations were expressed in micrograms per gram (µg/g) of wet tissue weight. All measurements were carried out in triplicate to ensure accuracy and reproducibility (Verma et al., 2023).

3.13 HISTOLOGICAL PROCESSING OF CEREBELLAR TISSUE

Briefly, the excised cerebellum tissues were fixed in 10% buffered formal saline and processed by paraffin embedding with sections cut at 5µm thickness. The paraffin wax embedding method of Drury and Wallington (1980) was used to prepare the tissues. They were each dehydrated for an hour at room temperature using ethanol concentrations of 70%, 90%, absolute ethanol I, and absolute ethanol II. Two xylene changes at room temperature, lasting an hour each, was used to clear dehydrated tissue. The tissues were soaked in two separate batches of molten paraffin wax for one hour each at 60 °C before being embedded in multi block paraffin wax molds. The paraffin blocked tissues were cut into smaller pieces and put on a wooden chuck for rotary microtome sectioning. A rotary microtome was used to slice the tissue blocks into sections that were 5 µm thick. To spread the folded ribbons, the sections were placed in a water bath at 40 °C. These pieces were fixed to a fresh, spotless glass slide. To increase the adherence of the sections to the slides, these were dried at 40 °C using a slide dryer.

3.14 HEMATOXYLIN AND EOSIN STAINING PROCEDURES

Haematoxylin and Eosin staining on the cerebelli sections was carried out according to methods described by Drury and Wallington (1980). The sections were dewaxed in two changes of xylene, spending approximately two minutes in each to effectively remove the paraffin. Following dewaxing, the tissues were rehydrated through descending grades of ethanol—

absolute ethanol II, absolute ethanol I, 95%, 90%, 70%, and 50%—with each step lasting two minutes. The rehydrated sections were then rinsed in distilled water for three minutes before being stained in hematoxylin for 15–20 minutes.

To remove excess hematoxylin, the slides were rinsed under running tap water for two to three minutes and examined microscopically to confirm the adequacy of nuclear staining. This was followed by differentiation in acid alcohol (0.5% HCl in 70% ethanol) for two to three minutes to achieve clearer nuclear definition. After differentiation, the slides were rinsed thoroughly in running water for 10–15 minutes, then counterstained in 1% aqueous eosin for two to four minutes to highlight the cytoplasm. Excess eosin stain was removed by washing in running water, and the sections were again observed under the microscope to verify appropriate staining intensity. The sections were then dehydrated in ascending grades of ethanol, cleared in xylene, and mounted using a synthetic resin mounting medium (DPX) for microscopic evaluation.

3.15 PHOTOMICROGRAPHY

The sections of the cerebellum were obtained and examined under an Olympus DP71 Digital Camera mounted on a 12.0 MP Eakins USB Digital Microscope Camera. The camera features 12 megapixels (3488×2616 pixel) high resolution colour digital camera and 0.5X reduction lengths connected to a laptop on which was installed ToUPView Software (version x64,3,7,71,49,2016). A view of the slides was captured using x10 and x40 objective lenses.

3.16 STATISTICAL ANALYSIS

The obtained data were analysed using the IBM Statistical Package for the Social Sciences (SPSS), Version 23 (International Business Machines Corporation [IBM], Armonk, NY, USA; 2015). All values were presented as mean ± standard error of the mean (SEM) for all experimental groups. Significance was determined using one-way analysis of variance (ANOVA) followed by Tukey's multiple comparisons *post hoc* test, and a *p*-value less than 0.05 ($p < 0.05$) was considered statistically significant.

CHAPTER FOUR

RESULTS

4.1 MYCOCHEMICAL SCREENING

Table 4.1 shows the qualitative mycochemical constituents of *Pleurotus ostreatus*. Results showed the presence of glycosides, Phenols, Terpenoids, Alkaloids, Flavonoids, Saponins and Tannins, while Eugenols, Steroids and Reducing sugars were absent.

Table 4.2 shows the quantitative estimation of mycochemical constituents of *Pleurotus ostreatus*. Results showed that the highest concentration was tannins, with Alkaloids having the least concentration.

Table 4.1: Qualitative screening of mycochemical constituents of *Pleurotus ostreatus* ethanol extract

S/N	CONSTITUENTS	RESULT
1.	Glycosides	+
2.	Saponins	+
3.	Phenols	+
4.	Eugenols	-
5.	Terpenoids	+
6.	Steroids	-
7.	Alkaloids	+
8.	Flavonoids	+
9.	Tannins	+
10.	Reducing Sugar	-

+: Present

-: Absent

Table 4.2: Quantitative estimation of mycochemical constituents of *Pleurotus ostreatus* ethanol extract

S/N	CONSTITUENTS	CONCENTRATION (mg/100g)
1.	Alkaloid	1.25 ±0.04
2.	Tannins	31.43 ±0.66
3.	Phenolics	29.41 ±0.48
4.	Saponins	18.95 ±1.15
5.	Flavonoid	25.45 ±1.33

4.2 PROXIMATE ANALYSIS

Table 4.3 shows the proximate composition of *Pleurotus ostreatus*. Results showed that carbohydrate content and ash content were the most composition, with protein content being the least.

Table 4.3: Proximate composition of ethanol extract of *Pleurotus ostreatus*

S/N	PARAMETERS	
1.	MOISTURE (%)	7.2
2.	PROTEIN (%)	4.0
3.	FAT (%)	5.0
4.	FIBRE (%)	5.1
5.	ASH (%)	8.4
6.	CARBOHYDRATE (%)	70.3

4.3 DPPH RADICAL SCAVENGING ACTIVITY

Figures 4.1 and 4.2 illustrate the DPPH radical scavenging activity of *Pleurotus ostreatus* and ascorbic acid (used as the standard antioxidant) across a concentration range of 0–250 µg/mL. Figure 4.1 presents the corresponding absorbance values, while Figure 4.2 displays the percentage inhibition of DPPH radicals. Results showed a clear concentration-dependent antioxidant effect with increased concentrations resulting in lower absorbance values and higher % inhibition. *Pleurotus ostreatus* exhibited notable radical scavenging activity that, while slightly lower, was comparable to that of Ascorbic acid.

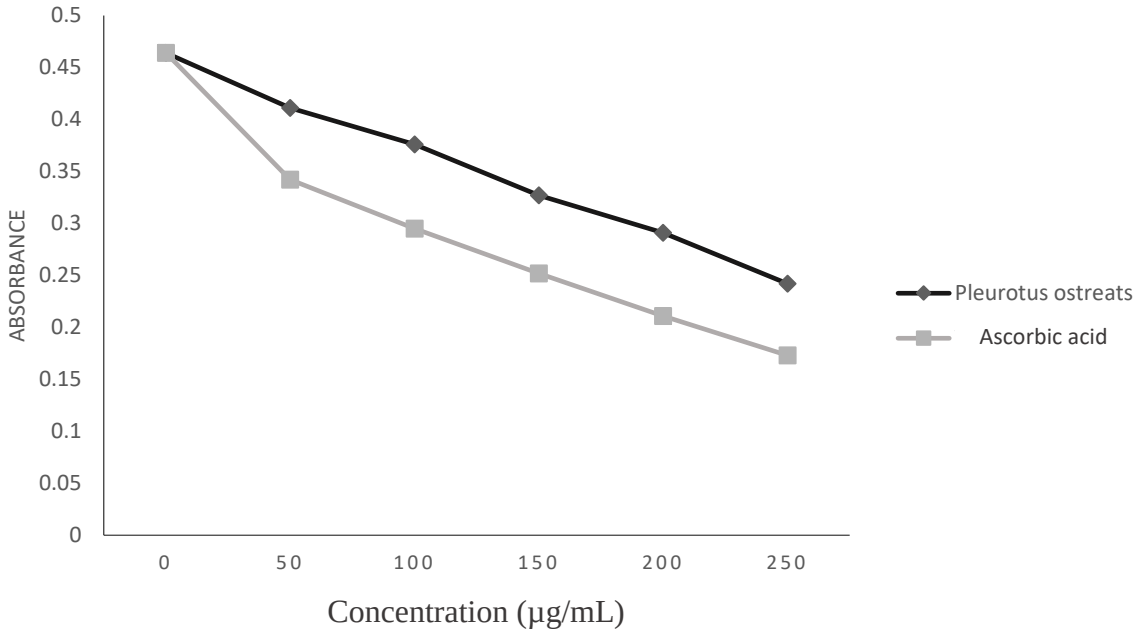

Figure 4.1: DPPH Absorbance of *Pleurotus ostreatus* and Ascorbic acid

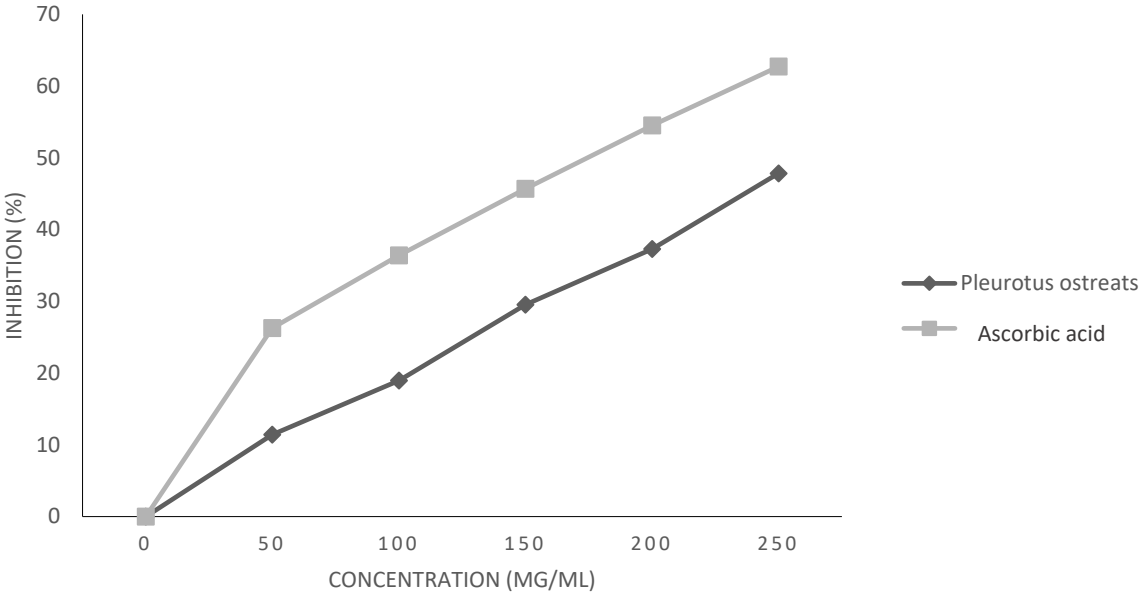

Figure 4.2: DPPH % Inhibition by *Pleurotus ostreatus* and ascorbic acid

4.4 EFFECT OF TREATMENT ON BODY AND BRAIN WEIGHTS

Figure 4.3 shows the initial body weights across the experimental groups. There was no significant difference (p >0.05) in the initial body weight across the experimental groups.

Figure 4.4 shows the final body weights across the experimental groups. There was a significant decrease (p <0.05) in the final body weight of rats treated with $HgCl_2$ compared to control. However, there was a significant increase (p <0.05) in the $HgCl_2$-exposed rats treated with *Pleurotus ostreatus w*hen compared to $HgCl_2$ only. There was no significant difference (p >0.05) in the *Pleurotus ostreatus* only groups when compared to control.

Figure 4.5 shows the body weight change (difference in initial and final body weights) across the experimental groups. There was a significant decrease (p <0.05) in the body weight change of rats treated with $HgCl_2$ only when compared to control. However, there was a significant increase (p <0.05) in the $HgCl_2$-exposed rats treated with *Pleurotus ostreatus w*hen compared to $HgCl_2$ only. There was no significant difference (p >0.05) in the *Pleurotus ostreatus* only groups when compared to control.

Figure 4.6 shows the whole brain weights across experimental groups. There was a significant decrease (p <0.05) in the whole brain weights of rats treated with $HgCl_2$ only when compared to control. However, there was a significant increase (p <0.05) in the $HgCl_2$-exposed rats treated with *Pleurotus ostreatus w*hen compared to $HgCl_2$ only. There was no significant difference (p >0.05) in the *Pleurotus ostreatus* only groups when compared to control.

Figure 4.7 shows the relative brain weights across experimental groups. There was a significant decrease (p <0.05) in the relative brain weights of rats treated with $HgCl_2$ only when compared to control. However, there was a significant increase (p <0.05) in the $HgCl_2$-exposed rats treated with *Pleurotus ostreatus w*hen compared to $HgCl_2$ only. There was no significant difference (p >0.05) in the *Pleurotus ostreatus* only groups when compared to control.

Figure 4.8 shows the cerebellar weights across the experimental groups. There was a significant decrease (p <0.05) in the cerebellar weights of rats treated with $HgCl_2$ only when compared to control. However, there was a significant increase (p <0.05) in the $HgCl_2$-exposed rats treated with *Pleurotus ostreatus w*hen compared to $HgCl_2$ only. There was no significant difference (p >0.05) in the *Pleurotus ostreatus* only groups when compared to control.

Figure 4.9 shows the relative cerebellar weights across the experimental groups. There was a significant decrease (p <0.05) in the relative cerebellar weights of rats treated with $HgCl_2$ only when compared to control. However, there was a significant increase (p <0.05) in the $HgCl_2$-exposed rats treated with *Pleurotus ostreatus w*hen compared to $HgCl_2$ only. There was no significant difference (p >0.05) in the *Pleurotus ostreatus* only groups when compared to control.

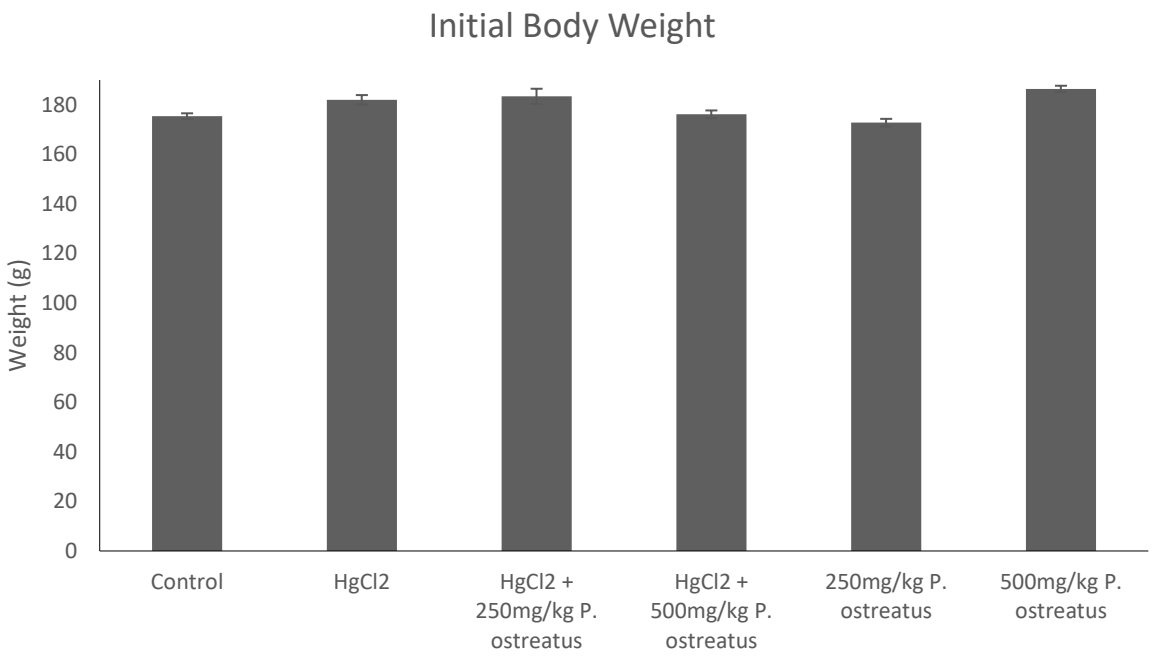

Figure 4.3: Initial body weight across experimental groups.

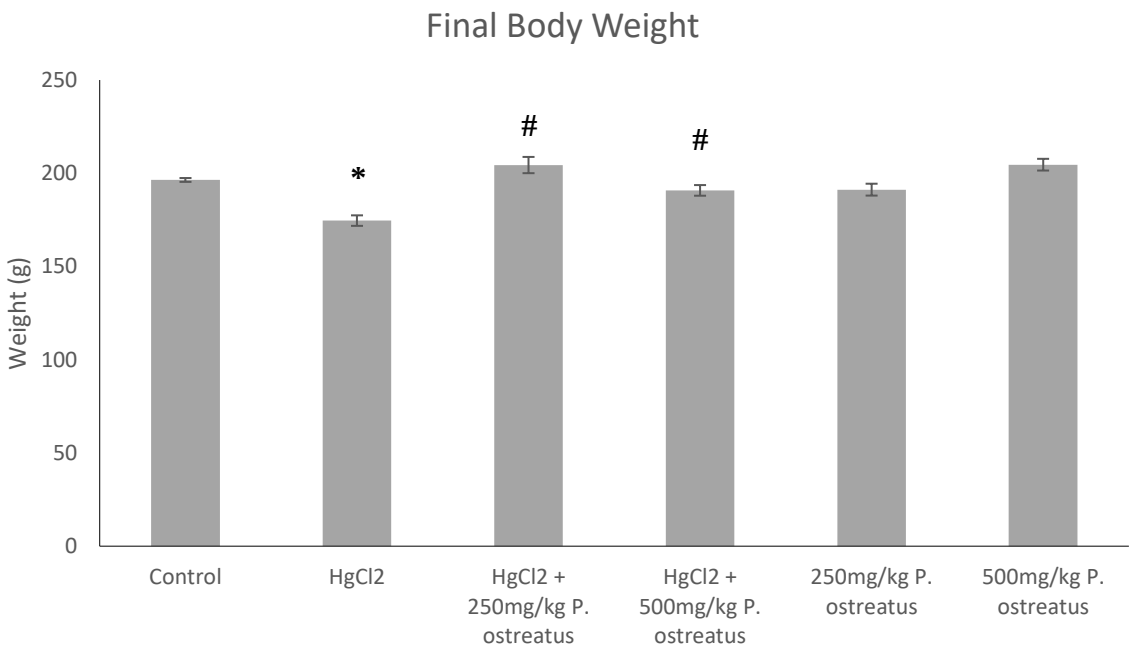

Figure 4.4: Final body weights across experimental groups.

* p <0.05 compared with control group; # p <0.05 compared with $HgCl_2$ only group.

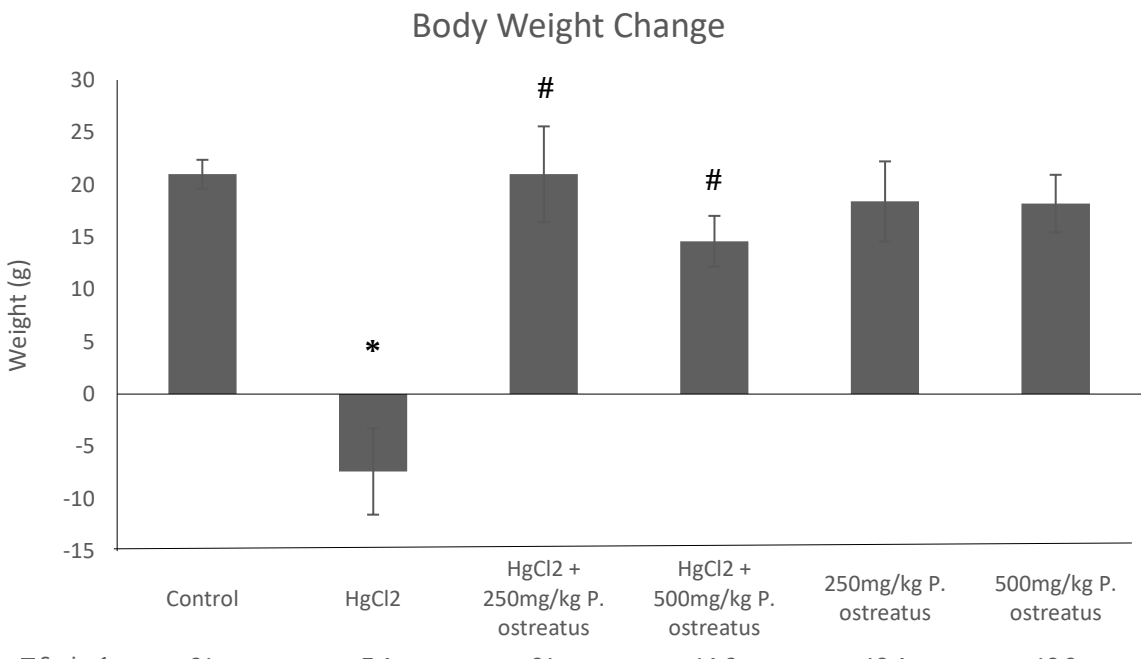

Figure 4.5: Body Weight Change (difference in initial and final body weights) across the experimental groups.

* p <0.05 compared with control group; # p <0.05 compared with $HgCl_2$ only group.

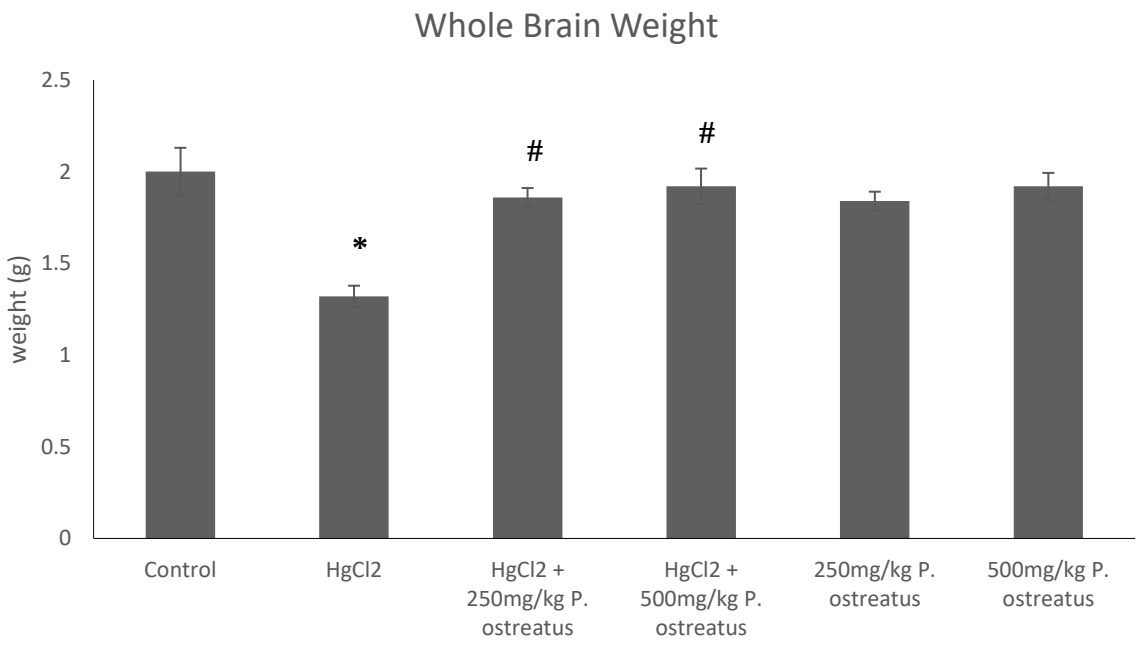

Figure 4.6: Whole Brain Weight across the experimental groups.

* p <0.05 compared with control group; # p <0.05 compared with $HgCl_2$ only group.

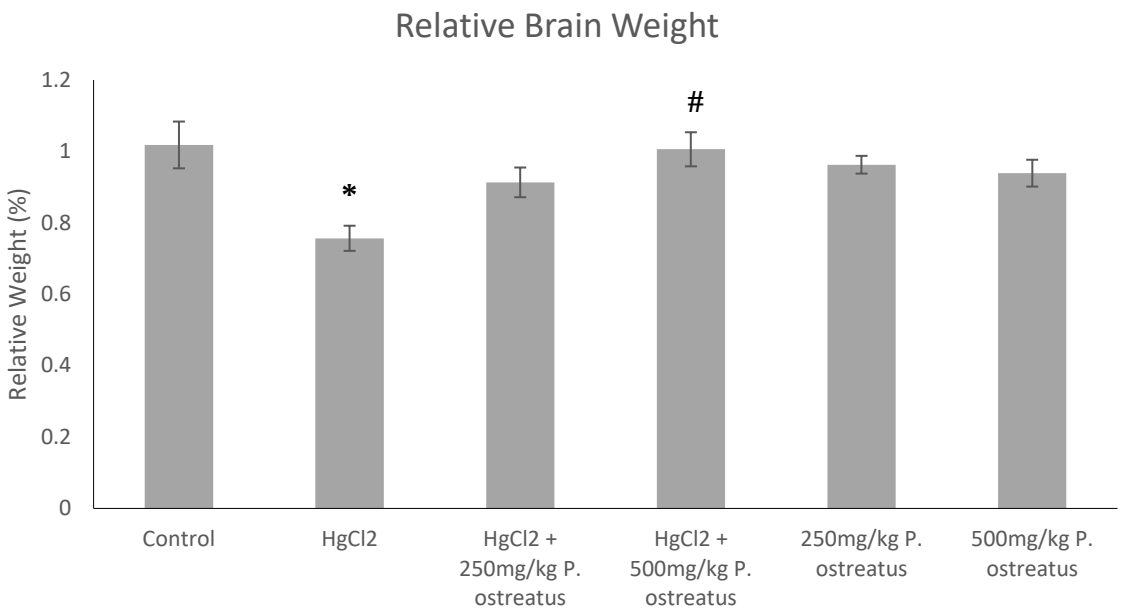

Figure 4.7: Relative Brain Weight across the experimental groups.

* p <0.05 compared with control group; # p <0.05 compared with $HgCl_2$ only group.

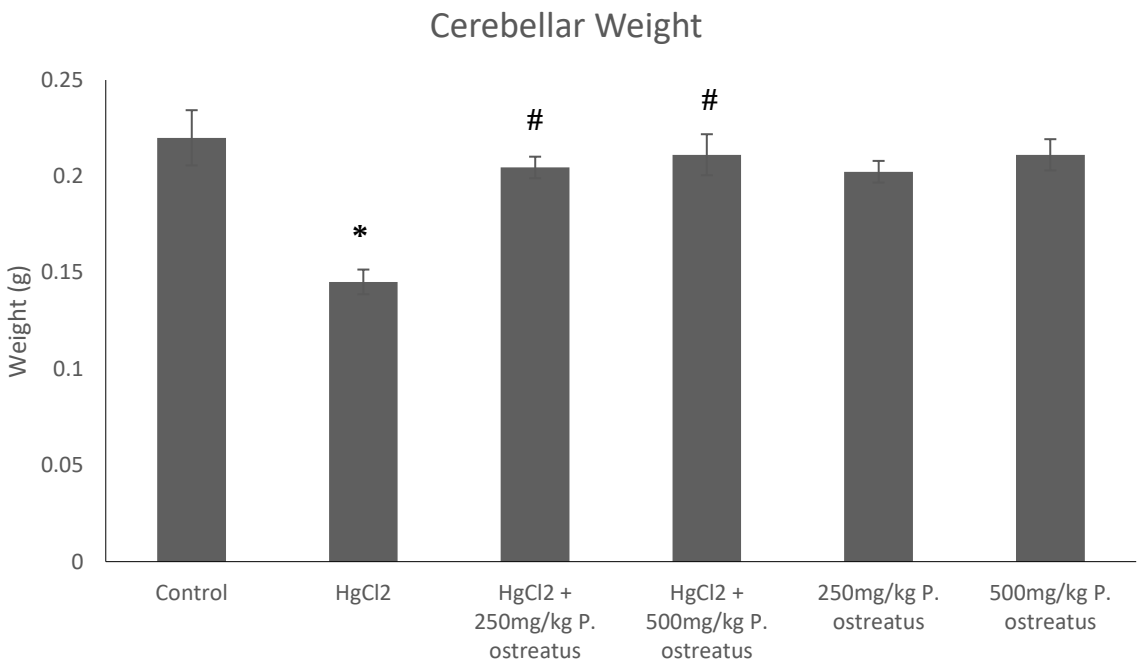

Figure 4.8: Cerebellar Weights across the experimental groups.

* p <0.05 compared with control group; # p <0.05 compared with $HgCl_2$ only group.

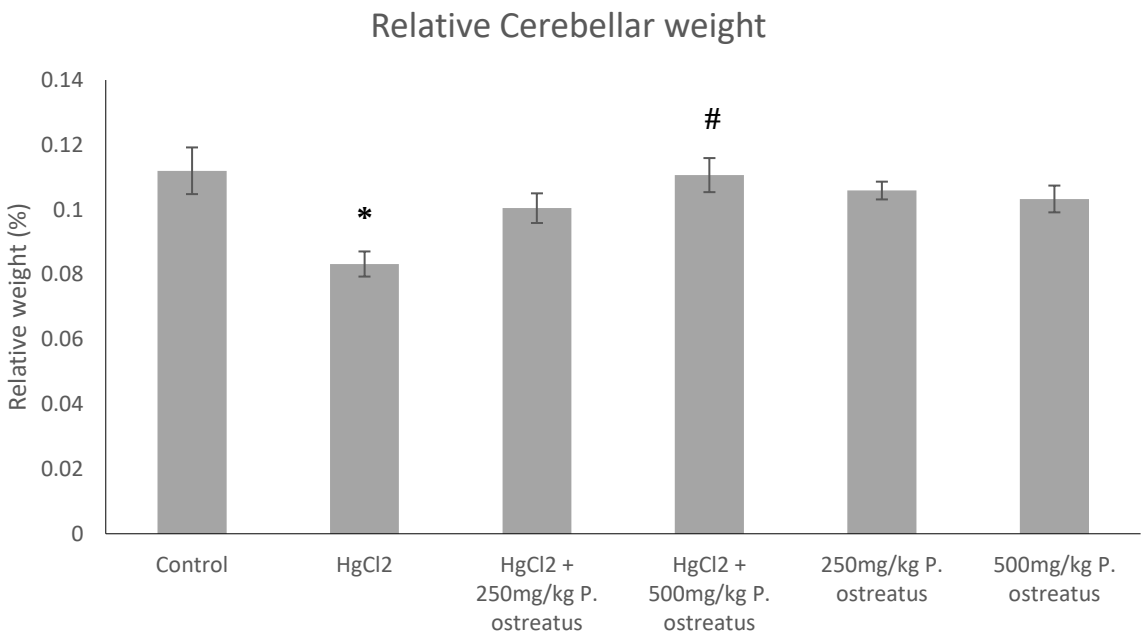

Figure 4.9: Relative cerebellar Weight across the experimental groups.

* p <0.05 compared with control group; # p <0.05 compared with $HgCl_2$ only group.

4.5 EFFECT OF TREATMENT ON NEUROBEHAVIOURAL ACTIVITY

4.5.1 Open Field Test

Figure 4.10 shows the rearing frequency across the experimental groups. There was a significant decrease (p <0.05) in the rearing frequency of rats treated with $HgCl_2$ only when compared to control. However, there was a significant increase (p <0.05) in the $HgCl_2$-exposed rats treated with *Pleurotus ostreatus w*hen compared to $HgCl_2$ only. There was no significant difference (p >0.05) in the *Pleurotus ostreatus* only groups when compared to control.

Figure 4.11 shows the grooming time across the experimental groups. There was a significant increase (p <0.05) in the grooming time of rats treated with $HgCl_2$ only when compared to control. However, there was a significant decrease (p <0.05) in the $HgCl_2$-exposed rats treated with *Pleurotus ostreatus w*hen compared to $HgCl_2$ only. There was no significant difference (p >0.05) in the *Pleurotus ostreatus* only groups when compared to control.

Figure 4.12 shows the ambulation duration across the experimental groups. There was a significant decrease (p <0.05) in the ambulation time of rats treated with $HgCl_2$ only when compared to control. However, there was a significant increase (p <0.05) in the $HgCl_2$-exposed rats treated with *Pleurotus ostreatus w*hen compared to $HgCl_2$ only. There was no significant difference (p >0.05) in the *Pleurotus ostreatus* only groups when compared to control.

Figure 4.13 shows the immobility time across the experimental groups. There was a significant increase (p <0.05) in the immobility time of rats treated with $HgCl_2$ only when compared to control. However, there was a significant decrease (p <0.05) in the $HgCl_2$-exposed rats treated with *Pleurotus ostreatus w*hen compared to $HgCl_2$ only. There was no significant difference (p >0.05) in the *Pleurotus ostreatus* only groups when compared to control.

Figure 4.14 shows the thigmotaxic frequency across the experimental groups. There was a significant increase (p <0.05) in the thigmotaxic frequency of rats treated with $HgCl_2$ only

when compared to control. However, there was a significant decrease (p <0.05) in the $HgCl_2$-exposed rats treated with *Pleurotus ostreatus w*hen compared to $HgCl_2$ only. There was no significant difference (p >0.05) in the *Pleurotus ostreatus* only groups when compared to control.

Figure 4.15 shows the sniffing time across the experimental groups. There was a significant increase (p <0.05) in the sniffing time of rats treated with $HgCl_2$ only when compared to control. However, there was a significant decrease (p <0.05) in the $HgCl_2$-exposed rats treated with *Pleurotus ostreatus w*hen compared to $HgCl_2$ only. There was no significant difference (p >0.05) in the *Pleurotus ostreatus* only groups when compared to control.

Figure 4.16 shows the central square entry across the experimental groups. There was a significant decrease (p <0.05) in the grooming time of rats treated with $HgCl_2$ only when compared to control. However, there was a significant increase (p <0.05) in the $HgCl_2$-exposed rats treated with *Pleurotus ostreatus w*hen compared to $HgCl_2$ only. There was no significant difference (p >0.05) in the *Pleurotus ostreatus* only groups when compared to control.

Figure 4.17 shows the crossing frequency across the experimental groups. There was a significant decrease (p <0.05) in the crossing frequency of rats treated with $HgCl_2$ only when compared to control. However, there was a significant increase (p <0.05) in the $HgCl_2$-exposed rats treated with *Pleurotus ostreatus w*hen compared to $HgCl_2$ only. There was no significant difference (p >0.05) in the *Pleurotus ostreatus* only groups when compared to control.

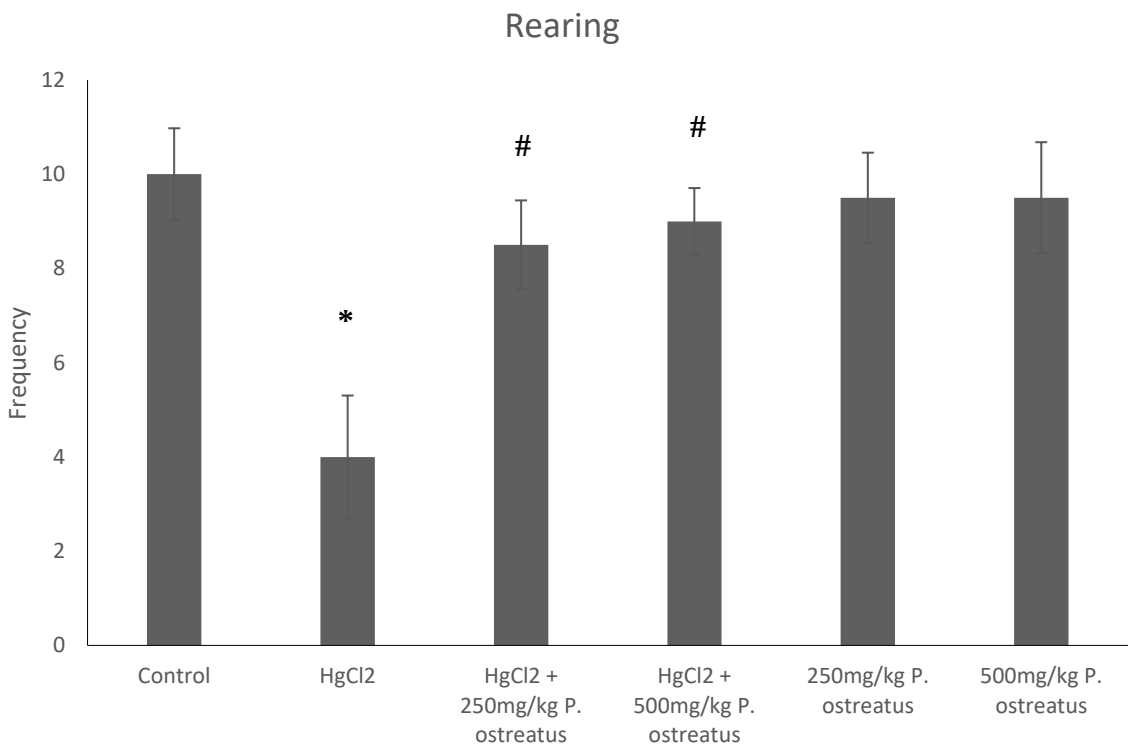

Figure 4.10: Rearing frequency across the experimental groups

* p <0.05 compared with control group; # p <0.05 compared with $HgCl_2$ only group.

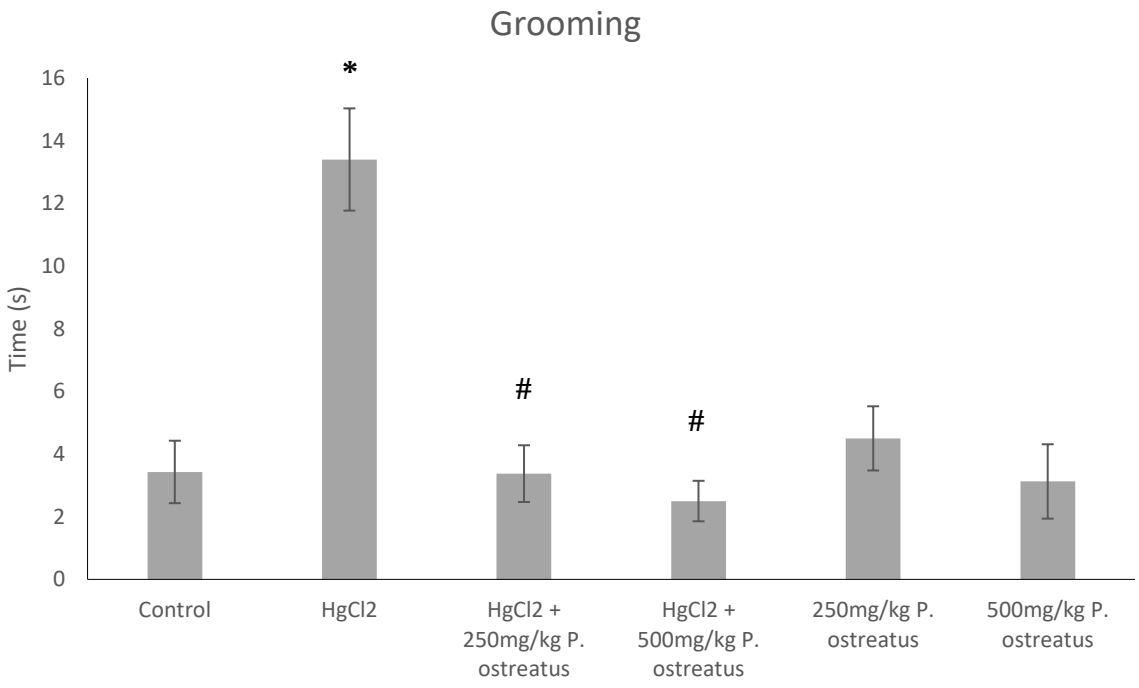

Figure 4.11: Grooming time across the experimental groups

* p <0.05 compared with control group; # p <0.05 compared with $HgCl_2$ only group.

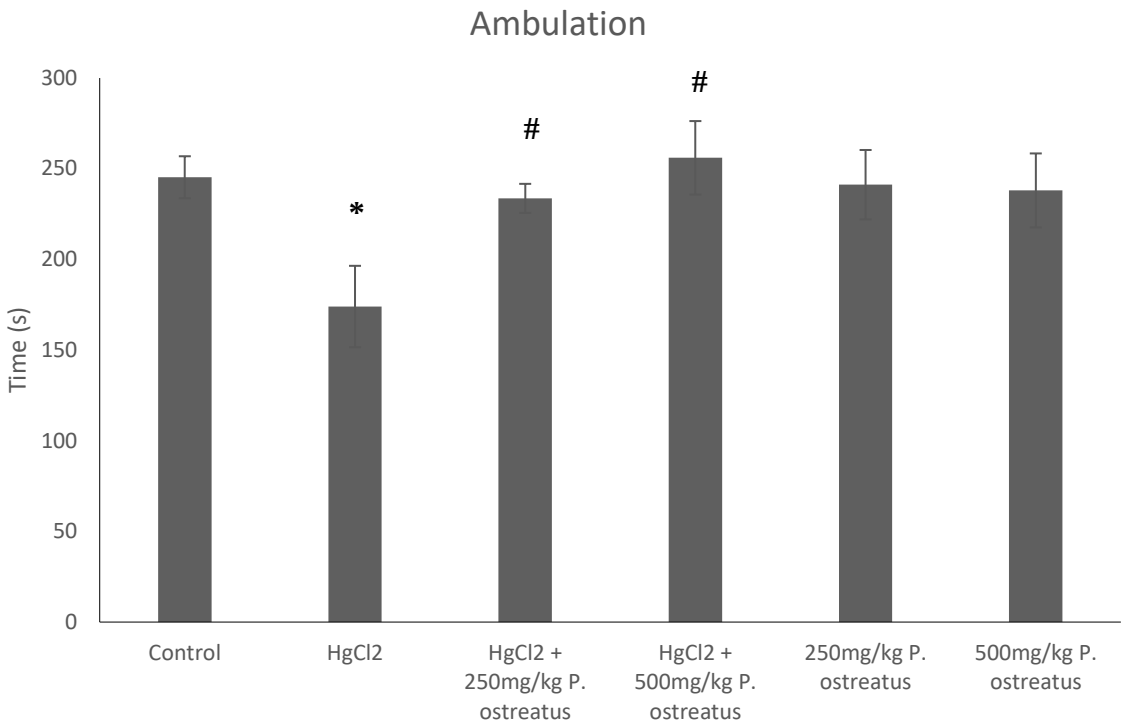

Figure 4.12: Ambulation time across the experimental groups

* p <0.05 compared with control group; # p <0.05 compared with $HgCl_2$ only group.

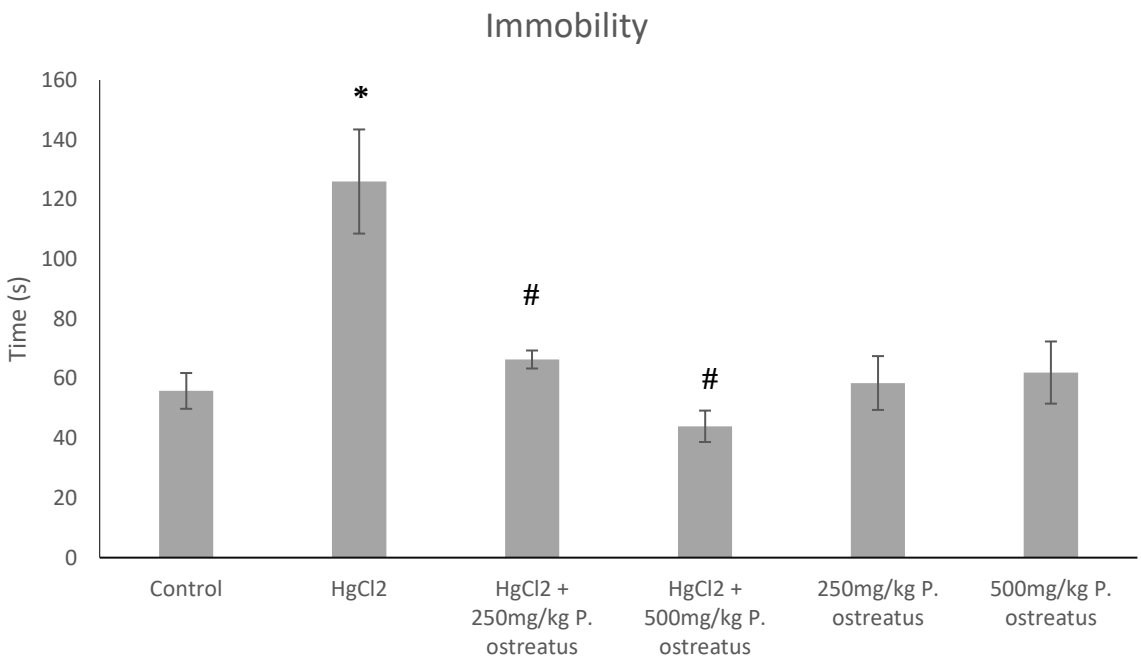

Figure 4.13: Immobility time across the experimental groups

* p <0.05 compared with control group; # p <0.05 compared with $HgCl_2$ only group.

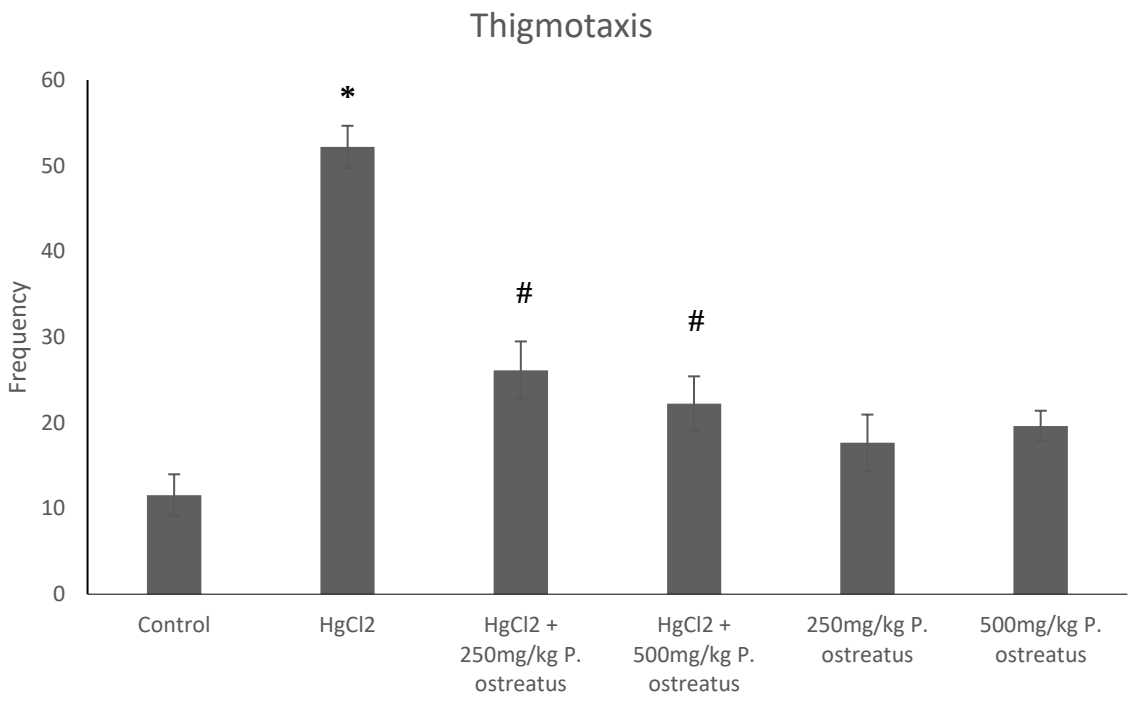

Figure 4.14: Thigmotaxis across the experimental groups

* p <0.05 compared with control group; # p <0.05 compared with $HgCl_2$ only group.

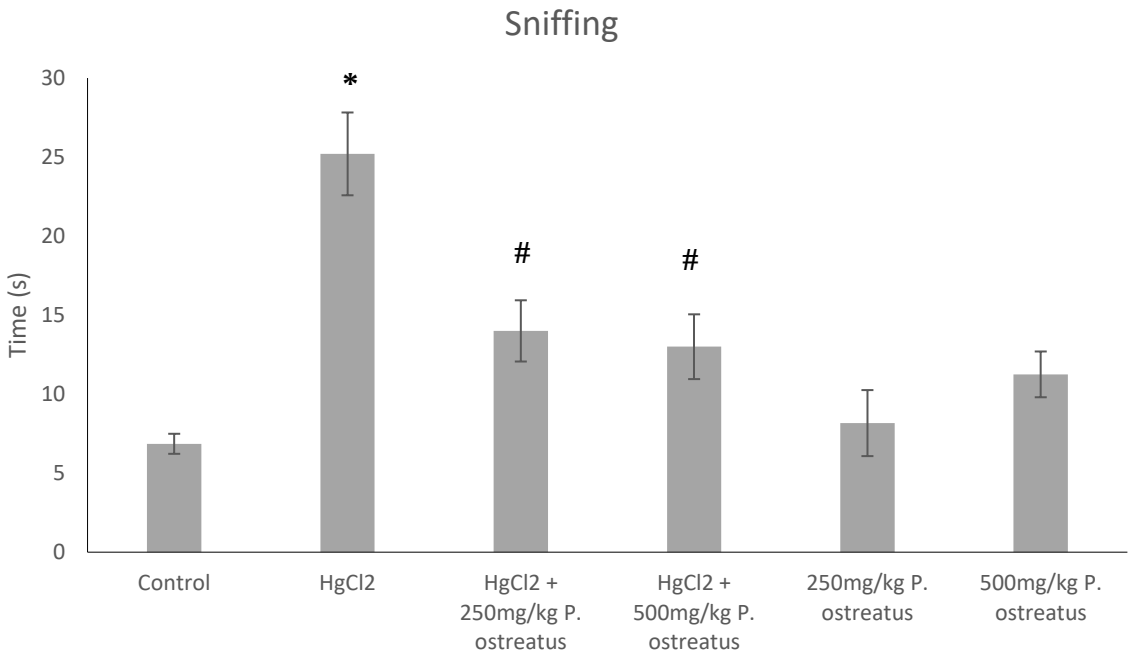

Figure 4.15: Sniffing time across the experimental groups

* p <0.05 compared with control group; # p <0.05 compared with $HgCl_2$ only group.

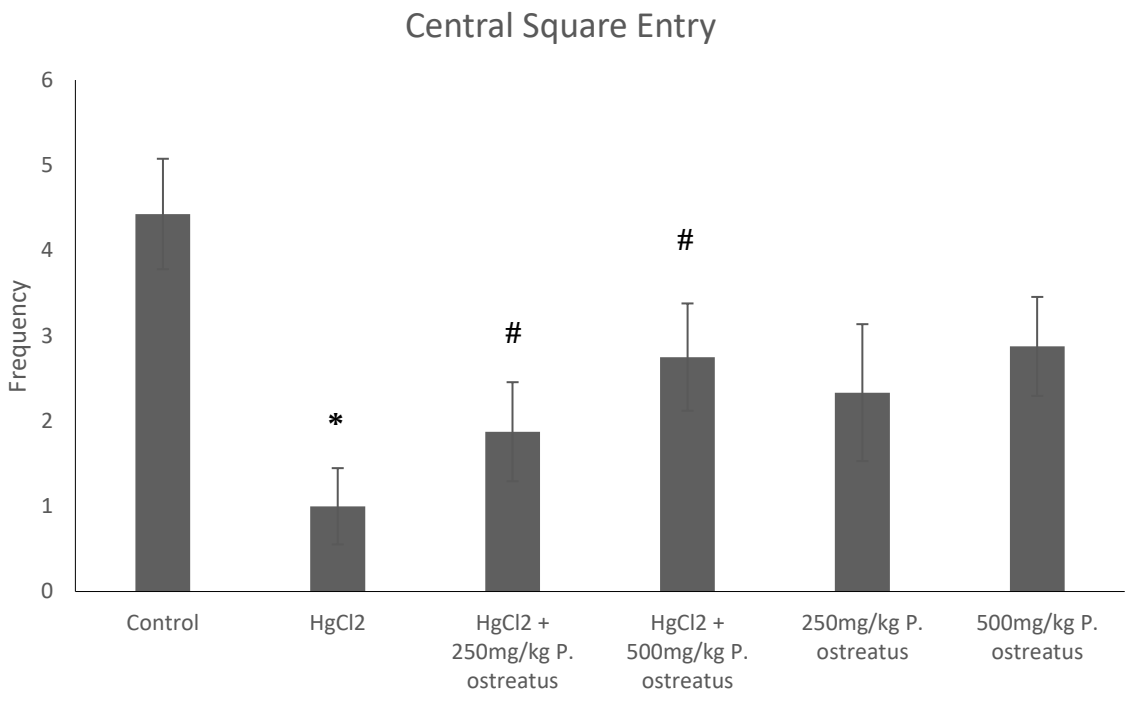

Figure 4.16: Central square entry frequency across the experimental groups

* p <0.05 compared with control group; # p <0.05 compared with $HgCl_2$ only group.

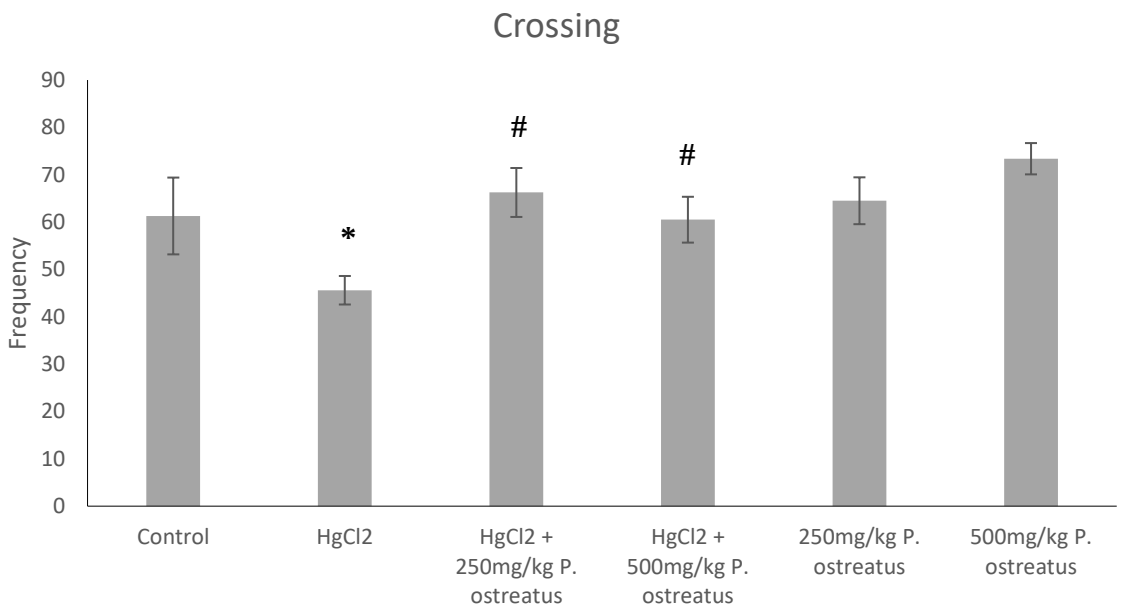

Figure 4.17: Crossing frequency across the experimental groups

* p <0.05 compared with control group; # p <0.05 compared with $HgCl_2$ only group.

4.5.2 String Test

Figure 4.18 shows the latency to grip loss across the experimental groups. There was a significant decrease (p <0.05) in the latency to grip loss of rats treated with $HgCl_2$-only when compared to control. However, there was a significant increase (p <0.05) in the $HgCl_2$-exposed rats treated with *Pleurotus ostreatus w*hen compared to $HgCl_2$ only. There was no significant difference (p >0.05) in the *Pleurotus ostreatus* only groups when compared to control.

Figure 4.19 shows the limb impairment score across the experimental groups. There was a significant decrease (p <0.05) in the latency to grip loss of rats treated with $HgCl_2$-only when compared to control. However, there was a significant increase (p <0.05) in the $HgCl_2$-exposed rats treated with *Pleurotus ostreatus w*hen compared to $HgCl_2$ only. There was no significant difference (p >0.05) in the *Pleurotus ostreatus* only groups when compared to control.

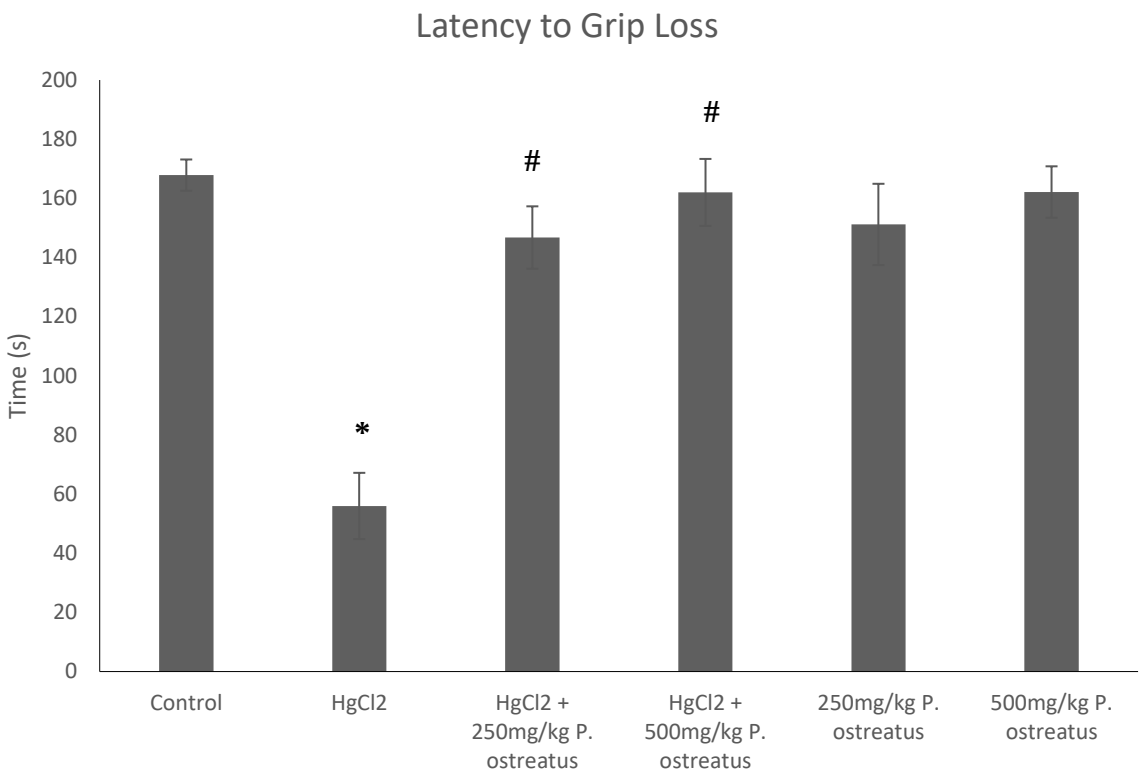

Figure 4.18: Latency to Grip Loss across the experimental groups

* p <0.05 compared with control group; # p <0.05 compared with $HgCl_2$ only group.

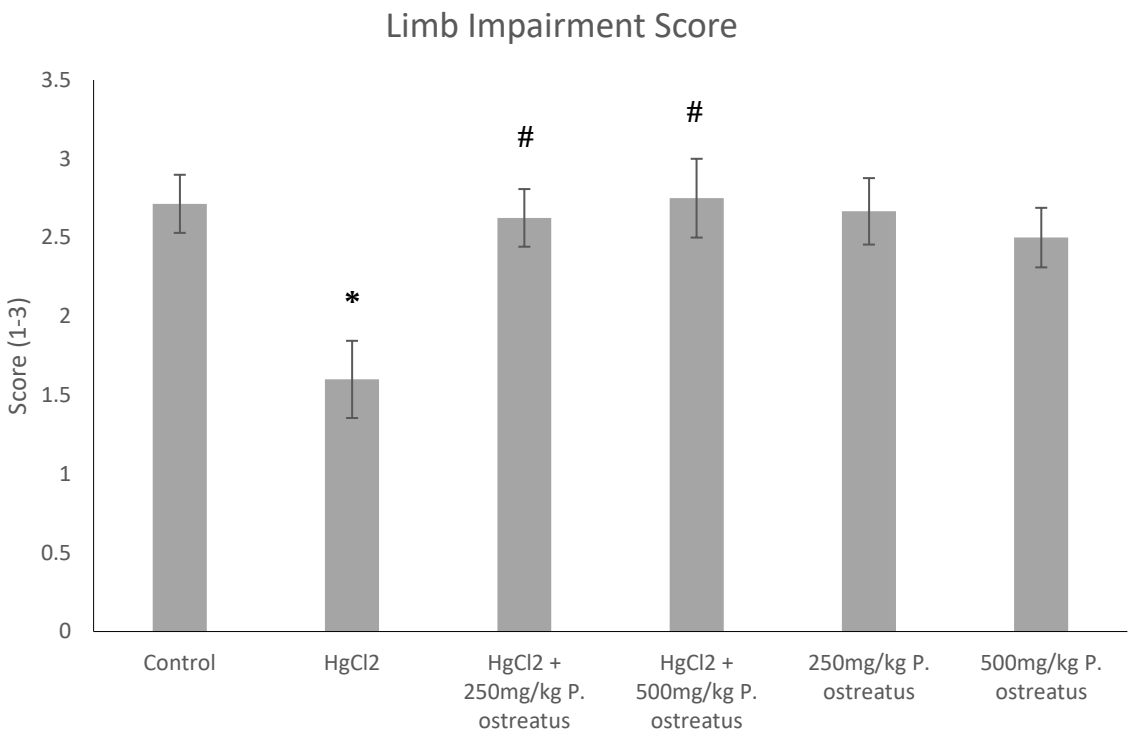

Figure 4.19: Latency impairment Score across the experimental groups

* p <0.05 compared with control group; # p <0.05 compared with $HgCl_2$ only group.

4.5.3 Movement Initiation Test

Figure 4.20 shows the movement initiation time across the experimental groups. There was a significant increase (p <0.05) in the movement initiation time of rats treated with $HgCl_2$-only when compared to control. Conversely, there was a significant decrease (p <0.05) in the $HgCl_2$-exposed rats treated with *Pleurotus ostreatus w*hen compared to $HgCl_2$ only. There was no significant difference (p >0.05) in the *Pleurotus ostreatus* only groups when compared to control.

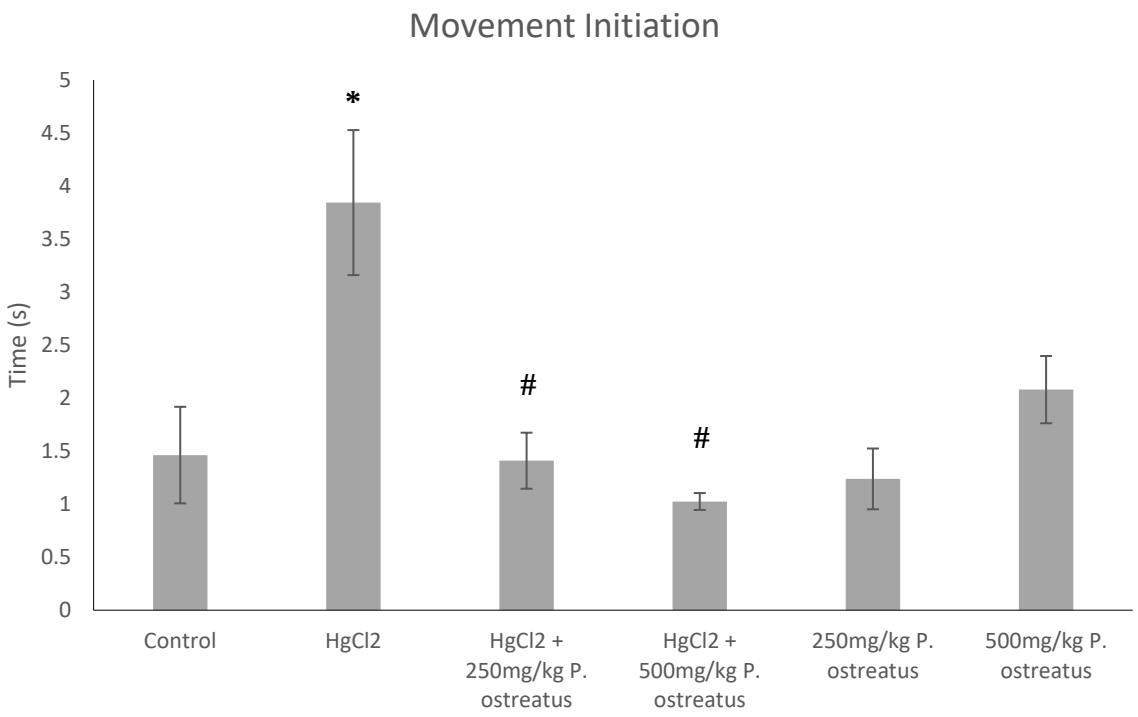

Figure 4.20: Movement Initiation time across the experimental groups

* p <0.05 compared with control group; # p <0.05 compared with $HgCl_2$ only group.

4.5.4 Step Test

Figure 4.21 shows the step test duration across the experimental groups. There was a significant decrease (p <0.05) in the movement initiation time of rats treated with $HgCl_2$-only when compared to control. Conversely, there was a significant increase (p <0.05) in the $HgCl_2$-exposed rats treated with *Pleurotus ostreatus w*hen compared to $HgCl_2$ only. There was no significant difference (p >0.05) in the *Pleurotus ostreatus* only groups when compared to control.

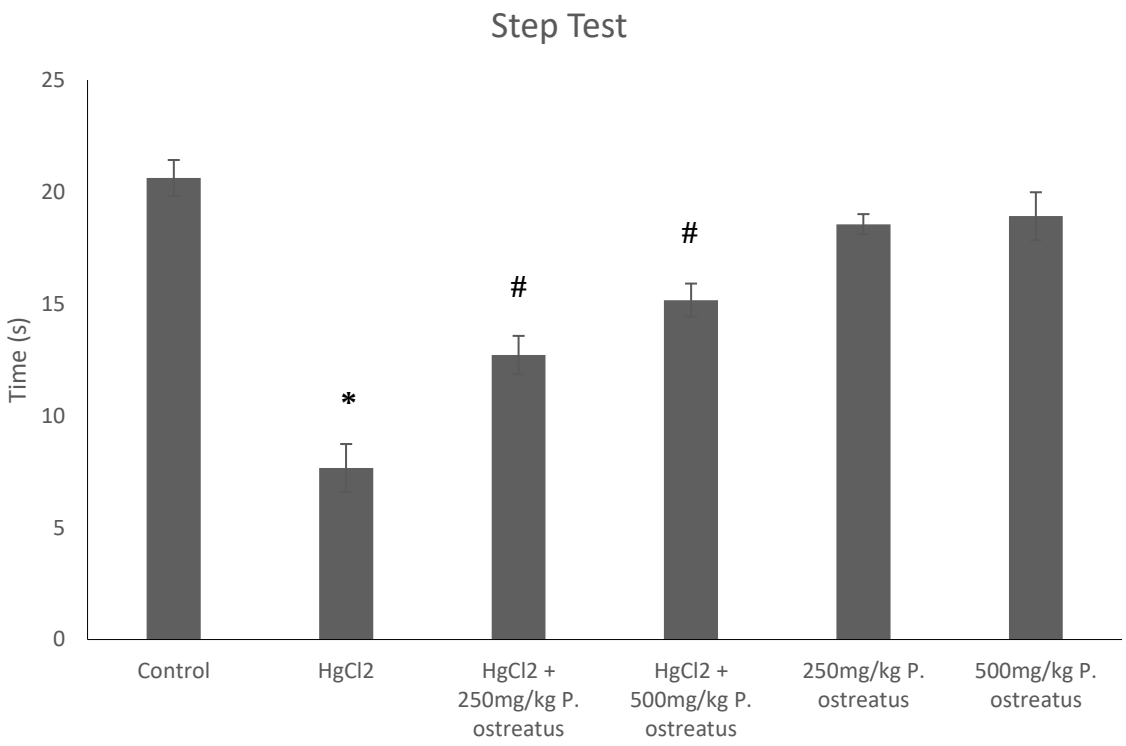

Figure 4.21: Step test time across the experimental groups

* p <0.05 compared with control group; # p <0.05 compared with $HgCl_2$ only group.

4.6 EFFECT OF TREATMENT ON ANTIOXIDANT ENZYMES ACTIVITY

Figure 4.22 shows the superoxide dismutase (SOD) activity across the experimental groups. There was a significant decrease (p <0.05) in SOD activity of rats treated with $HgCl_2$-only when compared to control. However, there was a significant increase (p <0.05) in the $HgCl_2$-exposed rats treated with *Pleurotus ostreatus w*hen compared to $HgCl_2$ only. There was no significant difference (p >0.05) in the *Pleurotus ostreatus* only groups when compared to control.

Figure 4.23 shows the Catalase (CAT) activity across the experimental groups. There was a significant decrease (p <0.05) in CAT activity of rats treated with $HgCl_2$-only when compared to control. However, there was a significant increase (p <0.05) in the $HgCl_2$-exposed rats treated with *Pleurotus ostreatus w*hen compared to $HgCl_2$ only. There was no significant difference (p >0.05) in the *Pleurotus ostreatus* only groups when compared to control.

Figure 4.24 shows the Glutathione peroxidase (GPx) activity across the experimental groups. There was a significant decrease (p <0.05) in GPx activity of rats treated with $HgCl_2$-only when compared to control. However, there was a significant increase (p <0.05) in the $HgCl_2$-exposed rats treated with *Pleurotus ostreatus w*hen compared to $HgCl_2$ only. There was no significant difference (p >0.05) in the *Pleurotus ostreatus* only groups when compared to control.

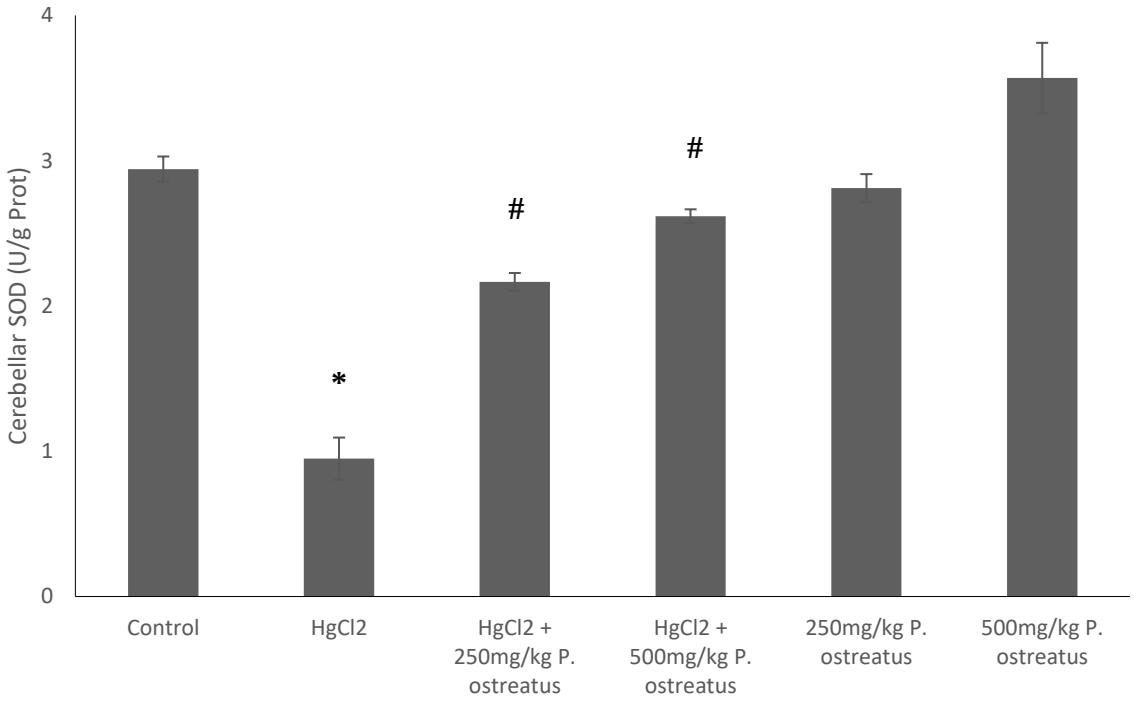

Figure 4.22: Superoxide dismutase (SOD) activity across the experimental groups

* p <0.05 compared with control group; # p <0.05 compared with $HgCl_2$ only group.

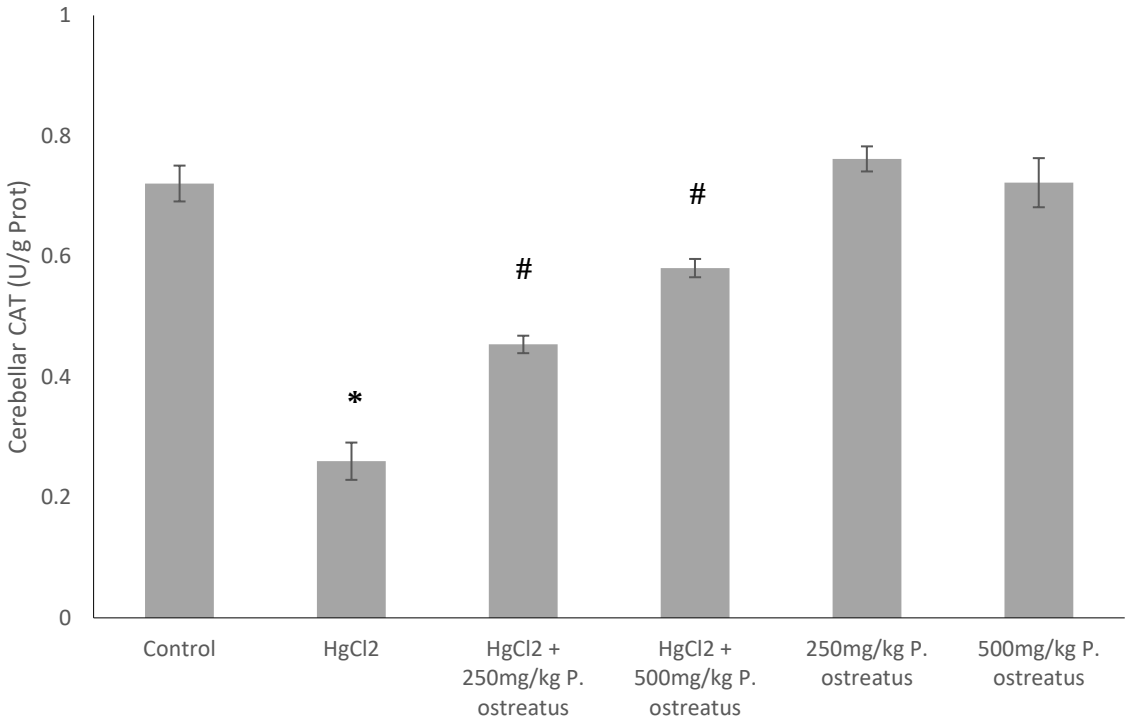

Figure 4.23: Catalase **(**CAT) activity across the experimental groups

* p <0.05 compared with control group; # p <0.05 compared with $HgCl_2$ only group.

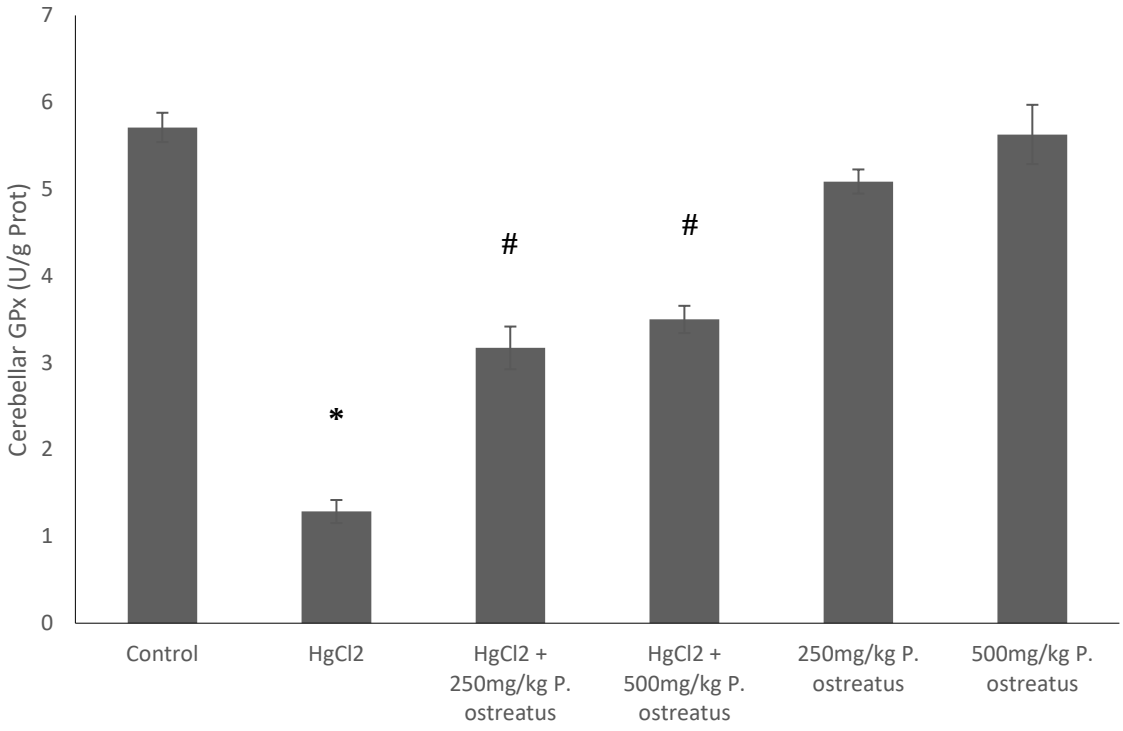

Figure 4.24: Glutathione peroxidase **(**GPx) activity across the experimental groups

* p <0.05 compared with control group; # p <0.05 compared with $HgCl_2$ only group.

4.7 EFFECT OF TREATMENT ON LIPID PEROXIDATION

Figure 4.25 shows the Malondialdehyde (MDA) concentration across the experimental groups. There was a significant increase (p <0.05) in MDA concentration of rats treated with $HgCl_2$-only when compared to control. However, there was a significant decrease (p <0.05) in the $HgCl_2$-exposed rats treated with *Pleurotus ostreatus w*hen compared to $HgCl_2$ only. There was no significant difference (p >0.05) in the *Pleurotus ostreatus* only groups when compared to control.

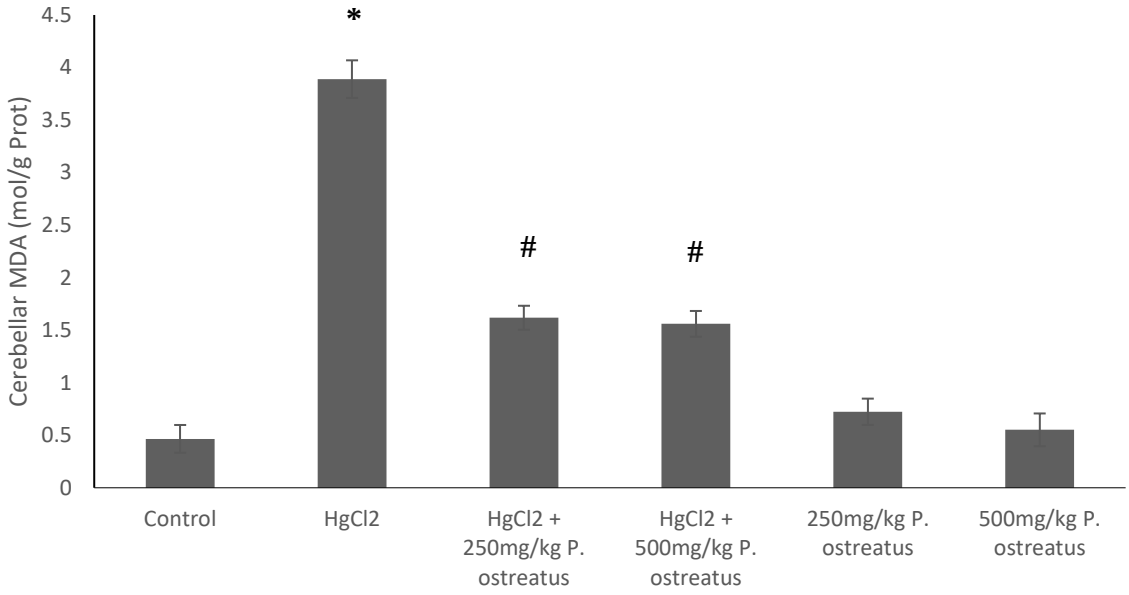

Figure 4.25: Malondialdehyde (MDA) concentration across the experimental groups

* p <0.05 compared with control group; # p <0.05 compared with $HgCl_2$ only group.

4.8 EFFECT OF TREATMENT ON MERCURY CONCENTRATION

Figure 4.26 shows the cerebellar mercury concentration across the experimental groups. There was a significant increase (p <0.05) in cerebellar mercury concentration of rats treated with $HgCl_2$-only when compared to control. However, there was a significant decrease (p <0.05) in the $HgCl_2$-exposed rats treated with *Pleurotus ostreatus w*hen compared to $HgCl_2$ only. There was no significant difference (p >0.05) in the *Pleurotus ostreatus* only groups when compared to control.

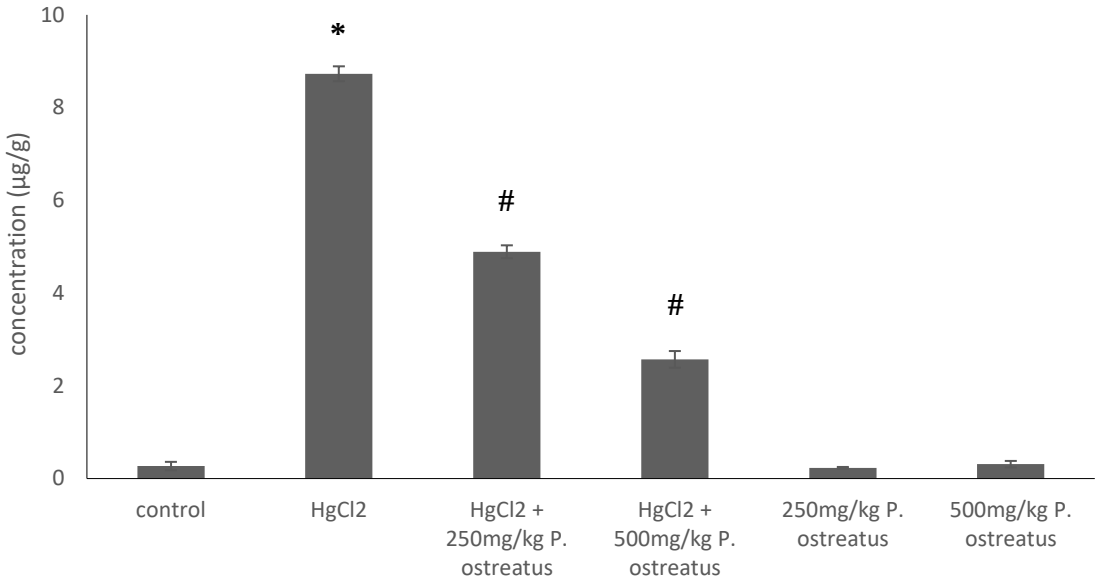

Figure 4.26: Cerebellar mercury concentration across the experimental groups.

* p <0.05 compared with control group; # p <0.05 compared with $HgCl_2$ only group.

4.9 EFFECT OF TREATMENT ON HISTOLOGY OF THE CEREBELLUM

Plate 4.1 - 4.6 shows the histology of the cerebellum of rats across experimental groups. Plate 4.1 (A and B) shows the cerebellum histology in control group with normal histological structure with distinct molecular, Purkinje, granular layers and white mater. Plate 4.2 (A and B) shows the cerebellum of rats treated with $HgCl_2$-only showing marked signs of damage, with Purkinje cell degeneration and molecular neuron degeneration. Plates 4.3 (A and B) and 4.4 (A and B) shows the cerebellum of $HgCl_2$-exposed rats treated with *Pleurotus ostreatus* – 250mg/kg and 500mg/kg respectively - showed relatively normal histological structure. Plate 4.5 (A and B) and Plate 4.6 shows the cerebellum of rats treated with *Pleurotus ostreatus* – 250mg/kg and 500mg/kg respectively – showed a relatively normal histological structure.

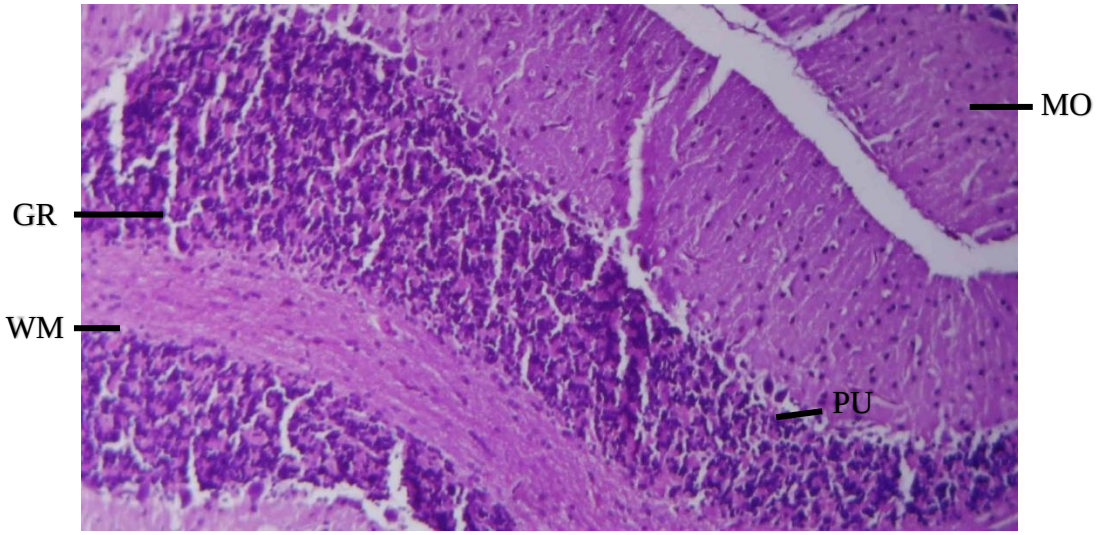

Plate 4.1A: Sections from control show: normal tissue architecture: molecular (MO), Purkinje (PU), granular (GR) layers and white mater (WM): H&E 100 X

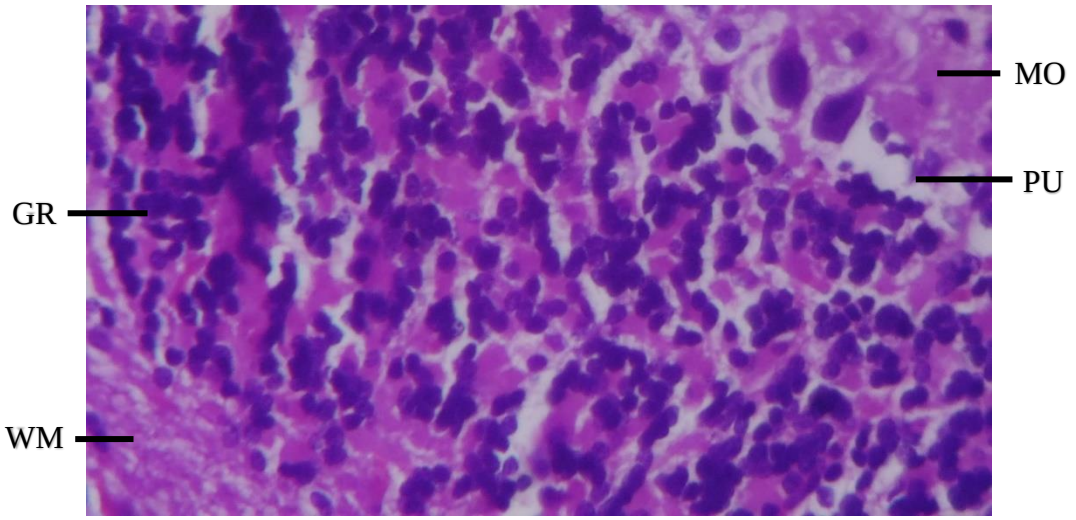

Plate 4.1B: Sections from control show: normal tissue architecture: molecular (MO), Purkinje (PU), granular (GR) layers and white mater (WM): H&E 400 X

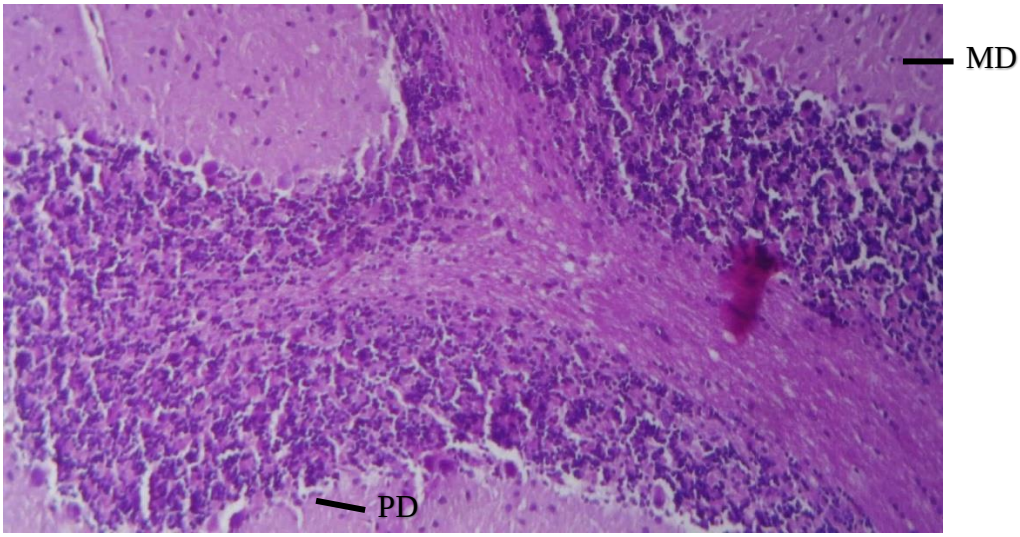

Plate 4.2A: Cerebellum given mercury chloride only show: Purkinje cell degeneration (PD) and molecular neuron degeneration (MD): H&E 100 X

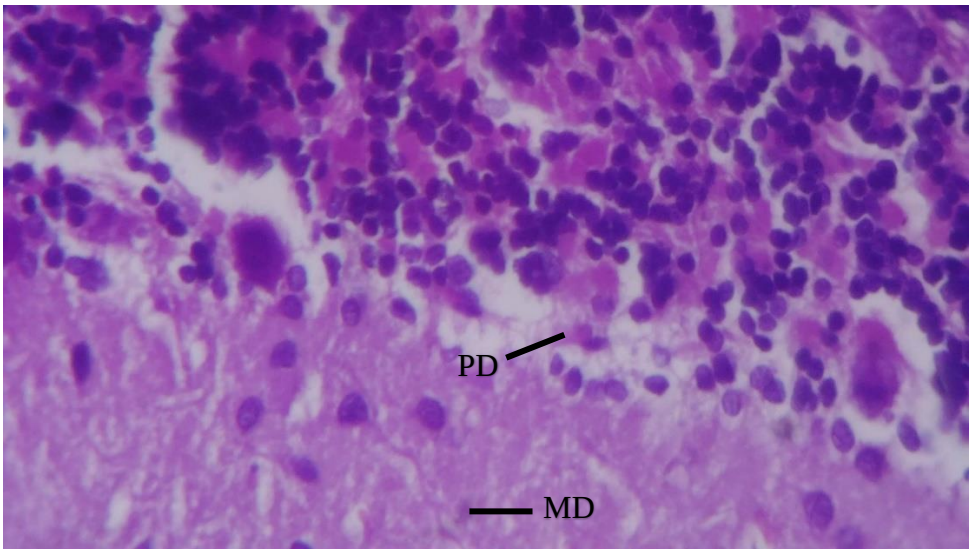

Plate 4.2B: Cerebellum given mercury chloride only show: Purkinje cell degeneration (PD) and molecular neuron degeneration (MD): H&E 400 X

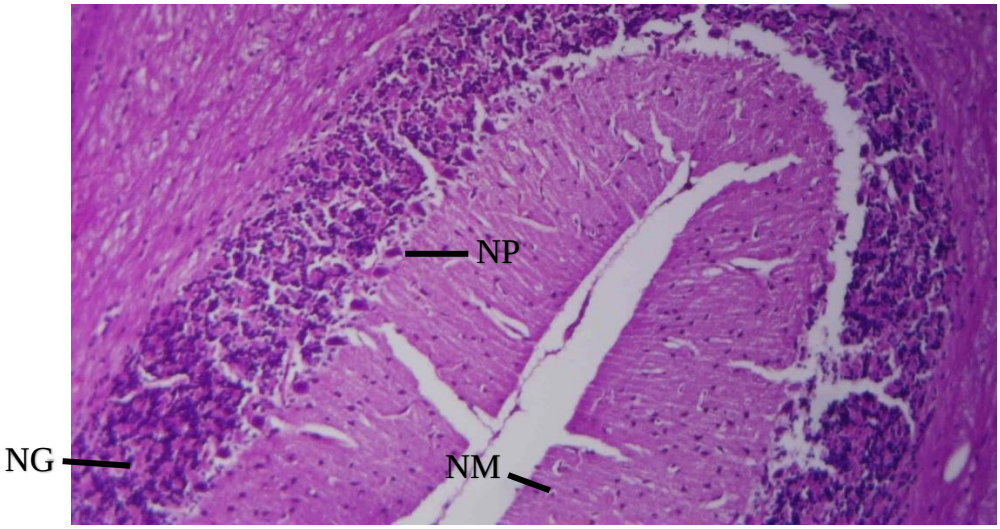

Plate 4.3A: Rat `cerebellum given Mercury Chloride + 250mg/kg *Pleurotus ostreatus* show: normal granular cell (NG), Purkinje (NP) and molecular cells (NM): H&E 100 X

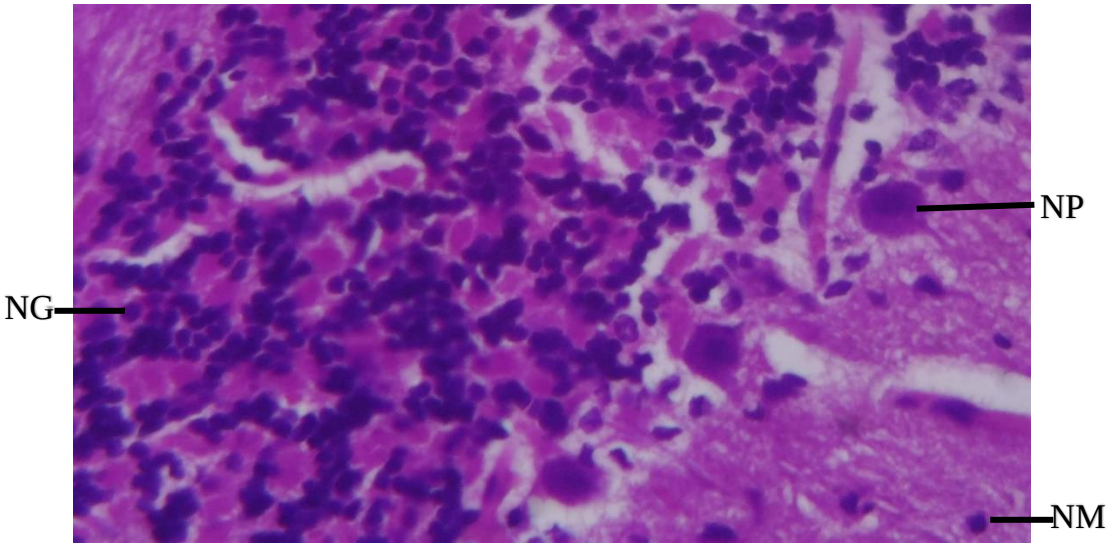

Plate 4.3B: Rat `cerebellum given Mercury Chloride + 250mg/kg *Pleurotus ostreatus* show: normal granular cell (NG), Purkinje (NP) and molecular cell (NM): H&E 400 X

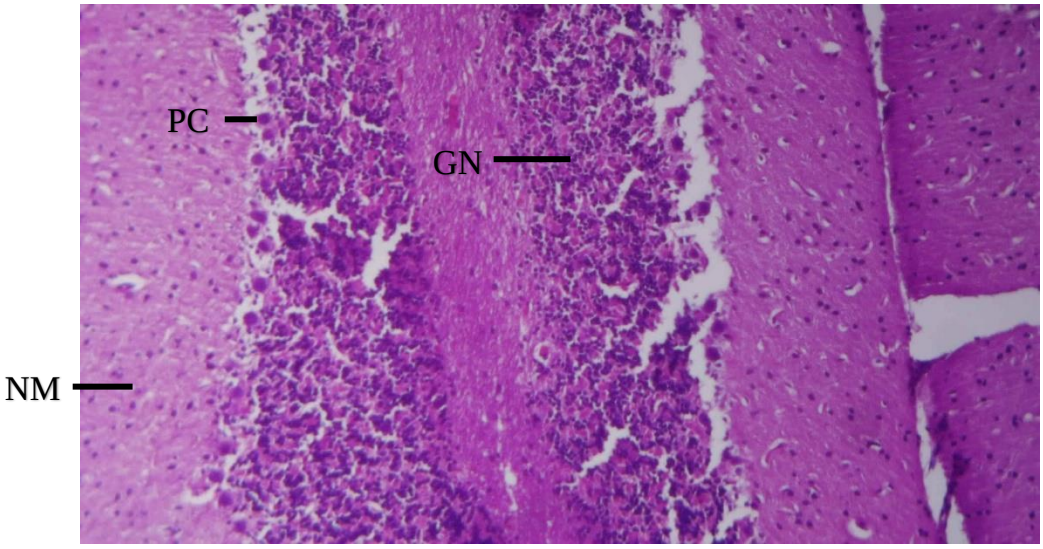

Plate 4.4A: Rat `cerebellum given Mercury Chloride + 500mg/kg *Pleurotus ostreatus* show: normal tissue architecture molecular (NM), Purkinje (PC) and granular (GN) neurons: H&E 100 X

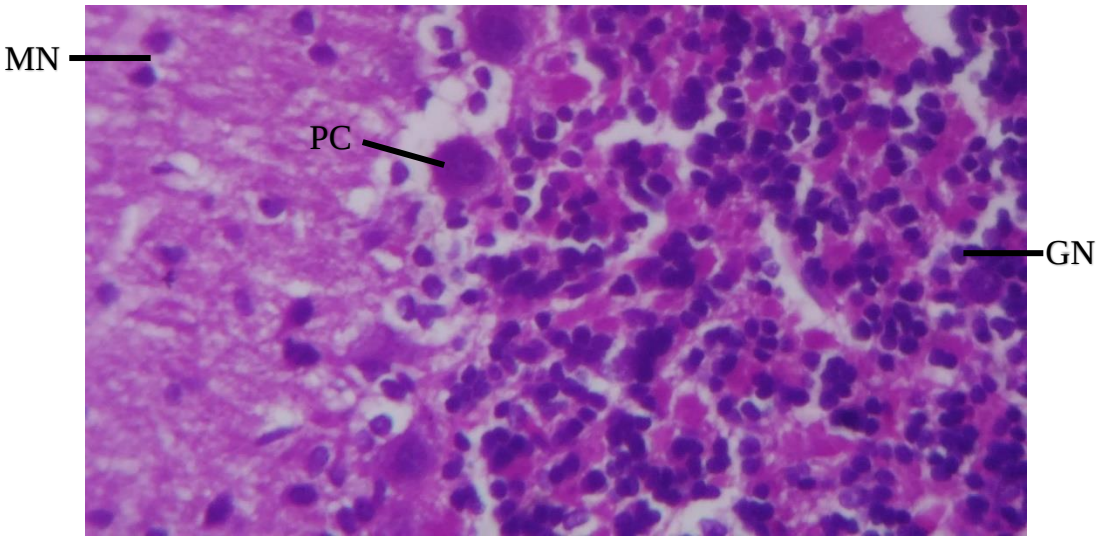

Plate 4.4B: Rat `cerebellum given Mercury Chloride + 500mg/kg *Pleurotus ostreatus* show: normal tissue architecture molecular (NM), Purkinje (PC) and granular (GN) neurons: H&E 400 X

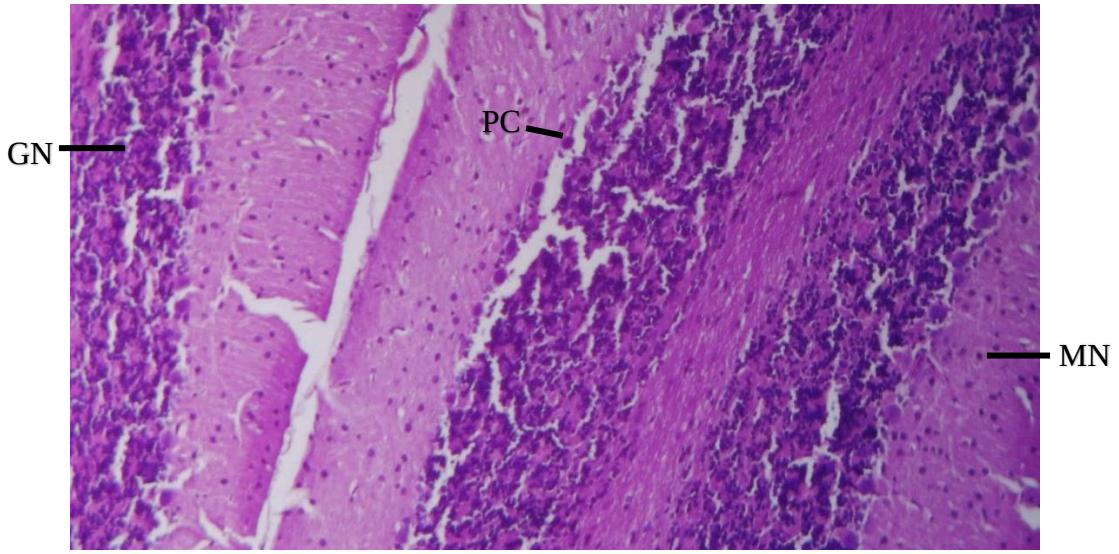

Plate 4.5A: Rat `cerebellum given 250mg/kg *Pleurotus ostreatus* only show: granular neurons (GN), Purkinje cells (PC), molecular neurons (MN), all normal: H&E 100 X.

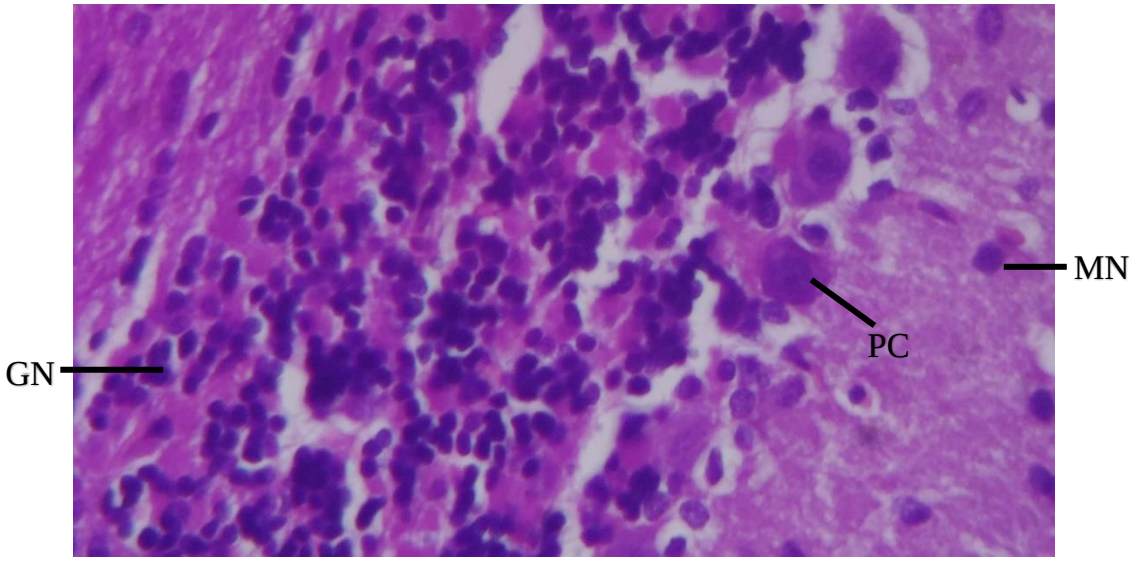

Plate 4.5B: Rat `cerebellum given 250mg/kg *Pleurotus ostreatus* only show: granular neurons (GN), Purkinje neurons (PC), molecular neurons (MN), all normal: H&E 400 X

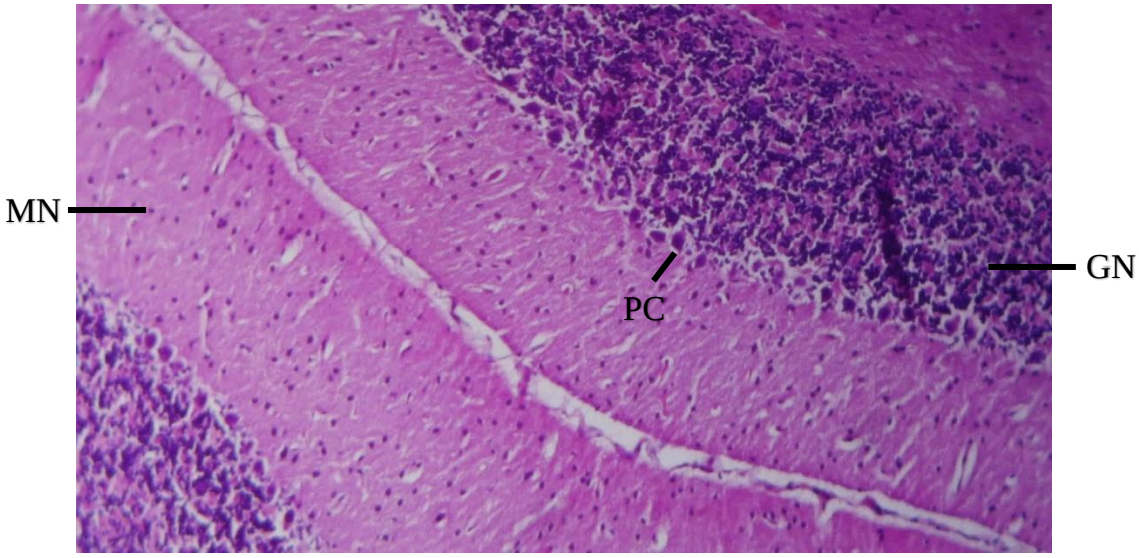

Plate 4.6A: Rat `cerebellum given 500mg/kg *Pleurotus ostreatus* only show: granular neurons (GN), Purkinje cells (PC) and molecular neurons (MN), all normal: H&E 100 X

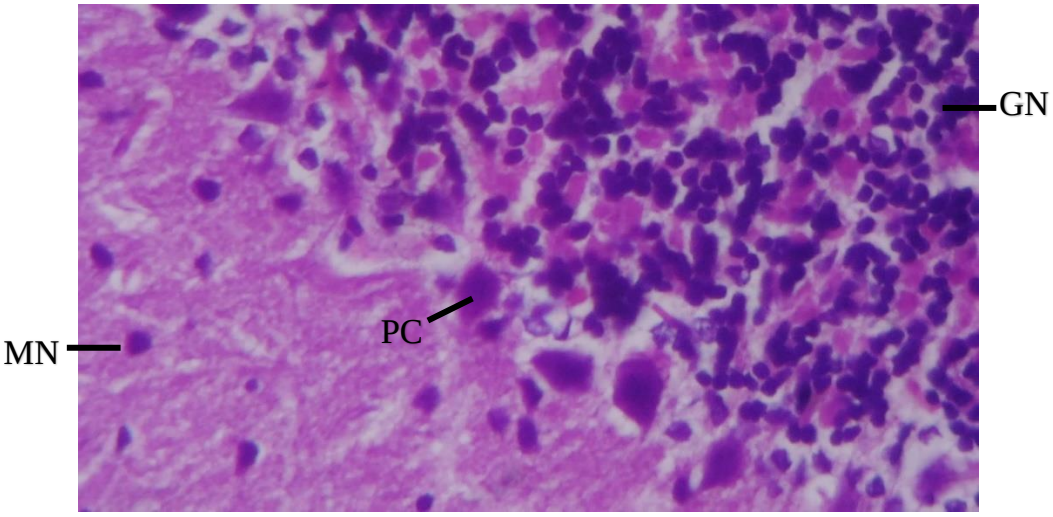

Plate 4.6B: Rat `cerebellum given 500mg/kg *Pleurotus ostreatus* only show: granular neurons (GN), Purkinje cells (PC) and molecular neurons (MN), all normal: H&E 400 X

CHAPTER FIVE

DISCUSSION, CONCLUSION AND RECOMMENDATION

5.1 DISCUSSION

5.1.1 *Pleurotus ostreatus* Possesses Bioactive and Antioxidant Properties

Pleurotus ostreatus continues to attract scientific attention for its dual role as both a nutritionally valuable food and a medicinally significant bioresource. Consistent with existing literature, findings from this study confirmed the presence of a diverse array of mycochemical constituents in the ethanol extract of *Pleurotus ostreatus*, including glycosides, saponins, phenols, terpenoids, alkaloids, flavonoids, and tannins. Notably, eugenols, steroids, and reducing sugars were absent. The presence of these secondary metabolites affirms the mushroom's biochemical richness and lends further support to the view that *Pleurotus ostreatus* is a functional food with considerable pharmacological potential (Sales-Campos *et al*., 2021; Sharma *et al*., 2021; Bulam *et al*., 2022).

Quantitative estimations revealed that tannins and phenolic compounds were the most abundant, followed by flavonoids and saponins, while alkaloids had the lowest concentration. This phytochemical distribution is of particular interest because tannins and phenolics are well-established antioxidants that exert multiple biological effects, including metal-chelating, anti-inflammatory, and enzyme-modulating activities (Soldado *et al*., 2021; Nemzer *et al*., 2021; Rana *et al*., 2022). Their abundance in *Pleurotus ostreatus* strengthens its potential as a neuroprotective agent, particularly in the mitigation of oxidative stress associated with heavy metal neurotoxicity.

The proximate composition of *Pleurotus ostreatus* further underscores its nutritional significance. Carbohydrates constituted the major component, followed by crude ash, fiber, fat, and moisture, with protein representing the lowest proportion. The high carbohydrate and fiber

content suggests its suitability as an energy-dense and gut-friendly dietary inclusion, supporting previous reports that mushrooms contribute positively to digestive health and energy metabolism (Cerletti *et al*., 2021; Bell *et al*., 2022; Zhang *et al*., 2022). Although relatively low in protein, *Pleurotus ostreatus* contains essential amino acids and bioactive peptides, making it a complementary component in balanced diets, especially when paired with higher-protein foods (Goswami *et al*., 2021; Lesa *et al*., 2022).

Critically, the antioxidant profile of *Pleurotus ostreatus* was validated through the DPPH radical scavenging assay. Results demonstrated a concentration-dependent increase in scavenging activity across the 0–250 µg/mL range, characterized by reduced absorbance and enhanced % inhibition. Although the antioxidant activity was slightly lower than that of the ascorbic acid, *Pleurotus ostreatus* still exhibited a comparably high radical-neutralizing effect. This strong antioxidant response is attributable to the substantial levels of phenolics and flavonoids present in the extract, both of which are capable of donating electrons or hydrogen atoms to neutralize free radicals (Tumilaar *et al*., 2024; Chouikh *et al*., 2025). These compounds may also interrupt radical chain reactions and stabilize reactive oxygen species (ROS), thereby limiting oxidative damage.

5.1.2 *Pleurotus ostreatus* Mitigates Mercury-induced Weight Loss

Body weight is a vital physiological indicator frequently used to assess systemic toxicity, especially in preclinical studies involving environmental toxicants (Idris *et al*., 2021; Dutta *et al*., 2022; Ding *et al*., 2024). Alterations in weight not only reflect disruptions in homeostasis but also offer critical insight into the biological burden exerted by xenobiotics such as heavy metals (Dutta *et al*., 2022). Among these, mercury remains a particularly hazardous neurotoxin with a well-documented profile of systemic toxicity, including marked reductions in somatic and organ-specific weights (Enogieru and Omoruyi, 2022; Zafar *et al*., 2024).

Inorganic mercury compounds, when ingested, can interfere with normal growth trajectories by impairing gastrointestinal function, inducing anorexia, and triggering metabolic derangements (Basu, 2023; Zafar *et al*., 2024). Mercury exposure is also known to generate reactive oxygen species (ROS), leading to cellular damage, muscle catabolism, and overall cachexia (Gouvêa *et al*., 2021; Rausch *et al*., 2021). The cumulative effect of these pathophysiological mechanisms often results in significant body weight loss, as well as decreased brain and cerebellar weights, particularly in developing animals (Enogieru and Inneh, 2022; Enogieru and Abhelemhen, 2025). Such neuroanatomical changes have critical implications for motor coordination and cognitive outcomes, further emphasizing the systemic reach of mercury toxicity.

In this study, a significant decrease in body, whole brain, and cerebellar weights was observed in rats administered $HgCl_2$. This is consistent with previous studies (Enogieru and Omoruyi, 2022; Imosemi and Oladejo, 2023; Kang *et al*., 2024). This weight reduction can be attributed to mercury-induced oxidative stress, gastrointestinal dysfunction, impaired nutrient assimilation, and reduced appetite. However, the treatment with *Pleurotus ostreatus*, markedly attenuated these toxic effects. The restoration of weight parameters in mercury exposed rats treated with *Pleurotus ostreatus* suggests a multifaceted protective role. *Pleurotus ostreatus* is rich in bioactive compounds, which may contribute to improved nutritional status and enhanced metabolic efficiency (Sen *et al*., 2021; Lesa *et al*., 2022). Moreover, its potent antioxidant capacity allows it to neutralize Hg-induced ROS, thereby preserving cellular integrity and limiting catabolic wasting. These antioxidative mechanisms not only mitigate tissue damage but may also promote the recovery of vital metabolic pathways necessary for growth and organ development.

5.1.3 *Pleurotus ostreatus* Mitigates Mercury-Induced Motor Deficits

The cerebellum plays a central role in the regulation of posture, balance, and finely coordinated voluntary movements (Langlois *et al*., 2024; Stańczak *et al*., 2025). Disruption of cerebellar integrity—such as that induced by neurotoxicants like mercury—can result in pronounced motor impairments that manifest as ataxia, tremors, and other locomotor abnormalities (Ganguly *et al*., 2022). Behavioural assessments are indispensable for quantifying these impairments in animal models (Sadler *et al*., 2022; Petković and Chaudhury, 2022), offering valuable insight into both neural dysfunction and therapeutic efficacy.

The Open Field Test (OFT) is a well-established and extensively used behavioural test for assessing general locomotor activity in rodent models. The OFT provides a quantitative measure of motor performance and anxiety-like behaviours by exposing the animal to a novel, open, and enclosed arena (Voikar and Stanford, 2022). In this study, ambulation, rearing, grooming, immobility, thigmotaxis, sniffing, frequency of central square entries, and crossings were assessed. Rearing behaviour, wherein the animal stands on its hind limbs with or without support, is closely linked to vertical exploratory activity and balance control. The cerebellum contributes significantly to postural adjustments required for rearing; thus, a decrease in rearing frequency may reflect cerebellar ataxia, motor impairment, or musculoskeletal weakness (Durosaro *et al*., 2021). Rodent grooming is a stereotyped sequence of self-directed behaviours—such as forepaw rubbing, facial cleaning, and body licking—that reflects both motor coordination and emotional regulation. It serves as a useful biomarker in neurotoxicological and behavioural studies (Idemudia and Enogieru, 2025). Ambulation, which refers to the movement of the rodent across the arena, is typically quantified as the total distance traveled or the number of floor grid crossings. It serves as a direct measure of overall motor activity and is sensitive to impairments in locomotion that may result from cerebellar or basal ganglia dysfunction (Gromer *et al*., 2021). A significant reduction in ambulation suggests

compromised neuromuscular coordination, hypoactivity, or possible sedative effects of test substances (Durosaro *et al*., 2021; Voikar and Stanford, 2022). Motor deficits can also affect the rodent's ability to move freely. For instance, increased immobility or freezing behaviour in the open field may be indicative of motor dysfunction or impaired motor planning and execution. Thigmotaxis, the tendency of rodents to remain close to the walls of the arena, is generally interpreted as an anxiety-related behaviour. A pronounced preference for the periphery and reluctance to explore the centre zone may not only reflect increased anxiety but could also stem from motor-related fear or impaired proprioception (Gromer *et al*., 2021; Voikar and Stanford, 2022). The frequency of sniffing behaviour in the open field test can be altered by motor impairments, as such behaviour depends on intact sensory-motor integration (Voikar and Stanford, 2022). Disruptions in motor coordination may reduce or modify sniffing patterns, reflecting underlying deficits in neuromuscular control and exploratory drive (Durosaro *et al*., 2021; Voikar and Stanford, 2022). Entries into the central zone and time spent therein serve as indicators of reduced anxiety or increased risk-taking, but in motor-deficient animals, they may also suggest physical limitations rather than purely emotional ones (Borba *et al*., 2025). The number of crossings—defined as transitions between zones within the open field arena—serves as a key indicator of motor competence and locomotor function. A marked decline in crossing frequency often signifies impaired gait or reduced voluntary movement (Durosaro *et al*., 2021; Borba *et al*., 2025). Findings from this study showed that $HgCl_2$-exposed rats exhibited significantly increased grooming, immobility, thigmotaxis, sniffing durations and decreased rearing, ambulation, central square entry and line crossing frequency when compared to control. This is consistent with previous studies by Ganguly *et al*. (2022) as well as Imosemi and Oladejo (2023), who reported similar findings. However, treatment with *Pleurotus ostreatus* significantly attenuated the mercury-induced motor deficits in rats, as

evidenced by the increased line crossing frequency, central square entry, ambulation, rearing as well as significantly decreased grooming, immobility, thigmotaxis, and sniffing durations.

The string test is a widely used behavioural assay for evaluating motor function in rodents. Two primary parameters assessed in this test are the latency to grip loss and the limb impairment score (Enogieru and Abhelemhen, 2025). Latency to grip loss refers to the duration a rodent can maintain its grip on a suspended string, serving as a quantitative measure of grip strength, muscular endurance, and coordination (Gromer *et al*., 2021). A shortened latency is indicative of compromised neuromuscular integrity, reflecting early signs of motor dysfunction. The limb impairment score, on the other hand, evaluates the functionality and coordination of the forelimbs and hindlimbs based on the rodent's ability to grasp, support, and manoeuvre along the string (Voikar and Stanford, 2022). Lower scores correspond to more pronounced motor deficits, such as limb weakness, uncoordinated movement, or reduced postural control. Significant reductions in both latency-to-grip loss and limb performance are strong indicators of underlying locomotor pathology (Voikar and Stanford, 2022). Results from this study showed that $HgCl_2$-only treated rats exhibited significant reductions in latency to grip loss and limb impairment score when compared to control. However, treatment with *Pleurotus ostreatus* increased both latency to grip loss and limb impairment score when compared to mercury-only treated rats, indicating *Pleurotus ostreatus'* ability to attenuate $HgCl_2$-induced motor deficits.

The movement initiation test is used to assess motor planning and execution by measuring the latency to initiate movement in response to a stimulus. This task is particularly sensitive to disruptions in neural circuits involved in voluntary motor control (Ganjuly *et al*., 2022; Heckman *et al*., 2023). Prolonged initiation times may indicate deficits in motor readiness, often observed in neurological disorders affecting basal ganglia or cortical motor regions (Heckman *et al*., 2023). Findings from this study showed that $HgCl_2$-exposed rats exhibited

increased movement initiation time in rats – indicative of impaired central control of motor functions. However, treatment with *Pleurotus ostreatus* showed significant improvement, exhibited as decreased movement initiation time compared to $HgCl_2$-only group.

The step test is a widely employed behavioral assay for assessing motor coordination and locomotor performance in rodents. It evaluates the animal's ability to make purposeful, coordinated stepping movements, serving as a reliable indicator of forelimb or hindlimb motor function (Dike *et al*., 2023). Higher step scores typically reflect intact motor performance and neuromuscular control, while reduced scores are associated with motor deficits such as impaired coordination, bradykinesia, or weakness (Eltokhi *et al*., 2021). Findings from this study showed a significant decrease in step test score in $HgCl_2$-only treated rats when compared to control. This is consistent with studies by Fagundes *et al*. (2022) and Dike *et al*. (2023), who both reported significant $HgCl_2$-induced deficits in step-test scores. However, treatment with *Pleurotus ostreatus* increased this step test score, an indication of improved motor performance.

Collectively, findings from this study demonstrate that $HgCl_2$ exposure induces significant motor and locomotor impairments in rodents, as evidenced by altered performance highlighting deficits in motor coordination, planning, and execution likely stemming from cerebellar dysfunction. Notably, treatment with *Pleurotus ostreatus* effectively mitigated these deficits across all tests, suggesting its therapeutic potential in reversing mercury-induced neuro-motor impairments through restoration of neuromuscular and locomotor function.

5.1.4 *Pleurotus ostreatus* Inhibits Mercury-Induced Oxidative Stress

Heavy metals, including mercury, are known to induce neurotoxicity through several mechanisms, of which initiation of oxidative stress is a major pathway (Balali-Mood *et al*., 2021; Thakur *et al*., 2021). This induction of oxidative stress is through the generation of free

radicals, resulting in an imbalance attributed to increased reactive oxygen species (ROS) production, decreased defensive mechanisms, or a combination of both factors (Novo *et al*., 2021; Thakur *et al*., 2021). Mercury is known to cross the blood-brain barrier leading to inhibition of several enzymes' activity (Azar *et al*., 2021).

Antioxidant enzymes play a pivotal role in cellular defense against oxidative stress by neutralizing reactive oxygen species (ROS) and preventing free radical-mediated damage. Among these, superoxide dismutase (SOD), catalase (CAT), and glutathione peroxidase (GPx) are key enzymatic antioxidants that work synergistically to maintain redox homeostasis and protect neural tissues from oxidative injury (Engwa *et al*., 2022; Demirci-Çekiç *et al*., 2022; Sadiq, 2023). SOD catalyzes the dismutation of superoxide anions —highly reactive species generated during aerobic metabolism—into molecular oxygen (O_2) and hydrogen peroxide (H_2O_2) (Andrés *et al*., 2023; Sadiq, 2023). This is particularly important in the brain, where high oxygen consumption and abundant polyunsaturated fatty acids render neuronal tissues, including the cerebellum, highly vulnerable to oxidative damage (Engwa *et al*., 2022). By limiting superoxide accumulation, SOD provides a crucial first line of defense in preserving neuronal integrity and motor function (Rosa *et al*., 2021). The hydrogen peroxide produced by SOD activity must be further detoxified to prevent its accumulation and conversion into more reactive hydroxyl radicals via the Fenton reaction. CAT performs this task efficiently by catalyzing the decomposition of hydrogen peroxide into water and oxygen (Dan *et al*., 2022; Khan *et al*., 2024). In doing so, CAT not only neutralizes a potent oxidant but also protects SOD from hydrogen peroxide-induced inactivation, thus maintaining the antioxidant defense system's functional continuity (Rosa *et al*., 2021; Khan *et al*., 2024). Deficiencies in CAT activity have been associated with increased oxidative burden and neuronal damage, particularly in cerebellar regions implicated in motor control (Dan *et al*., 2022; Engwa *et al*., 2022; Khan *et al*., 2024). GPx complements this enzymatic defense system by reducing

hydrogen peroxide and lipid hydroperoxides using glutathione (GSH) as a substrate, forming water and oxidized glutathione (GSSG) (Pisoschi *et al*., 2021; Pei *et al*., 2023). GPx is especially important in lipid-rich tissues such as the brain, where it prevents peroxidation of membrane lipids and helps maintain cellular structural integrity. Together, SOD, CAT, and GPx form an integrated antioxidant network that counteracts ROS-induced neuronal damage, making them critical biomarkers and therapeutic targets in conditions of heavy metal toxicity, including mercury and lead exposure (Pisoschi *et al*., 2021; Khan *et al*., 2024). Findings from this study showed that mercury significantly decreased SOD, CAT and GPx in the cerebellum. This agrees with previous studies that have reported the neurodegenerative effects of mercury through induction of oxidative stress characterized by reduced activity of antioxidant enzymes (Enogieru and Inneh, 2022; Imosemi and Oladejo, 2023; Yahyazadeh and Gur, 2024). However, treatment with *Pleurotus ostreatus* significantly improved these antioxidant enzymes activity in the cerebellum of experimental rats exhibited by significantly increased SOD, CAT and GPx activity. This improvement in the cerebellar antioxidant defense system could be attributed to the potent antioxidant property of *Pleurotus ostreatus*.

On the other hand, Malondialdehyde (MDA), a widely recognized and reliable biomarker of oxidative stress serving as a stable end product of lipid peroxidation, is primarily generated through the oxidative degradation of polyunsaturated fatty acids (PUFAs) within cellular membranes under conditions of elevated reactive oxygen species (ROS) (Bencivenga *et al*., 2023). Because neuronal tissues, including the cerebellum, are rich in PUFAs, they are particularly susceptible to lipid peroxidation during oxidative insults (Mohideen *et al*., 2023; Bencivenga *et al*., 2023). The accumulation of MDA reflects the extent of oxidative damage to membrane lipids, which compromises membrane fluidity, disrupts cellular signaling, and contributes to neurodegenerative processes (Bencivenga *et al*., 2023). Elevated MDA concentrations are indicative of impaired antioxidant defense and ongoing cellular damage,

especially under conditions of heavy metal exposure such as mercury or lead. Findings from this study showed a significant increase in cerebellar MDA concentrations in the $HgCl_2$-exposed rats. The increase in the cerebellum MDA levels observed in this study demonstrates the potency of mercury in the induction of lipid peroxidation. These findings are consistent with previous reports indicating that mercury exposure induces significant lipid peroxidation in the cerebellum, as evidenced by elevated MDA levels (Egba *et al*., 2022; Mousa and Ibrahim, 2023; Zahed *et al*., 2024). Notably, treatment with *Pleurotus ostreatus* effectively mitigated this oxidative damage, restoring MDA concentrations to near-control levels. This suggests that *Pleurotus ostreatus* exerts potent anti-peroxidative effects, likely through its antioxidant constituents that counteract mercury-induced lipid membrane degradation.

5.1.5 *Pleurotus ostreatus* Inhibits Mercury Accumulation in the Cerebellum

Accumulation of mercury in the cerebellum has been strongly implicated in the pathogenesis of cerebellar dysfunction, leading to impaired motor coordination, ataxia, and other neurological deficits (Ganguly *et al*., 2022; Chamoli and Karn, 2024). Mercury's high affinity for sulfhydryl groups in proteins allows it to disrupt critical enzymatic processes, promote oxidative stress, and induce neuronal apoptosis, particularly in the cerebellar cortex. As such, reducing mercury burden in neural tissues is a key therapeutic objective. One established strategy involves the use of chelating agents—chemical compounds with multiple electron-donating ligands capable of binding to heavy metal ions with high specificity (Fasae *et al*., 2021; Yudaev and Chistyakov, 2022). These agents form stable, water-soluble complexes with mercury, facilitating its mobilization and excretion via urine or feces, thereby reducing tissue toxicity and limiting further neuronal damage (Yudaev and Chistyakov, 2022).

Findings from this study demonstrated a significant increase in cerebellar mercury levels in rats exposed to $HgCl_2$, confirming the neurotoxic accumulation of mercury within motor

control centres of the brain (Ijomone *et al*., 2021; Imosemi and Oladejo, 2023). However, treatment with *Pleurotus ostreatus* markedly reduced cerebellar mercury concentrations, suggesting its potential as a natural chelating agent. This chelating effect is likely attributed to the mushroom's rich profile of bioactive compounds, including phenolics, flavonoids, and polysaccharides, which possess multiple electron-donating groups capable of binding heavy metal ions (Oyetayo *et al*., 2021; Effiong *et al*., 2024). By forming stable coordination complexes with mercury, these compounds may reduce its bioavailability, limit its ability to cross the blood–brain barrier, and ultimately prevent its deposition in sensitive neural tissues such as the cerebellum. This highlights *Pleurotus ostreatus* as a promising dietary intervention for mitigating mercury-induced neurotoxicity.

5.1.6 *Pleurotus ostreatus* Alleviates Mercury-Induced Cerebellar Histopathology

The cerebellum plays a central role in the regulation of fine motor coordination, postural balance, and sensorimotor integration. Given its complex architecture and high metabolic demand, it is particularly susceptible to damage from neurotoxicants such as mercury (Kumari and Chand, 2023; Chamoli and Karn, 2024). Among cerebellar neurons, Purkinje cells are especially vulnerable due to their extensive dendritic arborization and high oxidative sensitivity (Khaled *et al*., 2024; Dickmeiß *et al*., 2025). Disruption to this neuronal population can result in profound motor impairments and cerebellar dysfunction (Iskusnykh *et al*., 2024).

Histological analysis of cerebellar sections from rats exposed to $HgCl_2$-only revealed extensive neurodegenerative changes, characterized by Purkinje cell shrinkage, pyknotic nuclei, and widespread cellular disorganization. The molecular layer displayed dense, darkly stained degenerating neurons along with vacuolations, indicative of synaptic disruption and reactive gliosis. These structural abnormalities are consistent with mercury-induced oxidative damage and excitotoxicity, which disrupt mitochondrial function, elevate intracellular calcium, and

trigger neuronal apoptosis (Novo *et al*., 2021; Zahed *et al*., 2024). The vulnerability of Purkinje cells—given their metabolic demands and central role in cerebellar output—renders them a primary target of mercury neurotoxicity. However, treatment with *Pleurotus ostreatus* markedly preserved cerebellar architecture in a dose-dependent fashion. At 250 mg/kg, histological sections demonstrated appreciable protection of the Purkinje, granular, and molecular layers, with reduced evidence of neurodegeneration and vacuolations. This protective effect was more pronounced at 500 mg/kg, where the cerebellar cortex appeared largely comparable to the control group, with intact layering and minimal structural abnormalities.

These findings suggest that *Pleurotus ostreatus* attenuates mercury-induced histological alterations/damage, potentially by interfering with the toxicant's cellular targets or neutralizing its oxidative effects in real time. The neuroprotective capacity of *Pleurotus ostreatus* is likely mediated through its abundant phytochemicals—particularly phenolics, flavonoids, and polysaccharides—which possess antioxidative, anti-inflammatory, and metal-chelating properties (Olukemi *et al*., 2021; Michalska *et al*., 2025; Seethapathy *et al*., 2025). These compounds may act synergistically to reduce mercury accumulation, attenuate lipid peroxidation, chelate free mercury ions, stabilize cellular membranes and preserve mitochondrial integrity, thereby preventing apoptosis of Purkinje and cortical neurons. These results align with previous findings on natural antioxidants mitigating heavy metal neurotoxicity by preserving neural structure and function (Shohag *et al*., 2022; Murumulla *et al*., 2024). By restoring normal cerebellar histoarchitecture, *Pleurotus ostreatus* not only protects against structural degeneration but may also contribute to the preservation of motor function, as supported by parallel behavioural assessments in this study.

5.2 LIST OF FINDINGS

The findings from this study are as follows:

i. Ethanol extract of *P. ostreatus* mitigated mercuric chloride-induced weight loss.

ii. Ethanol extract of *P. ostreatus* mitigated mercuric chloride-induced locomotor and motor deficits.

iii. Ethanol extract of *P. ostreatus* inhibited mercuric chloride-induced dysregulation of antioxidant enzymes in the cerebellum of experimental rats.

iv. Ethanol extract of *P. ostreatus* protected against mercuric chloride-induced lipid peroxidation in the cerebellum of experimental rats.

v. Ethanol extract of *P. ostreatus* mitigated mercuric chloride-induced histological alterations in the cerebellum of experimental rats.

vi. Ethanol extract of *P. ostreatus* contains an array of bioactive phytochemicals such as glycosides, phenols, terpenoids, alkaloids, flavonoids, and tannins.

vii. Ethanol extract of *P. ostreatus* possesses comparable neuroprotective activity to ascorbic acid.

5.3 CONTRIBUTIONS TO KNOWLEDGE

This study has shown novel evidence and demonstrated that ethanol extract of *Pleurotus ostreatus*:

i. mitigates mercury-induced weight loss in the experimental rats.

ii. mitigates mercury-induced neurobehavioral deficits in the experimental rats.

iii. mitigates mercury-induced oxidative stress in the cerebellum of experimental rats.

iv. mitigates mercury accumulation in the cerebellum of experimental rats.

v. protects against mercury-induced cerebellar alterations in the experimental rats.

5.4 CONCLUSION

Results from this study show that *Pleurotus ostreatus* significantly mitigates mercury-induced cerebellar toxicity, primarily through its antioxidant, neuroprotective, and metal-chelating properties. These findings suggest that *Pleurotus ostreatus* may serve as a promising candidate for the development of novel therapeutic strategies aimed at managing mercury neurotoxicity and its associated motor impairments.

5.5 RECOMMENDATION

Comprehensive mechanistic studies using diverse *in vivo* and *in vitro* models should be undertaken to elucidate the precise molecular pathways through which *Pleurotus ostreatus* attenuates mercury-induced oxidative stress and neuronal damage, particularly within the cerebellum. Comparative evaluations between *Pleurotus ostreatus* and conventional chelating agents or synthetic antioxidants should be conducted to assess its relative efficacy and potential as a complementary or alternative therapeutic option. Given its dietary origin and promising neuroprotective profile, *Pleurotus ostreatus* warrants further exploration as a functional food or nutraceutical in populations at risk of chronic mercury exposure. Clinical studies are recommended to evaluate its potential in preventing or mitigating mercury-related neurodegenerative conditions.

REFERENCES

Abdelkader, M. A. E., Mediatrice, H., Lin, D., Lin, Z., & Aggag, S. A. (2024). Mitigating Oxidative Stress and Promoting Cellular Longevity with Mushroom Extracts. *Foods*, *13*(24), 4028.

Abidin, M. H. Z., Abdullah, N., & Abidin, N. Z. (2017). Therapeutic properties of Pleurotus species (oyster mushrooms) for atherosclerosis: A review. *International Journal of Food Properties*, *20*(6), 1251-1261.

Adetunji, C. O., Olaniyan, O. T., Adetunji, J. B., Osemwegie, O. O., & Ubi, B. E. (2022). African mushrooms as functional foods and nutraceuticals. *Fermentation and algal biotechnologies for the food, beverage and other bioproduct industries*, 233-251.

Agbagwa, S. S., Chuku, E. C., & Emiri, U. N. (2020). Determination of mineral and proximate compositions of *Pleurotus ostreatus* grown on three agrowaste. *International Journal of Research in Agriculture, Biology & Environment*, *1*(2), 22-27.

Agunloye, O. M., & Oboh, G. (2022). Blood glucose lowering and effect of oyster (*Pleurotus ostreatus*)-and shiitake (Lentinus subnudus)-supplemented diet on key enzymes linked diabetes and hypertension in streptozotocin-induced diabetic in rats. *Food Frontiers*, *3*(1), 161-171.

Ainsworth, E. A., & Gillespie, K. M. (2007). Estimation of total phenolic content and other oxidation substrates in plant tissues using Folin–Ciocalteu reagent. *Nature protocols*, *2*(4), 875-877.

Ajibade, A. J., Esho, J. O., Kehinde, B. D., & Adeleye, O. O. (2019). Histological and biochemical effects of mercury chloride on the kidney of adult Wistar rats. *Journal of Pharmacy and Pharmacology*, *1*, 21-7.

Akinsooto, O., Ogundipe, O. B., & Ikemba, S. (2024). Strategic policy initiatives for optimizing hydrogen production and storage in sustainable energy systems. *International Journal of Frontline Research and Reviews*, *2*(2), 001-021.

Althobaiti, N. A. (2024). Heavy metals exposure and Alzheimer's disease: Underlying mechanisms and advancing therapeutic approaches. *Behavioural Brain Research*, 115212.

Altunkaynak, B. Z., Akgül, N., Yahyazedeh, A., Makaracı, E., & Akgül, H. M. (2019). A stereological study of the effects of mercury inhalation on the cerebellum. *Biotechnic & Histochemistry*, *94*(1), 42-47.

Andrés, C. M. C., Pérez de la Lastra, J. M., Andrés Juan, C., Plou, F. J., & Pérez-Lebeña, E. (2023). Superoxide anion chemistry—Its role at the core of the innate immunity. *International Journal of Molecular Sciences*, *24*(3), 1841.

Anene, N. C., Dangulbi, B. M., & Veiga, M. M. (2024). Assessment of Gold and Mercury Losses in an Artisanal Gold Mining Site in Nigeria and Its Implication on the Local Economy and the Environment. *Minerals*, *14*(11), 1131.

Animoku Abdulrazaq, A., Suleiman, M. O., Iliyasu Musa, O., Bolaji, M. S., Ademola, Y. U., Omachonu, O. A., Muhammad, I.Z., & Simpa, M. J. (2019). Histomorphological Studies of the Cerebellum in Mercury Exposed Rats and the Role of Ascorbic Acid (Vitamin C). *Evaluation*, 4th.

Antunes dos Santos, A., Ferrer, B., Marques Gonçalves, F., Tsatsakis, A. M., Renieri, E. A., Skalny, A. V., Farina, M., Rocha, J. B., & Aschner, M. (2018). Oxidative stress in methylmercury-induced cell toxicity. *Toxics*, *6*(3), 47.

Araujo, A. P. B., Carpi-Santos, R., & Gomes, F. C. A. (2019). The role of astrocytes in the development of the cerebellum. *The Cerebellum*, *18*(6), 1017-1035.

Arslan, M., AÇAR, H., Cömert, A., & Tubbs, R. (2018). The cervical arteries: an anatomical study with application to avoid the nerve root and spinal cord blood supply. *Turkish Neurosurgery*, *28*(2).

Arumugam, N., & Parasher, R. K. (2019). Effect of physical exercises on attention, motor skill and physical fitness in children with attention deficit hyperactivity disorder: A systematic review. *ADHD Attention Deficit and Hyperactivity Disorders*, *11*(2), 125-137.

Auza, M. I., Abraham, S. M., Oladele, S. B., Bauchi, Z. M., & Danborno, A. M. (2024). Neuroprotective Effect of Ginkgo biloba and L-Ascorbic Acid on Mercury Chloride (HgCl2)-Induced Oxidative stress and Neuroinflammation in Adult Male Wistar Rats. *Biological Sciences*, *4*(3), 701-711.

Awogbami, S. O., Ogunyemi, O., Adebayo, P. A., & Raimi, M. O. (2024). Protecting the Health of Black Communities: Assessing the Impact of Environmental Hazards from Gold Mining Activities on Health Outcomes among Residents of Osun State, Nigeria. *Journal of Medical Internet Research Preprints*, *15*(09), 2024.

Aysin, F., Karaman, A., Yilmaz, A., Aksakal, Ö., Gezgincioğlu, E., & Kohnehshahri, S. M. (2020). Exogenous cysteine alleviates mercury stress by promoting antioxidant defence in maize (Zea mays L.) seedlings. *Turkish Journal of Agriculture and Forestry*, *44*(5), 506-516.

Azar, J., Yousef, M. H., El-Fawal, H. A., & Abdelnaser, A. (2021). Mercury and Alzheimer's disease: a look at the links and evidence. *Metabolic Brain Disease*, *36*, 361-374.

Badura, A., Verpeut, J. L., Metzger, J. W., Pereira, T. D., Pisano, T. J., Deverett, B., Bakshinskaya, D.E., & Wang, S. S. (2018). Normal cognitive and social development require posterior cerebellar activity. *Elife*, *7*, e36401.

Balali-Mood, M., Naseri, K., Tahergorabi, Z., Khazdair, M. R., & Sadeghi, M. (2021). Toxic mechanisms of five heavy metals: mercury, lead, chromium, cadmium, and arsenic. *Frontiers in pharmacology*, *12*, 643972.

Baran, O., Baydin, S., Mirkhasilova, M., Bayramli, N., Bilgin, B., Middlebrooks, E., Ozlen, F. & Tanriover, N. (2022). Microsurgical anatomy and surgical exposure of the cerebellar peduncles. *Neurosurgical Review*, 1-23.

Basu, M. (2023). Impact of mercury and its toxicity on health and environment: a general perspective. In *mercury toxicity: Challenges and solutions* (pp. 95-139). Singapore: Springer Nature Singapore.

Bell, V., Silva, C. R. P. G., Guina, J., & Fernandes, T. H. (2022). Mushrooms as future generation healthy foods. *Frontiers in Nutrition*, *9*, 1050099.

Bencivenga, D., Arcadio, F., Piccirillo, A., Annunziata, M., Della Ragione, F., Cennamo, N., Borriello, A., Zeni, L., & Guida, L. (2023). Plasmonic optical fiber biosensor development for point-of-care detection of malondialdehyde as a biomarker of oxidative stress. *Free Radical Biology and Medicine*, *199*, 177-188.

Bhushan, R., Ravichandiran, V., & Kumar, N. (2022). An overview of the anatomy and physiology of the brain. *Nanocarriers for Drug-Targeting Brain Tumors*, 3-29.

Billeri, L., & Naro, A. (2021). A narrative review on non-invasive stimulation of the cerebellum in neurological diseases. *Neurological Sciences*, *42*(6), 2191-2209.

Bittencourt, L. O., Chemelo, V. S., Aragão, W. A. B., Puty, B., Dionizio, A., Teixeira, F. B., Fernandes, M.S., Silva, M.C.F., Fernandes, L.M.P., de Oliveira, E.H.C., Buzalaf, M.A.R., & Lima, R. R. (2021). From molecules to behavior in long-term inorganic mercury intoxication: unraveling proteomic features in cerebellar neurodegeneration of rats. *International Journal of Molecular Sciences*, *23*(1), 111.

Błaszczyk, M., Ochwat, K., Necka, S., Kwiecińska, M., Ostrowski, P., Bonczar, M., Żytkowski, A., Walocha, J., Mituś, J., & Koziej, M. (2024). The Arterial Anatomy of the Cerebellum—A Comprehensive Review. *Brain Sciences*, *14*(8), 763.

Borba, J. V., Resmim, C. M., Fontana, B. D., Moraes, H. S., Müller, M. L., Blanco, L., Uchoa, A. E., Parker, M. O, & Rosemberg, D. B. (2025). Anxiogenic and anxiolytic modulators

differentially affect thigmotaxis and thrashing behavior in adult zebrafish during habituation to the open field test. *Behavioural Processes*, *228*, 105199.

Borst, K., Dumas, A. A., & Prinz, M. (2021). Microglia: Immune and non-immune functions. *Immunity*, *54*(10), 2194-2208.

Bostan, A. C., & Strick, P. L. (2018). The basal ganglia and the cerebellum: nodes in an integrated network. *Nature Reviews Neuroscience*, *19*(6), 338-350.

Boyken, J., Frenzel, T., Lohrke, J., Jost, G., & Pietsch, H. (2018). Gadolinium accumulation in the deep cerebellar nuclei and globus pallidus after exposure to linear but not macrocyclic gadolinium-based contrast agents in a retrospective pig study with high similarity to clinical conditions. *Investigative Radiology*, *53*(5), 278-285.

Bruckert, L., Shpanskaya, K., McKenna, E. S., Borchers, L. R., Yablonski, M., Blecher, T., Ben-Shachar, M., Travis, K.E., Feldman, H.M., & Yeom, K. W. (2019). Age-dependent white matter characteristics of the cerebellar peduncles from infancy through adolescence. *The Cerebellum*, *18*, 372-387.

Buege, J. A., & Aust, S. D. (1978). [30] Microsomal lipid peroxidation. In *Methods in enzymology* (Vol. 52, pp. 302-310). Academic press.

Bulam, S., Üstün, N., & Pekşen, A. (2022). Oyster mushroom (*Pleurotus ostreatus*) as a healthy ingredient for sustainable functional food production. *Mantar Dergisi*, *13*(3), 131-143.

Calao-Ramos, C., Bravo, A. G., Paternina-Uribe, R., Marrugo-Negrete, J., & Díez, S. (2021). Occupational human exposure to mercury in artisanal small-scale gold mining communities of Colombia. *Environment International*, *146*, 106216.

Cappelletti, S., Piacentino, D., Fineschi, V., Frati, P., D'Errico, S., & Aromatario, M. (2019). Mercuric chloride poisoning: symptoms, analysis, therapies, and autoptic findings. A review of the literature. *Critical Reviews in Toxicology*, *49*(4), 329-341.

Carey, M. R. (2024). The cerebellum. *Current Biology*, *34*(1), R7-R11.

Cariccio, V. L., Samà, A., Bramanti, P., & Mazzon, E. (2019). Mercury involvement in neuronal damage and in neurodegenerative diseases. *Biological Trace Element Research*, *187*(2), 341-356.

Çavdar, S., Özgur, M., Kuvvet, Y., & Bay, H. H. (2018). The cerebello-hypothalamic and hypothalamo-cerebellar pathways via superior and middle cerebellar peduncle in the rat. *The Cerebellum*, *17*, 517-524.

Ceccatelli, S., Daré, E., & Moors, M. (2010). Methylmercury-induced neurotoxicity and apoptosis. *Chemico-biological interactions*, *188*(2), 301-308.

Cerletti, C., Esposito, S., & Iacoviello, L. (2021). Edible mushrooms and beta-glucans: Impact on human health. *Nutrients*, *13*(7), 2195.

Chamoli, A., & Karn, S. K. (2024). The effects of mercury exposure on neurological and cognitive dysfunction in human: a review. *Mercury toxicity mitigation: sustainable nexus approach*, 117-135.

Chang, L. W., & Hartmann, H. A. (1972). Ultrastructural studies of the nervous system after mercury intoxication: II. Pathological changes in the nerve fibers. *Acta neuropathologica*, *20*, 316-334.

Charkiewicz, A. E., Omeljaniuk, W. J., Garley, M., & Nikliński, J. (2025). Mercury exposure and health effects: what do we really know?. *International Journal of Molecular Sciences*, *26*(5), 2326.

Chouikh, A., Chenguel, A., & Ali, A. B. (2025). Understanding the Role of Free Radicals, Oxidative Stress, and Antioxidants: A Comprehensive Review. *Letters in Applied NanoBioScience*, *14*(2), 66.

Chromý, V., Vinklárková, B., Šprongl, L., & Bittová, M. (2015). The Kjeldahl method as a primary reference procedure for total protein in certified reference materials used in clinical chemistry. I. A review of Kjeldahl methods adopted by laboratory medicine. *Critical reviews in analytical chemistry*, *45*(2), 106-111.

Ćilerdžić, J., Galić, M., Vukojević, J., & Stajic, M. (2019). *Pleurotus ostreatus* and Laetiporus sulphureus (Agaricomycetes): possible agents against Alzheimer and Parkinson diseases. *International Journal of Medicinal Mushrooms*, *21*(3).

Cohen, G., Dembiec, D., & Marcus, J. (1970). Measurement of catalase activity in tissue extracts. *Analytical biochemistry*, *34*(1), 30-38.

Consalez, G. G., Goldowitz, D., Casoni, F., & Hawkes, R. (2021). Origins, development, and compartmentation of the granule cells of the cerebellum. *Frontiers in neural circuits*, *14*, 611841.

Corrêa, M. G., Bittencourt, L. O., Nascimento, P. C., Ferreira, R. O., Aragão, W. A. B., Silva, M. C. F., Gomes-Leal, W., Fernandes, M. S., Dionizio, A., Buzalaf, M. R., Crespo-Lopez, M. E., & Lima, R. R. (2020). Spinal cord neurodegeneration after inorganic mercury long-term exposure in adult rats: Ultrastructural, proteomic and biochemical damages associated with reduced neuronal density. *Ecotoxicology and Environmental Safety*, *191*, 110159.

Cozza, M., & Boccardi, V. (2023). A narrative review on mild behavioural impairment: an exploration into its scientific perspectives. *Aging clinical and experimental research*, *35*(9), 1807-1821.

D'Angelo, E. (2021). Cerebellar granule cell. In *Handbook of the cerebellum and cerebellar disorders* (pp. 837-862). Cham: Springer International Publishing.

D'Arrigo, S., Loiacono, C., Ciaccio, C., Pantaleoni, C., Faccio, F., Taddei, M., & Bulgheroni, S. (2021). Clinical, cognitive and behavioural assessment in children with cerebellar disorder. *Applied Sciences*, *11*(2), 544.

Dan, M., Zhong, R., Hu, S., Wu, H., Zhou, Y., & Liu, Z. Q. (2022). Strategies and challenges on selective electrochemical hydrogen peroxide production: Catalyst and reaction medium design. *Chem Catalysis*, *2*(8), 1919-1960.

Demirci-Çekiç, S., Özkan, G., Avan, A. N., Uzunboy, S., Çapanoğlu, E., & Apak, R. (2022). Biomarkers of oxidative stress and antioxidant defense. *Journal of Pharmaceutical and Biomedical Analysis*, *209*, 114477.

Dickmeiß, J., Henning, Y., Stahlke, S., Weber, T., Theiss, C., & Matschke, V. (2025). Differential Protective Effects of Edaravone in Cerebellar and Hippocampal Ischemic Injury Models. *The Cerebellum*, *24*(2), 49.

Diedrichsen, J., King, M., Hernandez-Castillo, C., Sereno, M., & Ivry, R. B. (2019). Universal transform or multiple functionality? Understanding the contribution of the human cerebellum across task domains. *Neuron*, *102*(5), 918-928.

Dike, C., Antia, M., Bababtunde, B., Sikoki, F., & Ezejiofor, A. (2023). Cognitive, sensory, and motor impairments associated with aluminium, manganese, mercury and lead exposures in the onset of neurodegeneration. *IPS Journal of Public Health*, *2*(1), 1-17.

Ding, N., Li, S., Zhou, H., Tang, Z., Gao, T., Tian, M., Liu, C., Luo, X., Chen, H., Yu, L., Chen, Y., & Zhu, L. (2024). Exploring the complex dynamics of BMI, age, and physiological indicators in early adolescents. *BMC pediatrics*, *24*(1), 222.

Donnelly, L. (2023). The brain: functional divisions. *Anaesthesia & Intensive Care Medicine*, *24*(6), 358-363.

Douae, B., Samir, B., Meriam, E. A., Fatima-zahra, Y., & Youssef, A. (2025). Mercuric Chloride Aggravates Hyperglycemia-Induced Anxiety and Depressive-Like Behaviours in Type 2 Diabetic Rats: Breakdown of the Antioxidant Defense System. *Biological Trace Element Research*, 1-15.

Du, B., Zhang, X., Zhu, C., Wu, Y., Ji, H., Zhang, Y., & Yue, X. (2022). Immunomodulatory and Antioxidant Effects of Polysaccharides from *Pleurotus ostreatus* on Immunosuppressed Mice. *Starch-Stärke*, *74*(11-12), 2200009.

Duan, Z., Zhang, Y., Zhu, C., Wu, Y., Du, B., & Ji, H. (2020). Structural characterization of phosphorylated *Pleurotus ostreatus* polysaccharide and its hepatoprotective effect on carbon tetrachloride-induced liver injury in mice. *International Journal of Biological Macromolecules*, *162*, 533-547.

Dubey, P. R., Kaur, G., & Shukla, R. (2025). Nano-mediated management of metal toxicity-induced neurodegeneration: a critical review. *Molecular Neurobiology*, 1-20.

Durosaro, S. O., Iyasere, O. S., Oguntade, D. O., Ilori, B. M., Odubola, T. A., Adewunmi, A. P., Oyeniran, V. J., & Ozoje, M. O. (2021). Associations between plumage colour and fear behaviour in young Nigerian indigenous turkeys (Meleagris gallopavo). *Applied Animal Behaviour Science*, *244*, 105483.

Dutta, S., Gorain, B., Choudhury, H., Roychoudhury, S., & Sengupta, P. (2022). Environmental and occupational exposure of metals and female reproductive health. *Environmental Science and Pollution Research*, *29*(41), 62067-62092.

Echefu, B., Becker, M., Stein, D., & Ornoy, A. (2025). Methods for Assessing Neurodevelopmental Disorders in Mice: A Critical Review of Behavioral Tests and Methodological Considerations Searching to Improve Reliability. *NeuroSci*, *6*(2), 27.

Effiong, M. E., Umeokwochi, C. P., Afolabi, I. S., & Chinedu, S. N. (2024). Assessing the nutritional quality of *Pleurotus ostreatus* (oyster mushroom). *Frontiers in nutrition*, *10*, 1279208.

Effiong, M. E., Umeokwochi, C. P., Afolabi, I. S., & Chinedu, S. N. (2024). Comparative antioxidant activity and phytochemical content of five extracts of *Pleurotus ostreatus* (oyster mushroom). *Scientific Reports*, *14*(1), 3794.

Egba, S. I., Famurewa, A. C., & Omoruyi, L. E. (2022). Buchholzia coriacea seed extract attenuates mercury-induced cerebral and cerebellar oxidative neurotoxicity via NO signaling and suppression of oxidative stress, adenosine deaminase and acetylcholinesterase activities in rats. *Avicenna Journal of Phytomedicine*, *12*(1), 42.

Elhusseiny, S. M., El-Mahdy, T. S., Awad, M. F., Elleboudy, N. S., Farag, M. M., Yassein, M. A., & Aboshanab, K. M. (2021). Proteome analysis and in vitro antiviral, anticancer and antioxidant capacities of the aqueous extracts of Lentinula edodes and *Pleurotus ostreatus* edible mushrooms. *Molecules*, *26*(15), 4623.

Eltokhi, A., Kurpiers, B., & Pitzer, C. (2021). Comprehensive characterization of motor and coordination functions in three adolescent wild-type mouse strains. *Scientific reports*, *11*(1), 6497.

Engwa, G. A., Nweke, F. N., & Nkeh-Chungag, B. N. (2022). Free radicals, oxidative stress-related diseases and antioxidant supplementation. *Alternative Therapies in Health & Medicine*, *28*(1).

Enogieru, A. B., & Abhelemhen, G. I. (2025). Cerebellar alterations following mercury chloride exposure in Wistar rats: protective role of folic acid. *Scientia Africana*, *24*(2), 69-78.

Enogieru, A. B., & Inneh, C. A. (2022). Cadmium and Mercury exposure: oxidative, neurobehavioural and histological alterations to the Cerebellum of Wistar rats. *Ibom Medical Journal*, *15*(2), 141-147.

Enogieru, A. B., & Omoruyi, S. I. (2022). Exploration of aqueous Phyllanthus amarus leaf extract as a protective agent in mercury chloride-exposed Wistar rats: a neurobehavioural study. *Journal of Applied Sciences and Environmental Management*, *26*(4), 629-637.

Fadugba, A. E., Oyetayo, V. O., Osho, B. I., & Olaniyi, O. O. (2024). Assessment of the effect of iron and selenium fortification on the amino acids profile of *Pleurotus ostreatus*. *Vegetos*, *37*(2), 494-499.

Fagundes, B. H. F., Nascimento, P. C., Aragão, W. A. B., Chemelo, V. S., Bittencourt, L. O., Eiró-Quirino, L., Silva, M. C. F., Freire, M. A. M., Fernandes, L. M. P., Maia, C. D. S. F., Crespo-Lopez, M. E., & Lima, R. R. (2022). Methylmercury exposure during prenatal and postnatal neurodevelopment promotes oxidative stress associated with motor and cognitive damages in rats: an environmental-experimental toxicology study. *Toxicology reports*, *9*, 563-574.

Famii, Z. L., & Ebuka, U. C. (2019). Hepatoprotective activities of aqueous extract of oyster mushroom (*Pleurotus ostreatus*) against lead-induced hepatotoxicity in albino Wistar rats (Rattus norvegicus). *World Journal of Advanced Research and Reviews*, *3*(3), 033-037.

Famii, Z. L., & Favour, B. S. E. (2019). Morris water maze test on neuroprotective effects of ethanolic extract of oyster mushroom (*Pleurotus ostreatus*) against neurotoxicity of mercury chloride in albino rats (Rattus norvegicus). *World Journal of Advanced Research and Reviews*, *3*(1).

Farina, M., & Aschner, M. (2019). Glutathione antioxidant system and methylmercury-induced neurotoxicity: An intriguing interplay. *Biochimica et Biophysica Acta (BBA)-General Subjects*, *1863*(12), 129285.

Farina, M., Aschner, M., & Rocha, J. B. (2012). Redox state in mediating methylmercury neurotoxicity. *Methylmercury and Neurotoxicity*, 101-125.

Fasae, K. D., Abolaji, A. O., Faloye, T. R., Odunsi, A. Y., Oyetayo, B. O., Enya, J. I., Rotimi, J. A., Akinyemi, R. O., Whitworth, A. J., & Aschner, M. (2021). Metallobiology and therapeutic chelation of biometals (copper, zinc and iron) in Alzheimer's disease: Limitations, and current and future perspectives. *Journal of Trace Elements in Medicine and Biology*, *67*, 126779.

Fastenrath, M., Spalek, K., Coynel, D., Loos, E., Milnik, A., Egli, T., Schicktanz, N., Geissmann, L., Roozendaal, B., Papassotiropoulos, A., & de Quervain, D. J. F. (2022). Human cerebellum and corticocerebellar connections involved in emotional memory enhancement. *Proceedings of the National Academy of Sciences*, *119*(41), e2204900119.

Fernandes, T., Garrine, C., Ferrão, J., Bell, V., & Varzakas, T. (2021). Mushroom nutrition as preventative healthcare in Sub-Saharan Africa. *Applied Sciences*, *11*(9), 4221.

Flora, S. J., Jain, K., Panghal, A., & Patwa, J. (2022). Chemistry, pharmacology, and toxicology of monoisoamyl dimercaptosuccinic acid: a chelating agent for chronic metal poisoning. *Chemical research in toxicology*, *35*(10), 1701-1719.

Florimbi, G., Torti, E., Masoli, S., D'Angelo, E., & Leporati, F. (2021). Granular layEr simulator: design and multi-gpu simulation of the cerebellar granular layer. *Frontiers in computational neuroscience*, *15*, 630795.

Florio, T. M. (2025). Emergent Aspects of the Integration of Sensory and Motor Functions. *Brain Sciences*, *15*(2), 162.

Frei, K., & Truong, D. D. (2022). Medications used to treat tremors. *Journal of the neurological sciences*, *435*, 120194.

Fuller, R., Hanrahan, D., Kabay, V., Sanchez-Triana, E., Kayser, M., Lunga, W., Bridgewater, P., & Watson, R. (2025). Towards a prioritization screening framework for chemicals, wastes, and pollution. *Environmental Science & Policy*, *164*, 103994.

Ganguly, J., Kulshreshtha, D., & Jog, M. (2022). Mercury and movement disorders: the toxic legacy continues. *Canadian Journal of Neurological Sciences*, *49*(4), 493-501.

Gao, P. C., Wang, A. Q., Chen, X. W., Cui, H., Li, Y., & Fan, R. F. (2023). Selenium alleviates endoplasmic reticulum calcium depletion-induced endoplasmic reticulum stress and

apoptosis in chicken myocardium after mercuric chloride exposure. *Environmental Science and Pollution Research*, *30*(18), 51531-51541.

Gashaw, G., Fassil, A., & Redi, F. (2020). Evaluation of the antibacterial activity of Pleurotus spp. cultivated on different agricultural wastes in Chiro, Ethiopia. *International Journal of Microbiology*, *2020*(1), 9312489.

Geng, G., Yu, X., Jiang, J., & Yu, X. (2020). Aetiology and pathogenesis of paraneoplastic autoimmune disorders. *Autoimmunity Reviews*, *19*(1), 102422.

Goswami, B., Majumdar, S., Das, A., Barui, A., & Bhowal, J. (2021). Evaluation of bioactive properties of *Pleurotus ostreatus* mushroom protein hydrolysate of different degree of hydrolysis. *Lwt*, *149*, 111768.

Gouvêa, A. L., Gracindo Silva, M., Cabral, B., Martinez, C. G., Lauthartte, L. C., Rodrigues Bastos, W., & Kurtenbach, E. (2021). Progressive resistance exercise prevents muscle strength loss due to muscle atrophy induced by methylmercury systemic intoxication. *JCSM Clinical Reports*, *6*(3), 80-92.

Grimaldi, G. (2021). Cerebellar motor disorders. In *Handbook of the cerebellum and cerebellar disorders* (pp. 1827-1855). Cham: Springer International Publishing.

Gromer, D., Kiser, D. P., & Pauli, P. (2021). Thigmotaxis in a virtual human open field test. *Scientific Reports*, *11*(1), 6670.

Gu, L., Jin, F., Yang, T., Ruan, Y., Zhong, R., Han, Q., & Huang, Y. (2023). Mercuric chloride induced brain toxicity in mice: The protective effects of puerarin-loaded PLGA nanoparticles. *Journal of Biochemical and Molecular Toxicology*, *37*(10), e23425.

Guell, X., & Schmahmann, J. (2020). Cerebellar functional anatomy: a didactic summary based on human fMRI evidence. *The cerebellum*, *19*(1), 1-5.

Guell, X., Schmahmann, J. D., Gabrieli, J. D., & Ghosh, S. S. (2018). Functional gradients of the cerebellum. *elife*, *7*, e36652.

Habas, C. (2021). Functional connectivity of the cognitive cerebellum. *Frontiers in systems neuroscience*, *15*, 642225.

Hamdy, E., Ramadan, I., Mekky, J., Gaber, D., & Galeel, A. A. (2022). Middle cerebellar peduncle lesions and their relation to affective and cognitive impairment in multiple sclerosis. *International Clinical Neuroscience Journal*, *9*, e1.

Hammoud, N., & Jimenez-Shahed, J. (2019). Chronic neurologic effects of alcohol. *Clinics in liver disease*, *23*(1), 141-155.

Hatten, M. E. (2020). Adding cognitive connections to the cerebellum. *Science*, *370*(6523), 1411-1412.

Heckman, R. L., Ludvig, D., & Perreault, E. J. (2023). A motor plan is accessible for voluntary initiation and involuntary triggering at similar short latencies. *Experimental brain research*, *241*(10), 2395-2407.

Hematian, H. (2013). Cerebellum alterations in offspring of mercury treated rats. *Bulgarian Journal of Veterinary Medicine*, *16*(1).

Henriques, M. C., Loureiro, S., Fardilha, M., & Herdeiro, M. T. (2019). Exposure to mercury and human reproductive health: A systematic review. *Reproductive toxicology*, *85*, 93-103.

Hull, C., & Regehr, W. G. (2022). The cerebellar cortex. *Annual review of neuroscience*, *45*(1), 151-175.

Huo, M., & Zhou, R. (2025). Research On The Identification Of Key Industries For Soil And Groundwater Environmental Control And Their Pollution Characteristics In China. *Special Issue: Technologies and Their Effects on Real-Time Social Development*, *167*(A2 (S)).

Idemudia, O. U., & Enogieru, A. B. (2025). Upregulation of Caspase-3 and TNF-α in a rat model of cerebellar motor disorder: role of Cucumis sativus (cucumber). *Journal of Molecular Histology*, *56*(3), 1-11.

Idris, M., Uddin, J., Sullivan, M., McNeill, D. M., & Phillips, C. J. (2021). Non-invasive physiological indicators of heat stress in cattle. *Animals*, *11*(1), 71.

Ijomone, O. M., Iroegbu, J. D., Aschner, M., & Bornhorst, J. (2021). Impact of environmental toxicants on p38-and ERK-MAPK signaling pathways in the central nervous system. *Neurotoxicology*, *86*, 166-171.

Ijomone, O. M., Olaibi, O. K., Biose, I. J., Mba, C., Umoren, K. E., & Nwoha, P. U. (2014). Performance of motor associated behavioural tests following chronic nicotine administration. *Annals of Neurosciences*, *21*(2), 42.

Imosemi, I. O., & Oladejo, O. O. (2023). Aqueous Extract of Allium Sativum Linn. Protected the Cerebellum of Adult Female Wistar Rats against Mercury-induced Oxidative Stress. *African Journal of Biomedical Research*, *26*(1), 119-128.

Iqbal, T., Sohaib, M., Iqbal, S., & Rehman, H. (2024). Exploring therapeutic potential of *Pleurotus ostreatus* and Agaricus bisporus mushrooms against hyperlipidemia and oxidative stress using animal model. *Foods*, *13*(5), 709.

Irshad, A., Tahir, A., Sharif, S., Khalid, A., Ali, S., Naz, A., Sadia, H., & Ameen, A. (2023). Determination of Nutritional and Biochemical Composition of Selected Pleurotus spps. *BioMed Research International*, *2023*(1), 8150909.

Iskusnykh, I. Y., Zakharova, A. A., Kryl'skii, E. D., & Popova, T. N. (2024). Aging, neurodegenerative disorders, and cerebellum. *International Journal of Molecular Sciences*, *25*(2), 1018.

Jalili, C., Darakhshan, S., & Azimi, M. (2021). Harmine mitigates liver injury induced by mercuric chloride via the inhibition of oxidative stress. *Research Journal of Pharmacognosy*, *8*(3), 13-23.

Jang, S. H., & Do Lee, H. (2020). Relationship between ataxia and inferior cerebellar peduncle injury in patients with cerebral infarct. *Medicine*, *99*(9), e19344.

Jayasuriya, W. B. N., Handunnetti, S. M., Wanigatunge, C. A., Fernando, G. H., Abeytunga, D. T. U., & Suresh, T. S. (2020). Anti-inflammatory activity of *Pleurotus ostreatus*, a culinary medicinal mushroom, in Wistar rats. *Evidence-Based Complementary and Alternative Medicine*, *2020*(1), 6845383.

Jha, A., Saidullah, B., & Bubber, P. (2019). A study on prooxidative and neurotoxic effects of mercury chloride in rats. *EC Pharmacology and Toxicology*, *7*, 112-124.

Johnson Afolabi, F., Babafemi Babaniyi, R., Obagunwa, M., Onile, F. O., Ajagun, E. J., Oyedele, O. J., & Adedayo Fasiku, S. (2024). Ethnomycology of Pleurotus tuber-regium and its use in food, medicine and bioremediation. *Botanica Lithuanica*, *30*(4).

Joshua, A. M., Keswani, K. H., & Pai, R. (2022). Cerebellar Dysfunction. In *Physiotherapy for Adult Neurological Conditions* (pp. 371-422). Singapore: Springer Nature Singapore.

Jossinger, S., Mawase, F., Ben-Shachar, M., & Shmuelof, L. (2020). Locomotor adaptation is associated with microstructural properties of the inferior cerebellar peduncle. *The Cerebellum*, *19*, 370-382.

Junior, L. S. B., Lemos, N. B., De Lima, L. F. G., Dias, A. J. A., Neto, O. D. C. F., De Lira, C. C. S., Diniz, A. M. S., Rabelo, N. N., Barroso, L. K. V., Valença, M. M., & de Azevedo Filho, H. R. C. (2021). The anatomy of the brain–learned over the centuries. *Surgical Neurology International*, *12*, 319.

Kalisińska, E., Łanocha-Arendarczyk, N., & Kosik-Bogacka, D. I. (2019). Mercury, Hg. *Mammals and birds as bioindicators of trace element contaminations in terrestrial environments: An Ecotoxicological assessment of the northern hemisphere*, 593-653.

Kamtekar, S., Keer, V., & Patil, V. (2014). Estimation of phenolic content, flavonoid content, antioxidant and alpha amylase inhibitory activity of marketed polyherbal formulation. *Journal of Applied Pharmaceutical Science*, *4*(9), 061-065.

Kang, B., Wang, J., Guo, S., & Yang, L. (2024). Mercury-induced toxicity: Mechanisms, molecular pathways, and gene regulation. *Science of The Total Environment*, 173577.

Kaur, I., Behl, T., Aleya, L., Rahman, M. H., Kumar, A., Arora, S., & Akter, R. (2021). Role of metallic pollutants in neurodegeneration: effects of aluminum, lead, mercury, and arsenic in mediating brain impairment events and autism spectrum disorder. *Environmental Science and Pollution Research*, *28*, 8989-9001.

Kebschull, J. M., Casoni, F., Consalez, G. G., Goldowitz, D., Hawkes, R., Ruigrok, T. J., Schilling, K., Wingate, R., Wu, J., Yeung, J., & Uusisaari, M. Y. (2024). Cerebellum lecture: the cerebellar nuclei—core of the cerebellum. *The Cerebellum*, *23*(2), 620-677.

Khaled, M., Mohamed, R., & Sadek, N. (2024). Age-Related Changes of Purkinje Cells and Astrocytes in Rat Cerebellar Cortex: Histomorphometric, Immunohistochemical and Biochemical Study. *Zagazig University Medical Journal*, *30*(1), 1-13.

Khamas, W., Rutllant, J., & Smodlaka, H. (2024). Nervous system. *Anatomy and Histology of the Domestic Chicken*, 171-182.

Khan, S., Qaiser, M. A., Qureshi, W. A., Najeeb-uz-Zaman, H. S., Yu, X., Wang, W., & Liu, Q. (2024). Photocatalytic hydrogen peroxide production: Advances, mechanistic insights, and emerging challenges. *Journal of Environmental Chemical Engineering*, 114143.

Khinsar, K. H., Abdul, S., Hussain, A., Ud Din, R., Lei, L., Cao, J., Abbasi, M., Ur Rehman, A., Farooqui, N., Yi, X., Min, H., & Mintao, Z. (2021). Anti-tumor effect of polysaccharide from *Pleurotus ostreatus* on H22 mouse Hepatoma ascites in-vivo and hepatocellular carcinoma in-vitro model. *AMB Express*, *11*, 1-15.

Kim, J. J., Kim, Y. S., & Kumar, V. (2019). Heavy metal toxicity: An update of chelating therapeutic strategies. *Journal of Trace elements in Medicine and Biology*, *54*, 226-231.

King, M., Hernandez-Castillo, C. R., Poldrack, R. A., Ivry, R. B., & Diedrichsen, J. (2019). Functional boundaries in the human cerebellum revealed by a multi-domain task battery. *Nature neuroscience*, *22*(8), 1371-1378.

Kosmowska, B., & Wardas, J. (2021). The pathophysiology and treatment of essential tremor: the role of adenosine and dopamine receptors in animal models. *Biomolecules*, *11*(12), 1813.

Kumari, K., & Chand, G. B. (2023). Effects of Mercury: Neurological and Cellular Perspective. *Mercury Toxicity: Challenges and Solutions*, 141-162.

Lackey, E. P., Heck, D. H., & Sillitoe, R. V. (2018). Recent advances in understanding the mechanisms of cerebellar granule cell development and function and their contribution to behavior. *F1000Research*, *7*, F1000-Faculty.

Langlois, E. T., Bennequin, D., & de Marco, G. (2024). Role of the cerebellum in the construction of functional and geometrical spaces. *The Cerebellum*, *23*(6), 2538-2563.

Lara-Aparicio, S. Y., Laureani-Fierro, A. J., Morgado-Valle, C., Beltrán-Parrazal, L., Rojas-Durán, F., García, L. I., Toledo-Cárdenas, R., Hernández, M.E., Manzo, J., & Pérez, C. A. (2022). Latest research on the anatomy and physiology of the cerebellum. *Neurology perspectives*, *2*(1), 34-46.

Lesa, K. N., Khandaker, M. U., Mohammad Rashed Iqbal, F., Sharma, R., Islam, F., Mitra, S., & Emran, T. B. (2022). Nutritional Value, Medicinal Importance, and Health-Promoting Effects of Dietary Mushroom (*Pleurotus ostreatus*). *Journal of Food Quality*, *2022*(1), 2454180.

LeWitt, P. A., Hong, L., & Moehle, M. S. (2024). Anticholinergic drugs for parkinsonism and other movement disorders. *Journal of Neural Transmission*, 1-14.

Li, J., Liu, X. B., Zhao, Z. W., & Yang, Z. L. (2019). Genetic diversity, core collection and breeding history of *Pleurotus ostreatus* in China. *Mycoscience*, *60*(1), 14-24.

Lim, C. Y., Seo, Y., Sohn, B., Seong, M., Kim, S. T., Hong, S., Youn, J., & Kim, E. Y. (2025). The inferior cerebellar peduncle sign: A novel imaging marker for differentiating multiple system atrophy cerebellar type from spinocerebellar ataxia. *American Journal of Neuroradiology*, *46*(6), 1223-1230.

Liu, Q., Kong, W., Hu, S., Kang, Y., Zhang, Y., & Ng, T. B. (2020). Effects of Oudemansiella radicata polysaccharide on postharvest quality of oyster mushroom (*Pleurotus ostreatus*) and its antifungal activity against Penicillium digitatum. *Postharvest Biology and Technology*, *166*, 111207.

Llauradó Maury, G., Morris-Quevedo, H. J., Heykers, A., Lanckacker, E., Cappoen, D., Delputte, P., Vanden Berghe, W., Salgueiro, Z., & Cos, P. (2021). Differential induction pattern towards classically activated macrophages in response to an Immunomodulatory extract from *Pleurotus ostreatus* mycelium. *Journal of Fungi*, *7*(3), 206.

Loehrer, P. A., Zieger, L., & Simon, O. J. (2021). Update on paraneoplastic cerebellar degeneration. *Brain sciences*, *11*(11), 1414.

Lorincz, M. T. (2018). Wilson disease and related copper disorders. *Handbook of Clinical Neurology*, *147*, 279-292.

Luo, J., Ganesan, K., & Xu, B. (2024). Unlocking the power: New insights into the anti-aging properties of mushrooms. *Journal of Fungi*, *10*(3), 215.

Majesty, D., Ijeoma, E., Winner, K., & Prince, O. (2019). Nutritional, anti-nutritional and biochemical studies on the oyster mushroom, *Pleurotus ostreatus*. *EC nutrition*, *14*(1), 36-59.

Maraveas, C., Bayer, I. S., & Bartzanas, T. (2021). Recent advances in antioxidant polymers: From sustainable and natural monomers to synthesis and applications. *Polymers*, *13*(15), 2465.

Marchand, S., Langlade, A., Legois, Q., & Séverac Cauquil, A. (2025). A wide-ranging review of galvanic vestibular stimulation: from its genesis to basic science and clinical applications. *Experimental Brain Research*, *243*(5), 1-31.

Mariën, P., & Borgatti, R. (2018). Language and the cerebellum. *Handbook of clinical neurology*, *154*, 181-202.

Martini, D. N., & Broglio, S. P. (2018). Long-term effects of sport concussion on cognitive and motor performance: a review. *International journal of psychophysiology*, *132*, 25-30.

McCreary, J. K., Rogers, J. A., & Forwell, S. J. (2018). Upper limb intention tremor in multiple sclerosis: an evidence-based review of assessment and treatment. *International journal of MS care*, *20*(5), 211-223.

Metwally, M. I., Basha, M. A. A., AbdelHamid, G. A., Nada, M. G., Ali, R. R., Frere, R. A. F., & Elshetry, A. S. F. (2021). Neuroanatomical MRI study: reference values for the measurements of brainstem, cerebellar vermis, and peduncles. *The British journal of radiology*, *94*(1120), 20201353.

Miall, R. C. (2022). Cerebellum: Anatomy and function. In *Neuroscience in the 21st Century: From Basic to Clinical* (pp. 1563-1582). Cham: Springer International Publishing.

Miao, H. L., Zhang, D. Y., Wang, T., Jiao, X. T., & Jiao, L. Q. (2020). Clinical importance of the posterior inferior cerebellar artery: a review of the literature. *International journal of medical sciences*, *17*(18), 3005.

Michalska, A., Sierocka, M., Drzewiecka, B., & Świeca, M. (2025). Antioxidant and Anti-Inflammatory Properties of Mushroom-Based Food Additives and Food Fortified with Them—Current Status and Future Perspectives. *Antioxidants*, *14*(5), 519.

Mir, M. A., Parihar, K., Tabasum, U., & Kumari, E. J. J. M. P. S. (2016). Estimation of alkaloid, saponin and flavonoid, content in various extracts of Crocus sativa. *Journal of Medicinal Plants Studies*, *4*(5), 171-174.

Mishra, V., Tomar, S., Yadav, P., Vishwakarma, S., & Singh, M. P. (2022). Elemental analysis, phytochemical screening and evaluation of antioxidant, antibacterial and anticancer

activity of *Pleurotus ostreatus* through in vitro and in silico approaches. *Metabolites*, *12*(9), 821.

Misra, H. P., & Fridovich, I. (1972). The role of superoxide anion in the autoxidation of epinephrine and a simple assay for superoxide dismutase. *Journal of Biological chemistry*, *247*(10), 3170-3175.

Mitoma, H., Buffo, A., Gelfo, F., Guell, X., Fucà, E., Kakei, S., Lee, J., Manto, M., Petrosini, L., Shaikh, A.G., & Schmahmann, J. D. (2020). Consensus paper. Cerebellar reserve: from cerebellar physiology to cerebellar disorders. *The Cerebellum*, *19*, 131-153.

Mohideen, K., Chandrasekar, K., Ramsridhar, S., Rajkumar, C., Ghosh, S., & Dhungel, S. (2023). Assessment of oxidative stress by the estimation of lipid peroxidation marker malondialdehyde (MDA) in patients with chronic periodontitis: a systematic review and meta-analysis. *International Journal of Dentistry*, *2023*(1), 6014706.

Mousa, H. R., & Ibrahim, M. H. (2023). Evaluation of The Ameliorative Effect of Green Tea Versus Berberine on Methyl Mercury Toxicity of Cerebellum in Adult Male Albino Rats, Histological & Immunohistochemical Study. *Zagazig Journal of Forensic Medicine and Toxicology*, *21*(2), 1-26.

Murumulla, L., Bandaru, L. J. M., & Challa, S. (2024). Heavy metal mediated progressive degeneration and its noxious effects on brain microenvironment. *Biological Trace Element Research*, *202*(4), 1411-1427.

Musa, K. H., Abdullah, A., & Al-Haiqi, A. (2016). Determination of DPPH free radical scavenging activity: application of artificial neural networks. *Food chemistry*, *194*, 705-711.

Naraki, K., Keshavarzi, M., Razavi, B. M., & Hosseinzadeh, H. (2025). The protective effects of taurine, a non-essential amino acid, against metals toxicities: a review article. *Biological Trace Element Research*, *203*(2), 872-890.

National Research Council (2011). Environment, housing, and management. In *Guide for the Care and Use of Laboratory Animals. 8th edition*. The National Academies Press: Washington, DC, 246.

Nawabjan, S. A., Zhang, F., GS, M. I., Yu, X., Yan, W. T., Balu, K., & Chow, B. K. (2025). Preparation, characterization of pearl powder and its in vivo detoxification potential for heavy metals in mice. *Journal of Hazardous Materials Advances*, *17*, 100524.

Nazareth, L., St John, J., Murtaza, M., & Ekberg, J. (2021). Phagocytosis by peripheral glia: Importance for nervous system functions and implications in injury and disease. *Frontiers in Cell and Developmental Biology*, *9*, 660259.

Neely, K. A., Mohanty, S., Schmitt, L. M., Wang, Z., Sweeney, J. A., & Mosconi, M. W. (2019). Motor memory deficits contribute to motor impairments in autism spectrum disorder. *Journal of autism and developmental disorders*, *49*, 2675-2684.

Nemzer, B., Kalita, D., Yashin, A. Y., & Yashin, Y. I. (2021). Chemical composition and polyphenolic compounds of red wines: their antioxidant activities and effects on human health—a review. *Beverages*, *8*(1), 1.

Nigeria Health Online. (2019, May 22). *Gold rush: Over 850,000 at risk of mercury poisoning*. https://www.nigeriahealthonline.com/2019/05/22/gold-rush-over-850000-at-risk-of-mercury-poisoning.nho/

Nimgampalle, M., Chakravarthy, H., Sharma, S., Shree, S., Bhat, A. R., Pradeepkiran, J. A., & Devanathan, V. (2023). Neurotransmitter systems in the etiology of major neurological disorders: Emerging insights and therapeutic implications. *Ageing Research Reviews*, *89*, 101994.

Nnemolisa, S. C., Chukwurah, C. C., Edeh, S. C., Aguchem, R. N., Chibuogwu, C. C., Aham, E. C., Chukwu, M.C., Obiora, M.O., Anyebe, D.E., & Okagu, I. U. (2024). Antidiabetic and antioxidant potentials of *Pleurotus ostreatus*-derived compounds: An in vitro and in silico approach. *Food Chemistry Advances*, *4*, 100639.

Novo, J. P., Martins, B., Raposo, R. S., Pereira, F. C., Oriá, R. B., Malva, J. O., & Fontes-Ribeiro, C. (2021). Cellular and molecular mechanisms mediating methylmercury neurotoxicity and neuroinflammation. *International journal of molecular sciences*, *22*(6), 3101.

Nweze, C. C., Rasaq, N. O., & Istifanus, B. I. (2020). Ameliorating effect of Agaricus bisponus and *Pleurotus ostreatus* mixed diet on Alloxan-induced hyperglycemic rats. *Scientific African*, *7*, e00209.

O'Leary, T. P., Robertson, A., Chipman, P. H., Rafuse, V. F., & Brown, R. E. (2018). Motor function deficits in the 12-month-old female 5xFAD mouse model of Alzheimer's disease. *Behavioural brain research*, *337*, 256-263.

Ojone, A. S., & Ayodele, S. M. (2025). Ethno-Medicinal Potential of Mushrooms among the Igala People of Kogi State. *African Journal of Agricultural Science and Food Research*, *18*(1), 241-256.

Olopade, F. (2020). Behavioral and Histomorphological Changes in the Developing Brains of Vanadium-Exposed Mice Pups: Protective Role of Minocycline. *Archives of Basic and Applied Medicine*, *8*(2), 95-102.

Olufunmilayo, E. O., Gerke-Duncan, M. B., & Holsinger, R. D. (2023). Oxidative stress and antioxidants in neurodegenerative disorders. *Antioxidants*, *12*(2), 517.

Olukemi, B. C., Omomowo, I. O., Bukola, M. A., Elegbede, J. A., & Adebayo, E. A. (2021). Free radical scavenging ability, mechanisms of action and health implications of oyster mushrooms (pleurotus species): pleurotus species (oyster mushrooms): free radical scavenging capacity. *Journal of Microbiology, Biotechnology and Food Sciences*, *10*(4), 636-647.

Osman, A., & Toliba, A. O. (2019). Hepatoprotective effects of crude phenolic-rich extract from oyster mushroom (*Pleurotus ostreatus*). *Egyptian Journal of Food Science*, *47*(2), 157-164.

Owoeye, O., Akinbami, R. O., & Thomas, M. A. (2018). Neuroprotective potential of Citrullus lanatus seed extract and vitamin E against mercury chloride intoxication in male rat brain. *African Journal of Biomedical Research*, *21*(1), 43-49.

Oyetayo, V. O., Ogidi, C. O., Bayode, S. O., & Enikanselu, F. F. (2021). Evaluation of biological efficiency, nutrient contents and antioxidant activity of Pleurotus pulmonarius enriched with Zinc and Iron. *Indian Phytopathology*, *74*, 901-910.

Palejwala, A. H., Dadario, N. B., Young, I. M., O'Connor, K., Briggs, R. G., Conner, A. K., O'Donoghue, D. L., & Sughrue, M. E. (2021). Anatomy and white matter connections of the lingual gyrus and cuneus. *World neurosurgery*, *151*, e426-e437.

Pánek, M., Wiesnerová, L., Jablonský, I., Novotný, D., & Tomšovský, M. (2019). What is cultivated oyster mushroom? Phylogenetic and physiological study of *Pleurotus ostreatus* and related taxa. *Mycological Progress*, *18*, 1173-1186.

Paredes-Acuna, N., Utpadel-Fischler, D., Ding, K., Thakor, N. V., & Cheng, G. (2024). Upper limb intention tremor assessment: opportunities and challenges in wearable technology. *Journal of NeuroEngineering and Rehabilitation*, *21*(1), 8.

Parida, L., & Patel, T. N. (2023). Systemic impact of heavy metals and their role in cancer development: a review. *Environmental Monitoring and Assessment*, *195*(6), 766.

Paterska, M., Czerny, B., & Cielecka-Piontek, J. (2024). Macrofungal extracts as a source of bioactive compounds for cosmetical anti-aging therapy: a comprehensive review. *Nutrients*, *16*(16), 2810.

Pei, J., Pan, X., Wei, G., & Hua, Y. (2023). Research progress of glutathione peroxidase family (GPX) in redoxidation. *Frontiers in pharmacology*, *14*, 1147414.

Penticoff, H. B., & Fortin, J. S. (2023). Toxic/metabolic diseases of the nervous system. In *Neurobiology of Brain Disorders* (pp. 379-401). Academic Press.

Pérez-Bassart, Z., Falcó, I., Martínez-Sanz, M., Martínez-Abad, A., Sánchez, G., López-Rubio, A., & Fabra, M. J. (2024). Antiviral and technological properties of β-glucan-rich aqueous fractions from *Pleurotus ostreatus* waste biomass. *Food Hydrocolloids*, *146*, 109308.

Perrone, P., Spinelli, S., Mantegna, G., Notariale, R., Straface, E., Caruso, D., Falliti, G., Marino, A., Manna, C., Remigante, A., & Morabito, R. (2023). Mercury chloride affects band 3 protein-mediated anionic transport in red blood cells: Role of oxidative stress and protective effect of olive oil polyphenols. *Cells*, *12*(3), 424.

Petković, A., & Chaudhury, D. (2022). Encore: Behavioural animal models of stress, depression and mood disorders. *Frontiers in behavioral neuroscience*, *16*, 931964.

Pillay, B. J., Meyer, A., & Mokobane, M. (2019). Fine motor deficits and attention deficit hyperactivity disorder in primary school children. *South African Journal of Psychiatry*, *25*(1), 1-7.

Piscopo, M., Notariale, R., Tortora, F., Lettieri, G., Palumbo, G., & Manna, C. (2020). Novel insights into mercury effects on hemoglobin and membrane proteins in human erythrocytes. *Molecules*, *25*(14), 3278.

Pisoschi, A. M., Pop, A., Iordache, F., Stanca, L., Predoi, G., & Serban, A. I. (2021). Oxidative stress mitigation by antioxidants-an overview on their chemistry and influences on health status. *European Journal of Medicinal Chemistry*, *209*, 112891.

Pontillo, G., Castagna, A., Vola, E. A., Macerollo, A., Peluso, S., Russo, C., Baglio, F., Manganelli, F., Brunetti, A., Cocozza, S., & Esposito, M. (2020). The cerebellum in idiopathic cervical dystonia: a specific pattern of structural abnormalities?. *Parkinsonism & Related Disorders*, *80*, 152-157.

Poudel, P. P., Bhattarai, C., Ghosh, A., & Kalthur, S. G. (2023). Histomorphometry of the cortical layers and the dentate nucleus of the human fetal cerebellum. *Journal of Taibah University Medical Sciences*, *18*(2), 390-399.

Prati, J. M., Pontes-Silva, A., & Gianlorenço, A. C. L. (2024). The cerebellum and its connections to other brain structures involved in motor and non-motor functions: a comprehensive review. *Behavioural Brain Research*, 114933.

Raeeszadeh, M., Moradi, M., Ayar, P., & Akbari, A. (2021). The antioxidant effect of Medicago sativa L.(alfalfa) ethanolic extract against mercury chloride (HgCl2) toxicity in rat liver and kidney: an in vitro and in vivo study. *Evidence-Based Complementary and Alternative Medicine*, *2021*(1), 8388002.

Rahimi-Balaei, M., Bergen, H., Kong, J., & Marzban, H. (2018). Neuronal migration during development of the cerebellum. *Frontiers in cellular neuroscience*, *12*, 484.

Rana, A., Samtiya, M., Dhewa, T., Mishra, V., & Aluko, R. E. (2022). Health benefits of polyphenols: A concise review. *Journal of Food Biochemistry*, *46*(10), e14264.

Ranjan, R., Chourey, A., Kabir, Y., Mata, H. D. G., Tiepolo, E., Vinueza, I. L. F., Mohammed, C., Mohammed, S. F., Thottakurichi, A. A., Vinueza, I. L. F., & THOTTAKURICHI, A. A. (2024). Role of Neurosurgical Interventions in the Treatment of Movement Disorders Like Parkinson's Disease, Dystonia, and Tourette Syndrome. *Cureus*, *16*(10).

Rausch, V., Sala, V., Penna, F., Porporato, P. E., & Ghigo, A. (2021). Understanding the common mechanisms of heart and skeletal muscle wasting in cancer cachexia. *Oncogenesis*, *10*(1), 1.

Rehman, Q., Rehman, K., & Akash, M. S. H. (2021). Heavy metals and neurological disorders: from exposure to preventive interventions. In *Environmental contaminants and neurological disorders* (pp. 69-87). Cham: Springer International Publishing.

Rehman, Q., Rehman, K., & Akash, M. S. H. (2021). Heavy metals and neurological disorders: from exposure to preventive interventions. In *Environmental contaminants and neurological disorders* (pp. 69-87). Cham: Springer International Publishing.

Reumers, S. F., Bongaerts, F. L., de Leeuw, F. E., van de Warrenburg, B. P., Schutter, D. J., & Kessels, R. P. (2025). Cognition in cerebellar disorders: What's in the profile? A systematic review and meta-analysis. *Journal of Neurology*, *272*(3), 250.

Rivero-Pérez, N., Ayala-Martínez, M., Zepeda-Bastida, A., Meneses-Mayo, M., & Ojeda-Ramírez, D. (2016). Anti-inflammatory effect of aqueous extracts of spent *Pleurotus ostreatus* substrates in mouse ears treated with 12-O-tetradecanoylphorbol-13-acetate. *Indian Journal of pharmacology*, *48*(2), 141-144.

Rojas-Franco, P., Franco-Colín, M., Torres-Manzo, A. P., Blas-Valdivia, V., Thompson-Bonilla, M. D. R., Kandir, S., & Cano-Europa, E. (2019). Endoplasmic reticulum stress participates in the pathophysiology of mercury-caused acute kidney injury. *Renal Failure*, *41*(1), 1001-1010.

Rosa, A. C., Corsi, D., Cavi, N., Bruni, N., & Dosio, F. (2021). Superoxide dismutase administration: A review of proposed human uses. *Molecules*, *26*(7), 1844.

Rotruck, J. T., Pope, A. L., Ganther, H. E., Swanson, A. B., Hafeman, D. G., & Hoekstra, W. (1973). Selenium: biochemical role as a component of glutathione peroxidase. *Science*, *179*(4073), 588-590.

Rousseau, P. N., Chakravarty, M. M., & Steele, C. J. (2022). Mapping pontocerebellar connectivity with diffusion MRI. *NeuroImage*, *264*, 119684.

Rukhsar, S., Usman, M., Yousaf, N., Murtaza, G., Manzoor, M. A., & Azam, M. (2025). Mushrooms in modern cosmetics: unlocking anti-aging, antioxidant, and therapeutic potential. *Archives of Dermatological Research*, *317*(1), 542.

Sadiq, I. Z. (2023). Free radicals and oxidative stress: Signaling mechanisms, redox basis for human diseases, and cell cycle regulation. *Current molecular medicine*, *23*(1), 13-35.

Sadler, K. E., Mogil, J. S., & Stucky, C. L. (2022). Innovations and advances in modelling and measuring pain in animals. *Nature Reviews Neuroscience*, *23*(2), 70-85.

Sagar, S. C., Deep, S., Chauhan, S., & Tapadia, M. G. (2025). The Brain. In *Encyclopedia of Religious Psychology and Behavior* (pp. 1-12). Cham: Springer Nature Switzerland.

Sahoo, R. K., Gupta, T., Kumar, V., Rani, S., & Gupta, U. (2022). Aetiology and pathophysiology of neurodegenerative disorders. In *Nanomedical Drug Delivery for Neurodegenerative Diseases* (pp. 1-16). Academic Press.

Said, E. S., Ahmed, R. M., Mohammed, R. A., Morsi, E. M., Elmahdi, M. H., Elsayed, H. S., Mahmoud, R.H., & Nadwa, E. H. (2021). Ameliorating effect of melatonin on mercuric chloride-induced neurotoxicity in rats. *Heliyon*, *7*(7).

Salavoura, A. (2025). Metals and Disease. In *Chemical Environmental Pollutants and their Effect on Health* (pp. 55-214). Cham: Springer Nature Switzerland.

Sales-Campos, C., da Silva, J. F., do Nascimento, L. B. D. B., dos Santos Gouvêa, P. R., de Aguiar, L. V. B., Fariña, J. I., Pontes, G. S., & Chevreuil, L. R. (2021). Nutritional and bioactive properties of an amazon wild oyster culinary-medicinal mushroom, *Pleurotus ostreatus* (Agaricomycetes): contributions to functional food and human health. *International Journal of Medicinal Mushrooms*, *23*(7).

Sarnaik, R., & Raman, I. M. (2018). Control of voluntary and optogenetically perturbed locomotion by spike rate and timing of neurons of the mouse cerebellar nuclei. *Elife*, *7*, e29546.

Sathyanesan, A., Zhou, J., Scafidi, J., Heck, D. H., Sillitoe, R. V., & Gallo, V. (2019). Emerging connections between cerebellar development, behaviour and complex brain disorders. *Nature Reviews Neuroscience*, *20*(5), 298-313. Sathyanesan, A., Zhou, J., Scafidi, J., Heck, D. H., Sillitoe, R. V., & Gallo, V. (2019). Emerging connections between cerebellar development, behaviour and complex brain disorders. *Nature Reviews Neuroscience*, *20*(5), 298-313.

Sathyanesan, A., Zhou, J., Scafidi, J., Heck, D. H., Sillitoe, R. V., & Gallo, V. (2019). Emerging connections between cerebellar development, behaviour and complex brain disorders. *Nature Reviews Neuroscience*, *20*(5), 298-313.

Schmahmann, J. D. (2023). A brief history of the cerebellum. In *Essentials of Cerebellum and Cerebellar Disorders: A Primer For Graduate Students* (pp. 5-14). Cham: Springer International Publishing.

Seethapathy, P., Subramani, T., Ayrilmis, N., & Patil, H. (2025). Therapeutic and Environmental Potential of Mushrooms in Ancient and Modern Contexts: A Review. *International Journal of Medicinal Mushrooms*, *27*.

Seethapathy, P., Thangaraj, P., Pandita, A., Sankaralingam, S., & Pandita, D. (2023). Oyster Mushroom (*Pleurotus ostreatus*). In *Mushrooms* (pp. 302-321). CRC Press.

Semenova, E., Kurakov, A. V., Nazarov, V., Presnyakova, V., Markelova, N., Karaseva, E., Kurdyukov, E. E., Tsokalo, I., Minkina, T., & Rajput, V. D. (2023). Biotransformation of Wastes of Essential Oil Industry by Strains Agaricus bisporus (JE Lange) Imbach, Lentinula edodes (Berk.) Pegler, and *Pleurotus ostreatus* (Jacq.) P. Kumm. *Horticulturae*, *9*(4), 450.

Sen, P., Kosre, A., Koreti, D., Chandrawansi, N. K., & Jadhav, S. K. (2021). Nutrients and Bioactive compounds of *Pleurotus ostreatus* mushroom. *NewBioWorld*, *3*(2), 8-12.

Seo, D. J., & Choi, C. (2021). Antiviral bioactive compounds of mushrooms and their antiviral mechanisms: a review. *Viruses*, *13*(2), 350.

Sereno, M. I., Diedrichsen, J., Tachrount, M., Testa-Silva, G., d'Arceuil, H., & De Zeeuw, C. (2020). The human cerebellum has almost 80% of the surface area of the neocortex. *Proceedings of the National Academy of Sciences*, *117*(32), 19538-19543.

Sharma, A., Sharma, A., & Tripathi, A. (2021). Biological activities of Pleurotus spp. polysaccharides: A review. *Journal of Food Biochemistry*, *45*(6), e13748.

Sharma, T., Gamit, R., Acharya, R., & Shukla, V. J. (2021). Quantitative estimation of total tannin, alkaloid, phenolic, and flavonoid content of the root, leaf, and whole plant of Byttneria herbacea Roxb. *AYU (An International Quarterly Journal of Research in Ayurveda)*, *42*(3), 143-147.

Shohag, S., Akhter, S., Islam, S., Sarker, T., Sifat, M. K., Rahman, M. M., Islam, M. R., & Sharma, R. (2022). Perspectives on the molecular mediators of oxidative stress and antioxidant strategies in the context of neuroprotection and neurolongevity: an extensive review. *Oxidative Medicine and Cellular Longevity*, *2022*(1), 7743705.

Singh, R. (2020). Cerebellum: its anatomy, functions and diseases. In *Neurodegenerative Diseases-Molecular Mechanisms and Current Therapeutic Approaches*. IntechOpen 93064.

Siripongvutikorn, S., Pumethakul, K., Yupanqui, C. T., Seechamnanturakit, V., Detarun, P., Utaipan, T., Sirinupong, N., Chansuwan, W., Wittaya, T., & Samakradhamrongthai, R. S. (2024). Phytochemical profiling and antioxidant activities of the most favored ready-to-use Thai curries, Pad-Ka-Proa (spicy basil leaves) and Massaman. *Foods*, *13*(4), 582.

Soldado, D., Bessa, R. J., & Jerónimo, E. (2021). Condensed tannins as antioxidants in ruminants—Effectiveness and action mechanisms to improve animal antioxidant status and oxidative stability of products. *Animals*, *11*(11), 3243.

Sørensen, F. W., Larsen, J. O., Eide, R., & Schiønning, J. D. (2000). Neuron loss in cerebellar cortex of rats exposed to mercury vapor: a stereological study. *Acta neuropathologica*, *100*, 95-100.

Stańczak, M., Swinnen, B., Kacprzak, B., Pacek, A., & Surmacz, J. (2025). Neurophysiology of ACL Injury. *Orthopedic Reviews*, *17*, 129173.

Stephen, C. D., Brizzi, K. T., Bouffard, M. A., Gomery, P., Sullivan, S. L., Mello, J., MacLean, J. & Schmahmann, J. D. (2019). The comprehensive management of cerebellar ataxia in adults. *Current Treatment Options in Neurology*, *21*, 1-17.

Stephen, C. D., Vangel, M., Gupta, A. S., MacMore, J. P., & Schmahmann, J. D. (2024). Rates of change of pons and middle cerebellar peduncle diameters are diagnostic of multiple system atrophy of the cerebellar type. *Brain Communications*, *6*(1), fcae019.

Stoia, M., & Oancea, S. (2022). Low-molecular-weight synthetic antioxidants: classification, pharmacological profile, effectiveness and trends. *Antioxidants*, *11*(4), 638.

Sultan, S. M., & Abed, F. N. M. (2023). Plasma cholesterol level reduction in albino rats by β-d glucan (pleuran) from Plurotus ostreatus. *Medical Journal of Babylon*, *20*(Supplement 1), S75-S79.

Sultana, O. F., Bandaru, M., Islam, M. A., & Reddy, P. H. (2024). Unraveling the complexity of human brain: Structure, function in healthy and disease states. *Ageing Research Reviews*, *100*, 102414.

Sumathi, T., Shobana, C., Christinal, J., & Anusha, C. (2012). Protective effect of Bacopa monniera on methyl mercury-induced oxidative stress in cerebellum of rats. *Cellular and Molecular Neurobiology*, *32*, 979-987.

Sun, Q., Li, Y., Shi, L., Hussain, R., Mehmood, K., Tang, Z., & Zhang, H. (2022). Heavy metals induced mitochondrial dysfunction in animals: Molecular mechanism of toxicity. *Toxicology*, *469*, 153136.

Tanabe, H. C., Kubo, D., Hasegawa, K., Kochiyama, T., & Kondo, O. (2018). Cerebellum: anatomy, physiology, function, and evolution. *Digital Endocasts: From Skulls to Brains*, 275-289.

ten Donkelaar, H. J., ten Donkelaar, H. J., den Dunnen, W., van de Warrenburg, B., Lammens, M., & Wesseling, P. (2020). The cerebellum. *Clinical Neuroanatomy: Brain Circuitry and Its Disorders*, 539-589.

Thakur, M., Rachamalla, M., Niyogi, S., Datusalia, A. K., & Flora, S. J. S. (2021). Molecular mechanism of arsenic-induced neurotoxicity including neuronal dysfunctions. *International Journal of Molecular Sciences*, *22*(18), 10077.

Tiwari Pandey, A., Pandey, I., Kanase, A., Verma, A., Garcia-Canibano, B., Dakua, S. P., Balakrishnan, S., & Singh, M. P. (2021). Validating anti-infective activity of Pleurotus Opuntiae via standardization of its bioactive mycoconstituents through multimodal biochemical Approach. *Coatings*, *11*(4), 484.

Tiwari, B. K., Abidi, A. B., Rizvi, S. I., & Pandey, K. B. (2016). Phytochemical screening and evaluation of antioxidant potentials of some Indian medicinal plants and their composite extract. *Annals of Phytomedicine*, *5*(1), 99-103.

Törős, G., El-Ramady, H., Prokisch, J., Velasco, F., Llanaj, X., Nguyen, D. H., & Peles, F. (2023). Modulation of the gut microbiota with prebiotics and antimicrobial agents from *Pleurotus ostreatus* mushroom. *Foods*, *12*(10), 2010.

Tripathi, P., & Sieber, F. (2019). The adult central nervous system: anatomy and physiology. In *Essentials of Neurosurgical Anesthesia & Critical Care: Strategies for Prevention, Early Detection, and Successful Management of Perioperative Complications* (pp. 3-13). Cham: Springer International Publishing.

Tumilaar, S. G., Hardianto, A., Dohi, H., & Kurnia, D. (2024). A comprehensive review of free radicals, oxidative stress, and antioxidants: Overview, clinical applications, global perspectives, future directions, and mechanisms of antioxidant activity of flavonoid compounds. *Journal of Chemistry*, *2024*(1), 5594386.

Uddin, S., Afroz, H., Hossain, M., Briffa, J., Blundell, R., & Islam, M. R. (2023). Heavy metals/metalloids in food crops and their implications for human health. *Heavy metal toxicity and tolerance in plants: A biological, omics, and genetic engineering approach*, 59-86.

United Nations Environment Programme. (2019). *Global mercury assessment 2018: Sources, emissions and releases to the environment* (Chemicals and Health Branch). https://www.unep.org/resources/publication/global-mercury-assessment-2018.

Urrutia Desmaison, J. D., Sala, R. W., Ayyaz, A., Nondhalee, P., Popa, D., & Léna, C. (2023). Cerebellar control of fear learning via the cerebellar nuclei–Multiple pathways, multiple mechanisms?. *Frontiers in Systems Neuroscience*, *17*, 1176668.

Valappil, G. P., Julius, S., & Krishnankutty, J. K. (2020). Hypolipidemic Activity of Pleurotus florida against Triton WR 1339 Induced Hyperlipidaemia. *Letters in Applied NanoBioScience*, *10*, 2107-2116.

Van Essen, D. C., Donahue, C. J., & Glasser, M. F. (2018). Development and evolution of cerebral and cerebellar cortex. *Brain Behaviour and Evolution*, *91*(3), 158-169.

Van Noorden, C. J. F. (2005). First Joint Congress of the Society for Histochemistry and The Histochemical Society, Noordwijkerhout, The Netherlands, April 27–30, 2005. *Acta histochemica*, *107*, 379-410.

Verma, N., Rachamalla, M., Kumar, P. S., & Dua, K. (2023). Assessment and impact of metal toxicity on wildlife and human health. In *Metals in water* (pp. 93-110). Elsevier.

Vianna, A. D. S., Matos, E. P. D., Jesus, I. M. D., Asmus, C. I. R. F., & Câmara, V. D. M. (2019). Human exposure to mercury and its hematological effects: a systematic review. *Cadernos de saude publica*, *35*(2), e00091618.

Vlasenko, E., & Kuznetsova, O. (2020). The influence of complex additives on the synthesis of aroma substances by gray oyster culinary-medicinal mushroom, *Pleurotus ostreatus* (agaricomycetes) during the substrate cultivation. *International Journal of Medicinal Mushrooms*, *22*(3).

Voikar, V., & Stanford, S. C. (2022). The open field test. *Psychiatric vulnerability, mood, and anxiety disorders: tests and models in mice and rats*, 9-29.

Wang, D., Wang, J., Liu, H., Liu, M., Yang, Y., & Zhong, S. (2022). The main structural unit elucidation and immunomodulatory activity in vitro of a selenium-enriched polysaccharide produced by *Pleurotus ostreatus*. *Molecules*, *27*(8), 2591.

Warfvinge, K. (2000). Mercury distribution in the neonatal and adult cerebellum after mercury vapor exposure of pregnant squirrel monkeys. *Environmental Research*, *83*(2), 93-101.

Willett, R. T., Bayin, N. S., Lee, A. S., Krishnamurthy, A., Wojcinski, A., Lao, Z., Stephen, D., Rosello-Diez, A., Dauber-Decker, K.L., Orvis, G.D. & Joyner, A. L. (2019). Cerebellar nuclei excitatory neurons regulate developmental scaling of presynaptic Purkinje cell number and organ growth. *Elife*, *8*, e50617.

World Health Organization. (2019, May 22). Over 850,000 Nigerians in 12 states at risk of poisoning from mercury use. WHO Regional Office for Africa. https://www.afro.who.int/news/over-850000-nigerians-12-states-risk-poisoning-mercury-use

World Health Organization. (2024, October 24). *Mercury and health*. https://www.who.int/news-room/fact-sheets/detail/mercury-and-health.

Wu, Y. S., Osman, A. I., Hosny, M., Elgarahy, A. M., Eltaweil, A. S., Rooney, D. W., Chen, Z., Rahim, N.S., Sekar, M., Gopinath, S. C., Mat Rani, N.N.I., & Yap, P. S. (2024). The toxicity of mercury and its chemical compounds: molecular mechanisms and environmental and human health implications: a comprehensive review. *Acs Omega*, *9*(5), 5100-5126.

Xia, Y., Wang, M., & Zhu, Y. (2023). The effect of cerebellar rtms on modulating motor dysfunction in neurological disorders: a systematic review. *The Cerebellum*, *22*(5), 954-972.

Yahyazadeh, A., & Gur, F. M. (2024). Promising the potential of β-caryophyllene on mercury chloride–induced alteration in cerebellum and spinal cord of young Wistar albino rats. *Naunyn-Schmiedeberg's Archives of Pharmacology*, *397*(12), 10175-10189.

Yshii, L., Bost, C., & Liblau, R. (2020). Immunological bases of paraneoplastic cerebellar degeneration and therapeutic implications. *Frontiers in immunology*, *11*, 991.

Yudaev, P., & Chistyakov, E. (2022). Chelating extractants for metals. *Metals*, *12*(8), 1275.

Zafar, A., Javed, S., Akram, N., & Naqvi, S. A. R. (2024). Health risks of mercury. In *Mercury Toxicity Mitigation: Sustainable Nexus Approach* (pp. 67-92). Cham: Springer Nature Switzerland.

Zahed, M. A., Ebrahimi, M., Barmakhshad, N., Shemshadi, S., & Parsasharif, N. (2024). Mercury-mediated neurological diseases: Insight into molecular mechanisms, mutant proteins, and structure-based therapeutic inhibitors. *Toxicology and Environmental Health Sciences*, 1-22.

Zhang, H., Jiang, F., Zhang, J., Wang, W., Li, L., & Yan, J. (2022). Modulatory effects of polysaccharides from plants, marine algae and edible mushrooms on gut microbiota and related health benefits: A review. *International Journal of Biological Macromolecules*, *204*, 169-192.

Zhao, C., Jiang, S., Jin, F., Gu, L., Liang, M., Zhao, Y., & Han, Q. (2025). Studies on the toxic effects of acute mercuric chloride poisoning in mice: primary toxicity evaluation analysis of HgCl2. *Toxicology Mechanisms and Methods*, 1-13.

Zhao, M., Li, Y., & Wang, Z. (2022). Mercury and mercury-containing preparations: history of use, clinical applications, pharmacology, toxicology, and pharmacokinetics in traditional Chinese medicine. *Frontiers in Pharmacology*, *13*, 807807.

Zitte, L. F., & Bernard, S. E. F. (2019). Antitoxic Effects of Ethanoic Extract of Oyster Mushroom (*Pleurotus ostreatus*) Against Neurotoxic Mercury Chloride In Albino Rats. *International Digital Organization for Scientific Research Journal of Applied Sciences*, *4*(1) 107-113.

Zulaikhah, S. T., Wahyuwibowo, J., & Pratama, A. A. (2020). Mercury and its effect on human health: A review of the literature. *International Journal of Public Health Science*, *9*(2), 103-114.

Zwergal, A., Feil, K., Schniepp, R., & Strupp, M. (2020, February). Cerebellar dizziness and vertigo: etiologies, diagnostic assessment, and treatment. In *Seminars in Neurology* (Vol. 40, No. 01, pp. 087-096). Thieme Medical Publishers.

APPENDIX

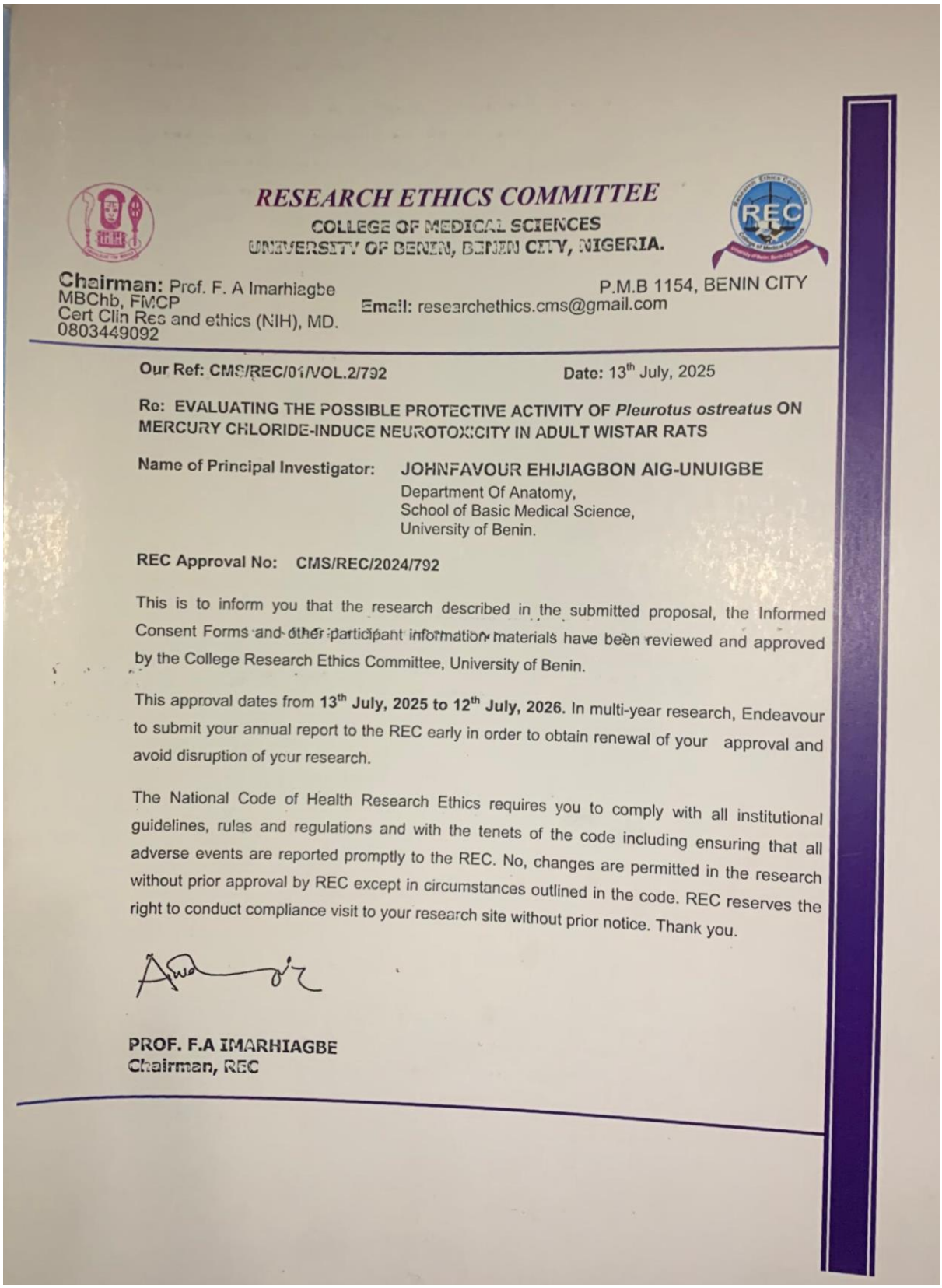

RESEARCH ETHICS COMMITTEE
COLLEGE OF MEDICAL SCIENCES
UNIVERSITY OF BENIN, BENIN CITY, NIGERIA.

Chairman: Prof. F. A Imarhiagbe
MBChb, FMCP
Cert Clin Res and ethics (NIH), MD.
0803449092

P.M.B 1154, BENIN CITY
Email: researchethics.cms@gmail.com

Our Ref: CMS/REC/01/VOL.2/792 **Date:** 13th July, 2025

Re: EVALUATING THE POSSIBLE PROTECTIVE ACTIVITY OF *Pleurotus ostreatus* ON MERCURY CHLORIDE-INDUCE NEUROTOXICITY IN ADULT WISTAR RATS

Name of Principal Investigator: **JOHNFAVOUR EHIJIAGBON AIG-UNUIGBE**
Department Of Anatomy,
School of Basic Medical Science,
University of Benin.

REC Approval No: **CMS/REC/2024/792**

This is to inform you that the research described in the submitted proposal, the Informed Consent Forms and other participant information materials have been reviewed and approved by the College Research Ethics Committee, University of Benin.

This approval dates from **13th July, 2025 to 12th July, 2026.** In multi-year research, Endeavour to submit your annual report to the REC early in order to obtain renewal of your approval and avoid disruption of your research.

The National Code of Health Research Ethics requires you to comply with all institutional guidelines, rules and regulations and with the tenets of the code including ensuring that all adverse events are reported promptly to the REC. No, changes are permitted in the research without prior approval by REC except in circumstances outlined in the code. REC reserves the right to conduct compliance visit to your research site without prior notice. Thank you.

PROF. F.A IMARHIAGBE
Chairman, REC